AD-759 952

MEASUREMENT OF RESISTANCE, ICE LOADS, AND ICE CHARACTERISTICS ON THE USCGC MACKINAW

R. Y. Edwards, Jr., et al

Teledyne Materials Research

Prepared for:

Coast Guard

5 February 1973

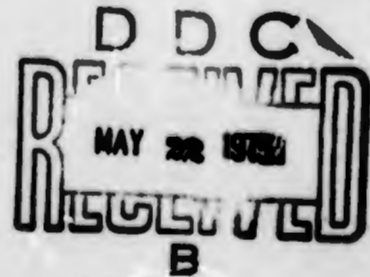# MEASUREMENT OF RESISTANCE, ICE LOADS, AND

ICE CHARACTERISTICS ON THE USCGC MACKINAW

AD 759952

D D C
RECEIVED
MAY 22 1973
B

FINAL TECHNICAL REPORT

Document is available to the public through the
National Technical Information Service,
Springfield, Virginia 22151

Prepared for

DEPARTMENT OF TRANSPORTATION
UNITED STATES COAST GUARD
Office of Research and Development
Washington, D.C. 20590

105

DATE __5 February 1973__

This report has been submitted in fulfillment of contract DOT-CG-11,730-A and is promulgated subject to the following qualifications:

The contents of this report reflect the views of the authors who are responsible for the facts and the accuracy of the data presented herein. The contents do not necessarily reflect the official views or policy of the Coast Guard. This report does not constitute a standard, specification, or regulation.

C. P. GLASS
Captain, U. S. Coast Guard
Chief, Marine Safety Technology Division
Office of Research and Development
U. S. Coast Guard Headquarters
Washington, D. C. 20590

1. Report No. E-1364(f)	2. Government Accession No.	3. Recipient's Catalog No.
4. Title and Subtitle Measurement of Resistance, Ice Loads, and Ice Characteristics on the USCGC MACKINAW		5. Report Date July 1971
		6. Performing Organization Code
7. Author(s) See below.		8. Performing Organization Report No.
9. Performing Organization Name and Address TELEDYNE MATERIALS RESEARCH 303 Bear Hill Road Waltham, Massachusetts 02154		10. Work Unit No.
		11. Contract or Grant No. DOT-CG-11,730-A
12. Sponsoring Agency Name and Address COMMANDANT (FSP-2/7/71) U. S. COAST GUARD HEADQUARTERS 400 Seventh Street, S.W. Washington, D. C. 20591		13. Type of Report and Period Covered Final Report Nov. 1970 - July 1971
		14. Sponsoring Agency Code

15. Supplementary Notes

Technical direction was by ARCTEC, Inc., with instrumentation provided by Teledyne Materials Research and the U. S. Coast Guard. Ice measurements by Cold Regions Res. & Eng. Lab.

16. Abstract

Authors:

R. Y. Edwards, Jr. *   * ARCTEC, Inc.
J. W. Wheaton   Wild Lake Village Center
G. Levine *   Columbia, MD
J. W. Lewis *

16. Abstract

Experimental Runs were made in ice of varying thickness at a number of different velocities and power levels to determine the effects of these and other variables on the resistance encountered by the ship. In addition, measurements of strain were made on the hull from which the force exerted on the hull by the ice was determined for each data point. The relationship force to other variables was also developed. The results of the trials are presented in the form of functions of a number of nondimensional variables.

17. Key Words resistance, icebreaking, hull structure, strain data	18. Distribution Statement

19. Security Classif. (of this report)	20. Security Classif. (of this page)	21. No. of Pages	22. Price
	- i -		

PREFACE

ABSTRACT

This report presents the results of full-scale trials of the
USCGC MACKINAW on the Great Lakes during February and March, 1971.
These trials are part of a long-range program to acquire data which
will improve the knowledge of how icebreaker power and strength are
related to speed and ice conditions. This knowledge, in turn, will
improve the accuracy with which an economic model of the Great Lakes
winter navigation system could be devised.

Experimental runs in ice of varying thickness were made at a
number of different velocities and power levels to determine the
effects of these and other variables on the resistance encountered
by the ship. In addition, measurements of strain were made on the
hull from which the force exerted on the hull by the ice was deter-
mined for a number of steady-state conditions. The relationship of
force to other variables was developed. The results of the trials
are presented in the form of functions of a number of non-dimensional
variables.

These experiments have shown that ice thickness, ship velocity,
and snow cover are the most significant variables in the equation for
ice resistance. The effect of the bow propeller upon ice resistance
was found to be small. In the range where there is data from both
WIND Class tests and MACKINAW tests, the dimensionless regression eq-
equations are almost identical. The resistance data acquired in the
course of these experiments span a range of velocity much wider than
any previous resistance tests in ice.

-i-2

ACKNOWLEDGEMENTS

TABLE OF CONTENTS

TABLE OF CONTENTS
(Continued)

iv

SUMMARY AND CONCLUSIONS

A full scale trial of the USCGC MACKINAW was conducted in Lake Huron, Lake Michigan and Green Bay during the period 3 February 1971 through 11 March 1971.

The purpose of the trial was twofold. The primary purpose was to determine the relationship between the resistance encountered by the ship while moving through an ice field and the following variables:

1. Ice thickness
2. Ship speed
3. Ratio of bow propeller power to total power
4. Snow cover depth
5. Ice strength

The second purpose was to obtain a relationship between the force exerted by the ice sheet on the hull of the ship and the following variables:

1. Ice thickness
2. Ship speed
3. Ice strength

The ship was equipped with an instrumentation package designed to measure and record the propeller thrust, torque, power and speed, strain in the hull plating and speed of the ship. The instrumentation package is described in Section III.

-/-

Thirty-five ice resistance experiments were conducted in a thirty-six day period. During most of the thirty-five tests, measurements of the bending strength of lake ice were obtained. The ice thickness and snow cover depth were also obtained for each test. The density of the ice was measured from time to time during the tests and showed insignificant variation.

The propulsion system data and ship velocity information were extracted from oscillograph records and hand prepared records and tabulations. The ice thickness and snow cover depth, recorded at intervals along the track of the ship, were combined with the ship propulsion and velocity data and punched on digital computer cards. The data were operated on by a reduction program which produced a printed record of each run. The record was a tabulation of propulsion, velocity and ice data for specified distances along the test run in the order of increasing distance. Intervals in these tabulations for which velocity and ice thickness were steady were selected. The average value of all of the measurements in these intervals was obtained. A relationship between the average thrust and the relevant variables was obtained by use of regression analysis. Only first and second order combinations of the five variables were considered. The result of this analysis was:

$$\Sigma T = 4.59 + 3.61 \; h \cdot v + 134.14 \; \overline{SC} - 0.644 \; \sigma_f \cdot \overline{SC} - 32.71 \; \overline{SC} \cdot \overline{CF}$$
$$+ \; 0.00313 \; W^2 \cos\theta + .00611 \; W^2 \sin\theta \qquad \qquad [1]$$

where

ΣT = sum of the calculated thrusts of the three propellers (tons)

h = ice thickness (ft)

σ_f = flexural strength of the ice cover (psi)

-2-

v = ship speed (ft/sec)

$\overline{SC}$ = snow cover depth (ft)

$\overline{CF}$ = coupling factor ($SHP_{bow}/\Sigma SHP$)

W = wind velocity (ft/sec)

Θ = angle on the bow of the relative wind

The raw data were converted to dimensionless numbers. For each test point, the following dimensionless numbers were formed:

1. $\alpha = \dfrac{\Sigma T - R_{water} - R_{wind}}{\rho_W (1 - \frac{\rho_i}{\rho_W}) g B h}$ dimensionless load (based on total thrust less wind and water resistance)

2. $V = \dfrac{v \; \mu_{iw}}{\rho_W \; gBh} \times 10^7$ dimensionless velocity

3. $\overline{SIGND} = \dfrac{\sigma_f}{\rho_W \; g \; h}$ dimensionless strength

4. $\dfrac{\overline{SC}}{h}$ dimensionless snow cover depth

5. $\overline{CF} = \dfrac{SHP_{bow}}{SHP_{total}}$ coupling factor

Regression analysis was used to develop a relationship between dimensionless load and the remaining four dimensionless numbers. Only first and second order combinations were permitted. Only those combinations which were significant at the 95 percent confidence level were retained. The resulting relationship is:

$$\mathcal{L}_{T-R_{wi}-R_{wa}} = 77.005 + 85.714\ V + 27.978\ V^2 + 70.369\ V \cdot \overline{SC}/h +$$
$$133.734\ V \cdot \overline{CF} - 114.822\ \overline{CF} + 176.362\ \overline{SC}/h -$$
$$0.0427\ V \cdot \overline{SIGND} \qquad\qquad [2]$$

It may be concluded on the basis of these experiments that ice thickness, ship velocity and snow cover are the most significant variables in the equation for determining ice resistance. The effect of the bow propeller upon ice resistance is small. The effect is beneficial at values of dimensionless velocity less than 0.868×10^{-7} and detrimental at higher values. The physical reason for the apparent ineffectiveness of the bow propeller is the tendency of the ship to become skewed in the broken channel due to the asymmetrical thrust produced by the single bow propeller. The additional resistance associated with this behavior evidently overshadowed any resistance reduction caused by the flushing capability of the bow screw.

The force exerted on the hull was determined by measuring the strain on the inside flange of the hull stiffeners 28, 30, 32, and 34 during each resistance test. The sensitivity of the gauges to external force was determined by applying known loads to the hull with a hydraulic ram, and measuring the strain. This calibration data was used to convert the array of observed strains during icebreaking tests to estimated values of external ice force. The computed impact force values over over intervals of the test for which ice thickness and velocity were steady were related to ice thickness, ship speed, and ice strength. Graphical analysis indicated that products of dimensionless groups would reduce the data.

A best fit line to the data indicates that the dimensionless impact load may be expressed as follows:

$$\frac{F_{ice}}{\rho_w gh^3} = 50\left[\frac{v_{ir}}{\sqrt{gh}} \cdot \frac{\sigma_f}{\rho_w gh}\right]^{1.2} \qquad [3]$$

where

F_{ice} = peak normal force on hull surface

ρ_w = mass density of the water

g = gravitational constant

v_{ir} = reduced impact velocity

Since v_{ir} in equation [3] contains a direction cosine which may be calculated for any hull, this equation should be applicable for any hull shape. Additional experimentation is required in order to establish definitely that hull shape is accounted for properly, however.

The resistance data acquired in the course of these experiments span a range of velocity much wider than any previous resistance tests in ice. In the range where there is data from both WIND Class tests and MACKINAW tests, i.e. ($v\mu/\rho_w gBh \times 10^7 \leq 1.0$) the dimensionless regression equations are almost identical. In both experiments, regression analysis reveals what has been suspected by ship operators for a long time: that snow cover depth is an extremely important factor in the determination of resistance to motion through ice fields. Ice thickness is the major factor. Ship speed is important when $v\mu/\rho_w gBh \times 10^7$ exceeds 1.0. The effect of ice strength is a second-order effect. The effectiveness of the bow propeller in reducing the ice resistance of the USCGC MACKINAW is small.

The total thrust deduction factor for the USCGC MACKINAW was available only for the total power range of 7,000 to 10,000 HP, and for coupling factors of 0, 0.33, and 0.5. In the speed range of 0 to 6 knots and coupling factor range of 0 to 0.50, the total thrust deduction factor varies between 0.895 and 0.96. The omission of the thrust deduction factor, therefore, would not appear to have a significant effect on the validity of the results.

Figures 1, 2, and 3 are presented as a summary of the test results. Figure 1 shows tow rope pull plotted against ship speed with ice thickness plotted as a parameter. This figure is based upon the dimensionless regression equation [2] with snow cover and coupling factor set to zero. Entering the curve with velocity and ice thickness, the required tow rope pull or horsepower may be obtained. Figure 2 is a cross-plot of Figure 1. Figure 3 demonstrates the augmentation of resistance caused by snow cover.
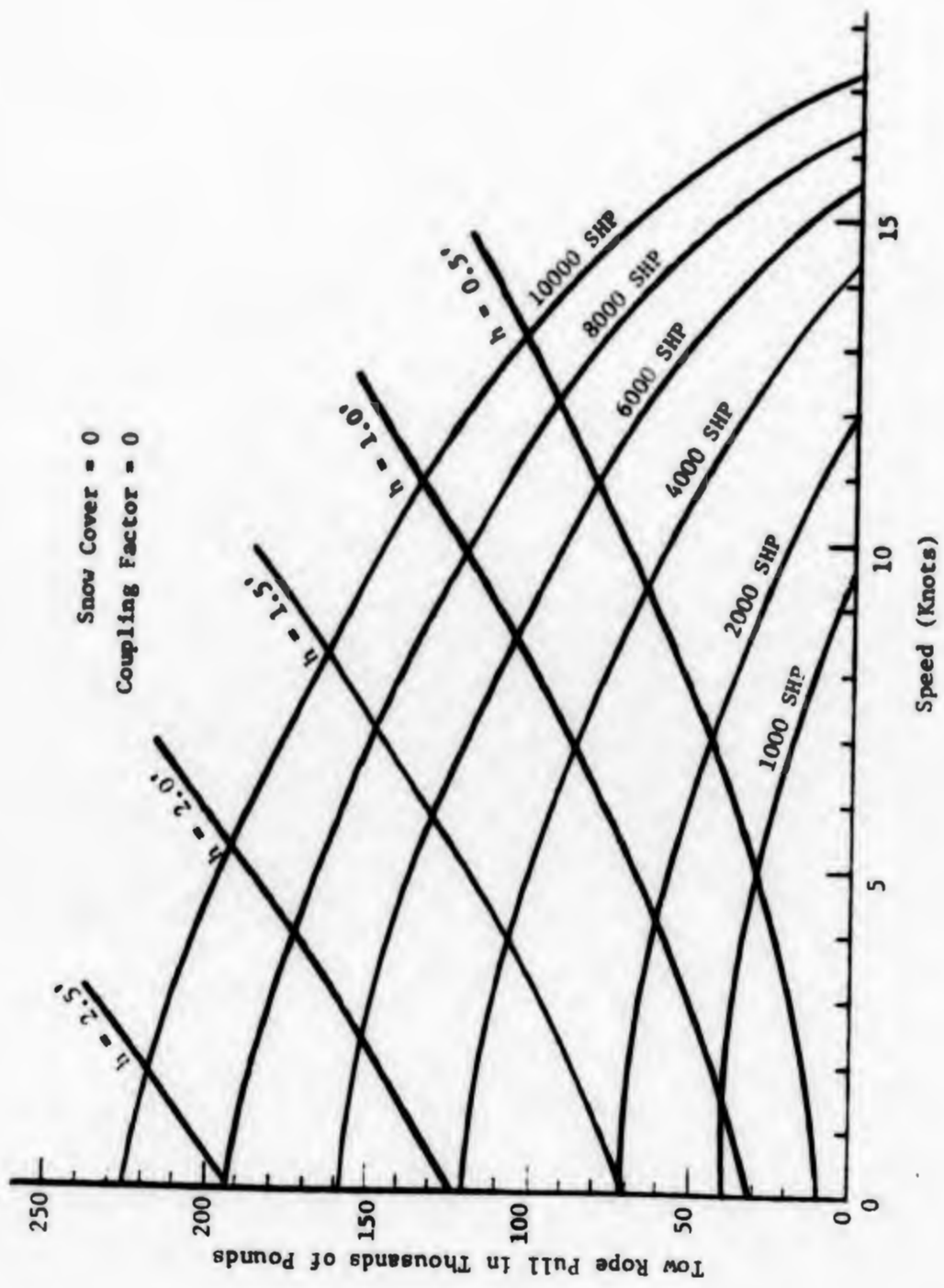
Figure 1
USCGC MACKINAW Performance in Ice
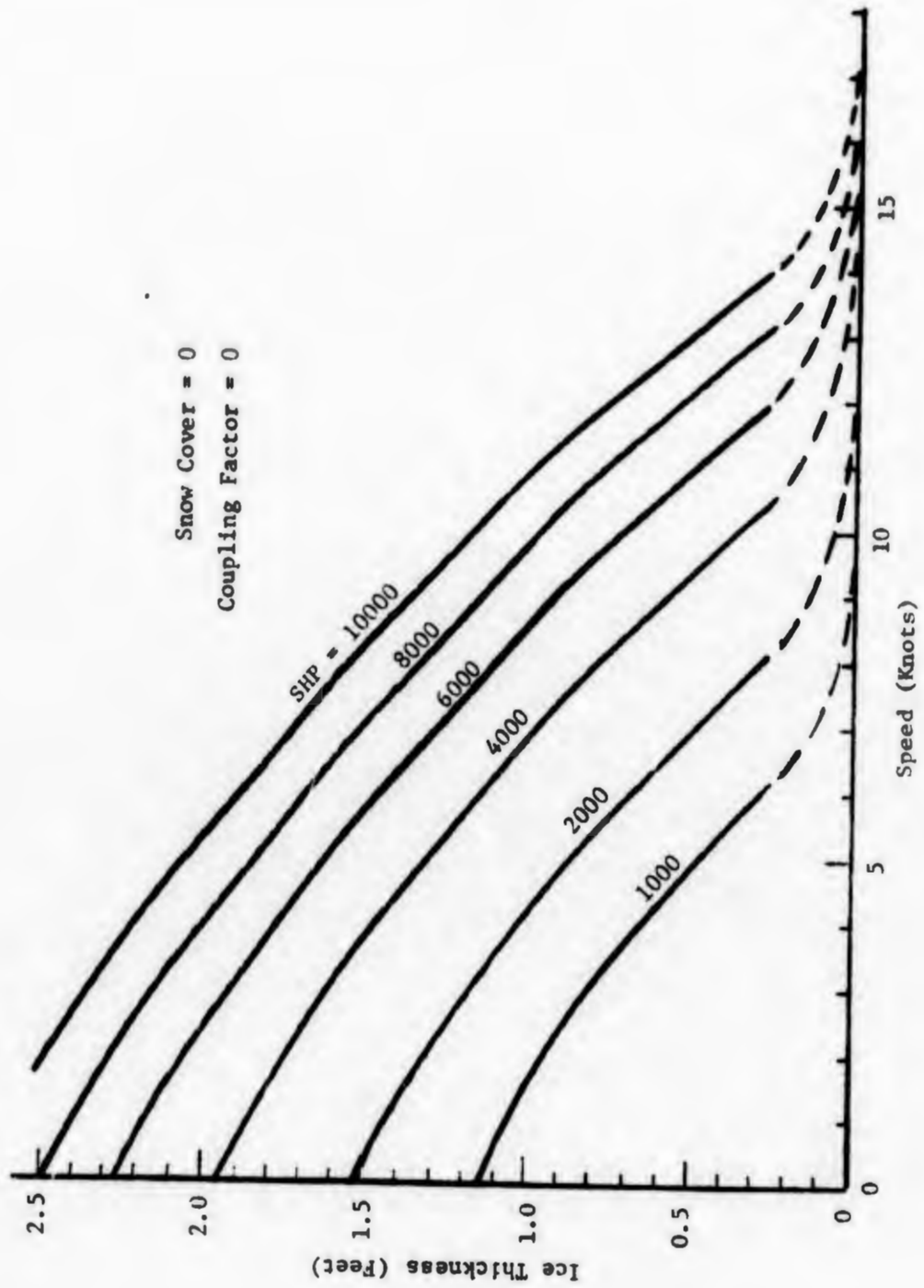
Figure 2

USCGC MACKINAW

Cross-Plot of Performance in Ice
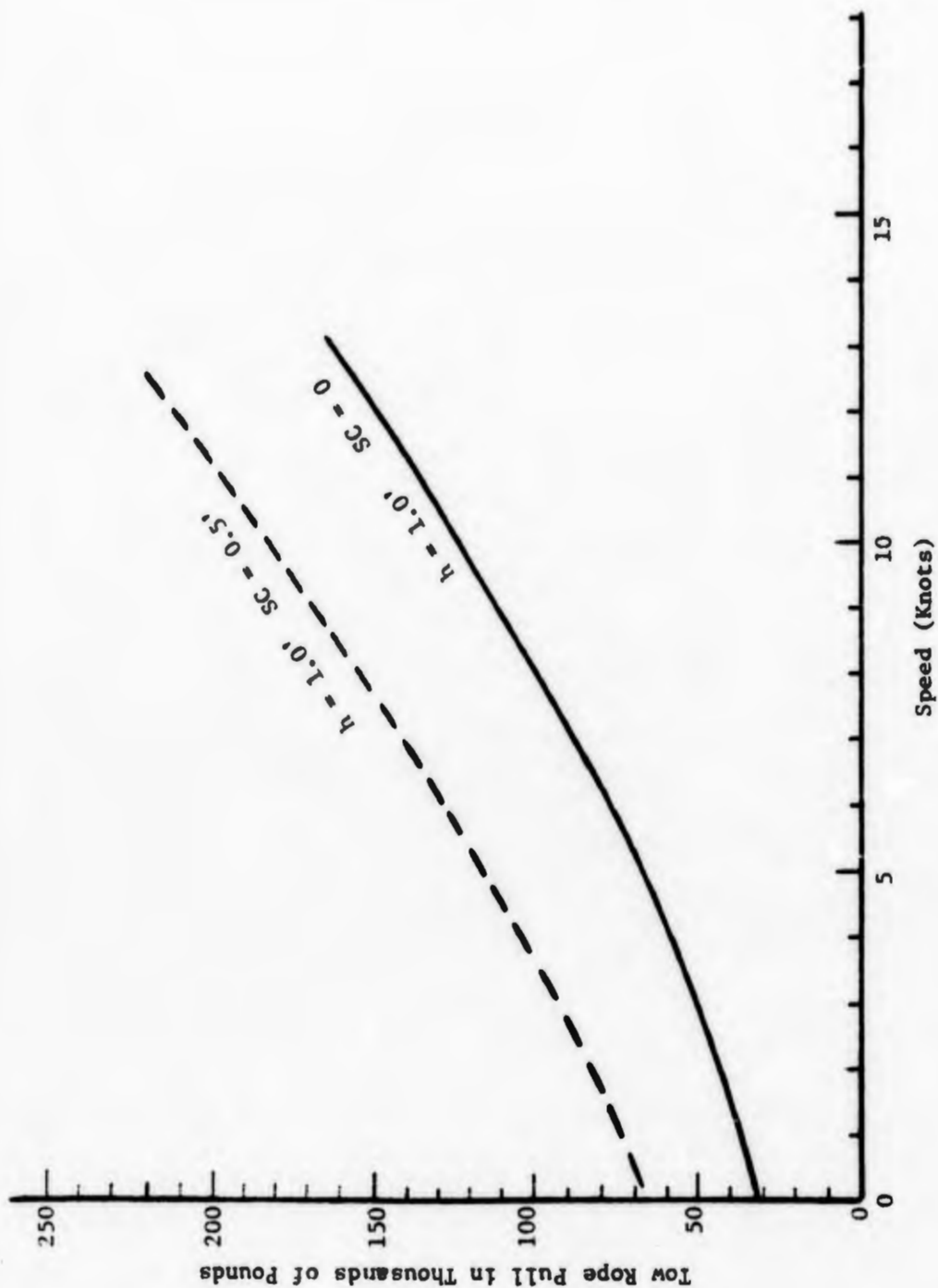
Figure 3

USCGC MACKINAW

Typical Increase in Resistance Due to Presence
of 6" of Snow Cover

I. INTRODUCTION

A. BACKGROUND

The feasibility of maintaining the Great Lakes Basin open for navigation on a year-round basis is under investigation by the Department of Transportation and other government organizations. One of the objectives of the investigation is to balance the costs of maintaining the transportation system viable through the winter against the overall benefits which will accrue to that region and even to the nation as a whole as a result of the navigation season extension.

A major portion of the costs of a winter navigation system will arise from the construction and operation of the icebreakers and ice-strengthened cargo ships which form the mobile portion of the transportation system. The construction costs of a ship of any type depend heavily upon the structural weight. Intuitively, one might assume that the structural weight of an icebreaking or ice-going ship will depend upon the thickness and strength of the ice and upon the relative velocity between the ship and the ice sheet. A relationship between the structural requirements and these factors will be of considerable use in determining the cost of constructing icebreakers and/or strengthening cargo ships. The powering requirements for icebreaking escort vessels (and to some extent, of the cargo vessels) are determined mainly by desired convoy speed and ice conditions. An equation relating the powering requirements to desired advance velocity and ice conditions is a sine qua non for intelligent analysis of the economics of the winter transportation system. Table I-1 lists on the left side general transportation system parameters

TABLE I-1

REQUIREMENTS		ESCORT PARAMETERS
Velocity	}	Power
Ice Conditions		Structural Strength
Navigational Constraints	}	Beam Draft
Cargo Ship Size	}	Beam
Number of Cargo Ships in Motion	}	Number of Escorts

and on the right side, the affected icebreaker parameters. Although the table is a generalization, to an extent it demonstrates that the desired cargo flow rate and the ice conditions have a strong influence on the number, size, and power level of the escort vessels and hence upon the cost of the system. It appears that data which improve the knowledge of how icebreaker power and strength are related to speed and ice conditions would in turn improve the accuracy with which an economic model of the Great Lakes winter navigation system could be devised. Furthermore, such data will improve the knowledge of the controlling phenomena and when properly analyzed, may point out areas where substantial improvements in icebreaker design and operating techniques can be realized. Improvements in these areas may be reflected as reduced capital and operating costs for a future Great Lakes winter navigation system.

B. OBJECTIVES

The U.S. Coast Guard Cutter MACKINAW is the most powerful icebreaker assigned to the Great Lakes Basin. It was selected as a subject for a series of experiments to determine:

   a. An expression relating the ice resistance of the MACKINAW to the following variables:

   1. ice thickness
   2. ship speed
   3. snow cover depth
   4. ice strength
   5. ratio of bow propeller power to total shaft horsepower

-8-

b. An expression relating the local force exerted upon the hull of the MACKINAW by the ice field to the following variables:

     1. ice thickness

     2. ship speed relative to the ice field

     3. ice bending strength

These experiments represent initial steps in the development of predictive data for the speed and power of icebreakers and for the strength requirements of icebreakers. Further, the output of the resistance tests was to provide an evaluation of bow propeller performance. When compared with tests of the USCGC STATEN ISLAND, the MACKINAW tests were to provide an estimate of the influence of ice strength upon ice resistance. In summary, the objectives of the test series were to:

a. Improve icebreaker resistance prediction equations

b. Evaluate bow propeller effectiveness in reducing resistance

c. Evaluate the effect of ice strength on resistance

d. Develop an ice-hull load prediction equation

In mathematical terms the objectives of the experiment are to determine the functions f_1 and f_2 below

$$R_{ice} = f_1 \left[h, v, \sigma_f, B, \rho_i, \rho_w, \mu_{iw}, g, HP_{bow}/\Sigma HP, \overline{SC} \right] \qquad [I-1]$$

and

$$F_{ice} = f_2 \left[h, v_i, \sigma_f, \sigma_{cr}, f, E, \beta, \alpha, \gamma, \psi, M_s, I_s, \rho_i, \rho_w, g, \overline{x} \right]$$

$\qquad\qquad\qquad\qquad [I-2]$

where

R_{ice} = resistance to the forward motion of the ship

F_{ice} = peak normal force on hull surface

h = ice thickness

v = ship speed

v_i = impact velocity

σ_f = flexural strength of ice

σ_{cr} = unconfined crushing strength of ice

B = ship beam

ρ_i = mass density of the ice

ρ_w = mass density of the water

μ_{iw} = absolute viscosity of the water

g = gravitational constant

E = elastic modulus of ice (bending)

$\overline{SC}$ = snow cover depth

$\dfrac{HP_{bow}}{HP}$ = ratio of bow horsepower to total power (referred to as coupling factor, CF)

ψ = spread angle of the wedge-shaped ice slab with which the hull makes contact

α = angle between a plane tangent to the ship's side at the contact point and the ship's center line

M_s = mass of the ship

I_s = longitudinal moment of inertia of the ship about the axis normal to the water surface

f = friction coefficient between hull and ice

β = angle between a plane tangent to the ship's side at the contact point and a normal to the ice surface

γ = angle between a line tangent to the buttock at the contact point and the waterplane

$\overline{x}$ = distance from the ship's center of gravity to the contact point

The techniques of dimensional analysis result in a dimensionless expression which is equivalent to equation [I-1] but which incorporates significant re-

-10-

duction in variables. Hence, it is ideal from the standpoint of control of the experiment.

$$\frac{R_{ice}}{\rho_w (1-\frac{\rho_i}{\rho_w})gBh^2} = f_3 \left[\frac{\mu_{iw} v}{\rho_w gBh}, \overline{CF}, \frac{\sigma_f}{\rho_w gh}, \frac{\overline{SC}}{h} \right] \qquad [I-3]$$

Since the ice load experiment was restricted to steady motion of the ship rather than ramming, accelerations are small and M_s, I_s, and $\overline{x}$ were dropped from equation I-2 which now becomes:

$$F_{ice} = f_3 \left[h, v_1, \sigma_f, \sigma_{cr}, E, \beta, \alpha, \gamma, \psi, \rho_i, \rho_w, g, f \right] \qquad [I-4]$$

Considering in advance that E could not be measured, dimensional analysis produces:

$$\frac{F_{ice}}{\rho_w gh^3} = f_4 \left[\left(\frac{v^2}{gh} \right), \left(\frac{\sigma_f}{\rho_w gh} \right), \left(\frac{\sigma_{cr}}{\sigma_f} \right), \left(\frac{\rho_i}{\rho_w} \right), \alpha_1, \psi, f \right] \qquad [I-5]$$

where

$$\alpha_1 = \sqrt{\frac{\sin^2\alpha \cos^2\gamma + \sin^2\alpha \cos^2\beta \sin^2\gamma}{1 + \sin^2\alpha \cos^2\beta \sin^2\gamma}}$$

(direction cosine for the vector normal to the hull surface at the contact point)

In the course of the full-scale experiment the cusp angle ψ could not be measured. The friction factor and unconfined crushing strength turned out to be relatively constant ($\overline{f} = 0.145$ and $\overline{\sigma}_{cr} = 340$ lb/in^2). Hence the experiment consisted in attempting to document the following relationship:

$$\frac{F_{ice}}{\rho_w gh^3} = f_5 \left[\left(\frac{v_{ir}}{\sqrt{gh}} \right), \left(\frac{\sigma_f}{\rho_w gh} \right) \right] \qquad [I-6]$$

In this equation the term v_{ir} appears. It is the reduced impact velocity, i.e., the speed of the ship in a direction normal to the surface of the hull at contact with the ice edge.

-11-

Equations I-3 and I-6 express in concrete terms the objectives of the tests. The data acquired during the experiments should include measurements of all of the variables mentioned in equations I-3 and I-6 and should be of sufficient quantity to permit determination of f_3 and f_5 within reasonable confidence intervals. In addition, the acquisition of data should be arranged to obtain the heaviest concentration of data in the regions where the most uncertainty exists in the measurement of key variables. Appendix E is devoted to the development of an experimental plan and contains an error analysis.

The specific techniques for measuring these variables will be described in Sections II and III.

II. EXPERIMENTAL PROCEDURES

A. INTRODUCTION

This section of the report lists the pertinent variables which must be measured to accomplish the objectives described in Section I and delineates the procedure for measuring those variables. The procedure for conducting the continuous icebreaking experiment is described in detail.

B. DELINEATION OF TEST VARIABLES

In Section I, two functional relationships were presented which incorporated ice resistance and hull ice loads into dimensionless numbers and related them to other dimensionless terms.

$$\frac{R_{ice}}{\rho_w \left(1 - \frac{\rho_i}{\rho_w}\right) g B h^2} = f_3 \left[\frac{\mu_{iw} V}{\rho_w g B h} , \overline{CF}, \frac{\sigma_f}{\rho_w g h} , \frac{SC}{h} \right] \qquad \begin{array}{c} [I-3] \\ \text{repeated} \end{array}$$

$$\frac{F_{ice}}{\rho_w g h^3} = f_5 \left[\left(\frac{V_{ir}}{\sqrt{gh}}\right) , \left(\frac{\sigma_f}{\rho_w g h}\right) \right] \qquad \begin{array}{c} [I-6] \\ \text{repeated} \end{array}$$

Each variable included in these two equations must be either measured or inferred from other measurements. Each one will be treated briefly.

1. <u>Ice resistance (R_{ice})</u>. Ice resistance may be determined in several ways from various propulsion system measurements. Sufficient propulsion system measurements were made aboard USCGC MACKINAW to insure

that regardless of the malfunction of individual sensors from time to time, sufficient data would always be available to compute ice resistance. Ice resistance is defined as the force which is available from the propulsion system to cause forward motion of the ship through ice covered water. It is the total estimated thrust developed by the propulsion system corrected for open water resistance. The thrust available from the propulsion system was measured directly with strain gages. The thrust was also calculated from torque in the propeller shafts using a technique described in Section IV. Propeller shaft torque was also measured directly with strain gages attached to the shafts. Torque was also determined from measurements of horsepower and propeller rotational velocity as follows:

$$Q = \frac{5250 \ SHP}{N} \qquad [II-1]$$

where

Q = torque in foot-lbs.

N = propeller speed (RPM)

SHP = shaft horsepower

SHP was determined by recording observations of main motor current and voltage and correcting the observations by an estimate of motor and shafting efficiency (95 percent).

$$SHP(elec.) = \frac{E \times I \times .95}{746} \qquad [II-2]$$

It is possible to determine thrust from observations of ship speed and propeller RPM and entering propeller curves. However, this requires an

-14-

accurate estimate of the wake fraction behavior over the full range of
the advance ratio of the tests, usually extracted from model tests.
Wake fraction data is subject to severe scaling error. Consequently,
this technique was not used.

2. <u>Ship speed (v)</u>. The speed of the ship relative to the ice was
obtained by a modified chip log system. A team of three men was assigned
to the task. One man threw numbered blocks onto the ice approximately
50-75 feet off to the side of the ship. A second observer, upon sighting
the block along a gunsight-type device, pushed a button which caused a
mark to be placed on a recorder. A third observer, a known distance from
the first one also caused a mark (distinguishable from the first one)
to be placed on a recorder by depressing a similar button. All three
members of this team were equipped with sound-powered phones.
Consequently, personnel operating the instrumentation below decks could
keep track of what blocks were passing and keep separate records for
later use in interpreting the recorded data. Since the distance be-
tween the shipboard observers was constant for any particular run, and
in most cases measurements of the distance between blocks were made
as they lay on the ice after a test, three independent values of velocity
could be obtained per block.

3. <u>Ice thickness (h)</u>. Ice thickness was measured using a 1-1/2
inch ice drill and a special measuring tape with a toggle which engaged
the underside of the ice sheet. Measurements were obtained at each block
along the test track at the conclusion of a run.

4. Snow cover (SC). The depth of the snow cover was measured and recorded at each block at the same time ice thickness was obtained.

5. Flexural strength of the ice (σ_f). Ice flexural strength was obtained by breaking large in-situ cantilever beams, measuring the force required to cause failure and measuring the dimensions of the beam. Equation [II-3] was used to compute ice flexural strength.

$$\sigma_f = \frac{6 P_0 \ell}{b h^2} \qquad\qquad [II-3]$$

where

σ_f = flexural strength

P_0 = failure load

ℓ = length of the beam

h = ice thickness

b = width of the beam

6. Ice density (ρ_i). Ice density was measured by cutting rectangular prisms of ice,measuring their volume and weighing them on a precision balance.

7. Absolute viscosity of water (μ_{iw}). The viscosity was inferred from data available in reference (2) which provides a table of μ vs. water temperature. Temperature was assumed to be 32.0° F.

8. Mass density of the water (ρ_w). A table of ρ_w is also available in reference (2) for this variable.

9. Coupling factor (CF). Coupling factor is a name given to the quantity SHP_{bow}/TOTAL SHP. It was obtained from the same measurements from which resistance is computed.

10. <u>Elastic Modulus (E)</u>. Elastic modulus was not measured.

11. <u>Ice force</u> (F_{ice}). The force which ice exerts on the hull
was estimated from strain measurements obtained along the flanges of
four vertical stiffeners spaced every other frame between frames 28
and 34. Strain was sensed with semiconductor strain gauges arranged
in a three-level rectangular array totaling 12 gauges. (A description
of the gauged "panel" and accompanying instrumentation may be found in
Section III.) The outputs of these twelve gauges were recorded con-
tinuously during the test runs. Appendix A describes the physical
calibration which was used to convert the twelve time records of
internal hull strain to an estimate of ice force on the exterior of the
hull over selected time intervals during the test runs.

12. <u>Wind velocity and direction</u>. These variables are not shown
in equations [I-3] & [I-4]. However, Baier, Spooner and McClure (1)
in analysis of tests of the USCGC MACKINAW in 1948 found that the
wind velocity caused significant resistance. Consequently, these
variables were monitored and included in a regression analysis to re-
move the effect of wind from the ice resistance estimates.

13. <u>Beam (B)</u>. The beam of the USCGC MACKINAW varies with draft.
Appendix E contains an equation relating beam to the draft forward and
aft. Drafts were obtained daily from observations made on the ice.

-17-

14. **Hull-ice friction factor (f).** Friction factor was measured by towing a 55-lb. steel plate on the surface of the ice sheet and measuring the tangential force. The measurements indicated very little variation in dynamic friction on the ice surface. Consequently, f was not included in the regression analysis. The average value was 0.145.

15. **Ice crushing strength (σ_{cr}).** The crushing strength of ice was determined from unconfined crushing strength tests. Rectangular ice samples were placed in a compression tester. Load was applied with a hand-turned screw and the maximum force measured with a proving ring. Crushing strength was calculated using the measured load and the sample size cross-sectional area.

C. **EXPERIMENTAL PLANNING AND CONTROL**

Prior to the full-scale trials of the USCGC MACKINAW pre-experimental analysis was undertaken. The purpose of this work was to develop a plan for conducting the experiment which would insure that:

1. Sufficient data was acquired to determine the form of functions f_3 and f_5 over the range of interest.

2. Data points would be distributed in such a way that, where there existed uncertainty in measuring the arguments of the functions,

more data would be available to offset the measurement errors by increasing sample density.

The pre-experimental analysis is described in Appendix E. It included the following important functions:

1. Simplification of equation [I-3] to the point where it included only variables over which the test team had some degree of control.

2. Error analysis to determine the expected measurement error of the prime variables over the expected range of the tests.

3. Development of a "priority" schedule based upon the error analysis which provided the test team with direction as to how, ideally, sampling density should vary over the desired range of the experiment.

4. Development of a technique for controlling the primary test variable by exercising control of the horsepower of the test ship.

Equation [I-3] was reduced to its simplest form by removing $\sigma_f / \rho_w\, g\, h$, and $\overline{SC}/h$ and assuming a simple relationship between dimensionless load and $\overline{CF}$ at constant dimensionless V.

$$\mathcal{L} = f_6\ (V,\ \overline{CF}) \tag{II-5}$$

where

$$\mathcal{L} = \frac{R_{ice}}{\rho_w\ (1- \dfrac{\rho_i}{\rho_w})\ g\ B\ h^2} \qquad \text{dimensionless load}$$

$$V = \frac{\mu_{iw}\ v}{\rho_w\ g\ B\ h}\ \times 10^7 \qquad \text{dimensionless velocity}$$

$$\overline{CF} = \frac{SHP_{bow}}{\Sigma \ SHP} \qquad \qquad \text{Coupling factor}$$

An error analysis was performed on all of the variables in these three dimensionless numbers. The result was an error surface which shows the expected variation in measurment error as a function of the three dimensionless numbers $\mathcal{L}$, V, and $\overline{CF}$. Figure II-1 shows a plot of $\mathcal{L}$ vs V with $\overline{CF}$ equal to zero which illustrates how the error bounds vary with V. Based upon the error analysis of Appendix E, Table II-1 was prepared which is essentially the test schedule.

Note that the variable v/h used in the Table is dimensional. It is a simplification of V. The variables μ_{iw}, ρ_w, g and B have been replaced with the mean expected values for the MACKINAW trials. The units of v_K/h are knots/ft., user's units. The analysis described in the foregoing paragraphs provides the test director with a quantitatively expressed goal; i.e. obtain N data points at a coupling factor of X_1 and a v_K/h of X_2.

The question remains -- How does one control $\overline{CF}$ and v_K/h? Appendix E describes in detail the procedure for developing a scheme for controlling these variables. Briefly it consists of obtaining an estimate of the MACKINAW's ice resistance as a function of ice thickness and velocity from Figure II-1 and superimposing the results on a plot of tow rope pull versus velocity with SHP as a parameter. This plot is shown in Figure E-3. Cross plotting this data judiciously results in the plot shown in Figure II-2. This plot was used to determine the total shaft

FIGURE II-1

ESTIMATED DIMENSIONLESS LOAD
VS.
DIMENSIONLESS VELOCITY
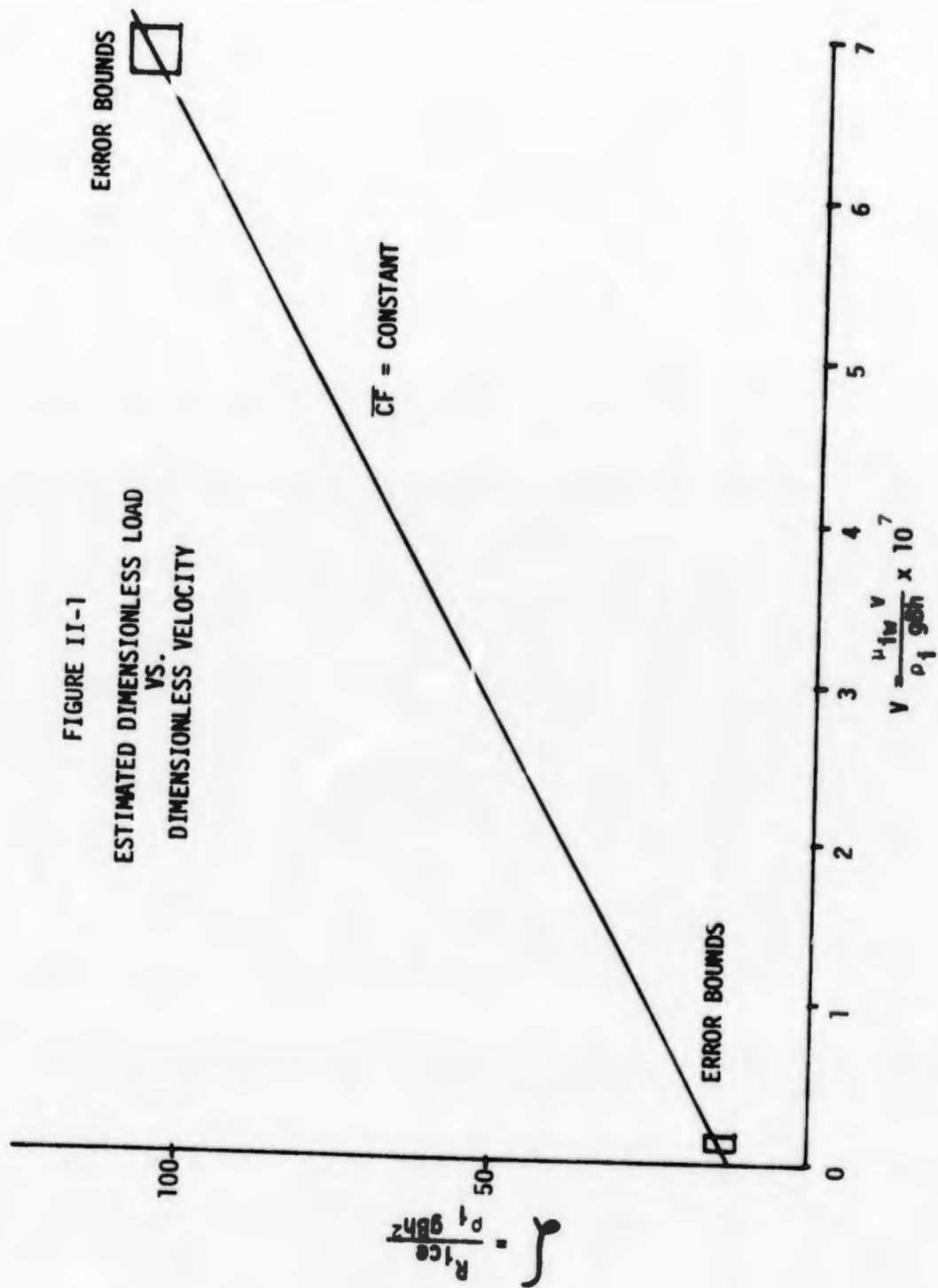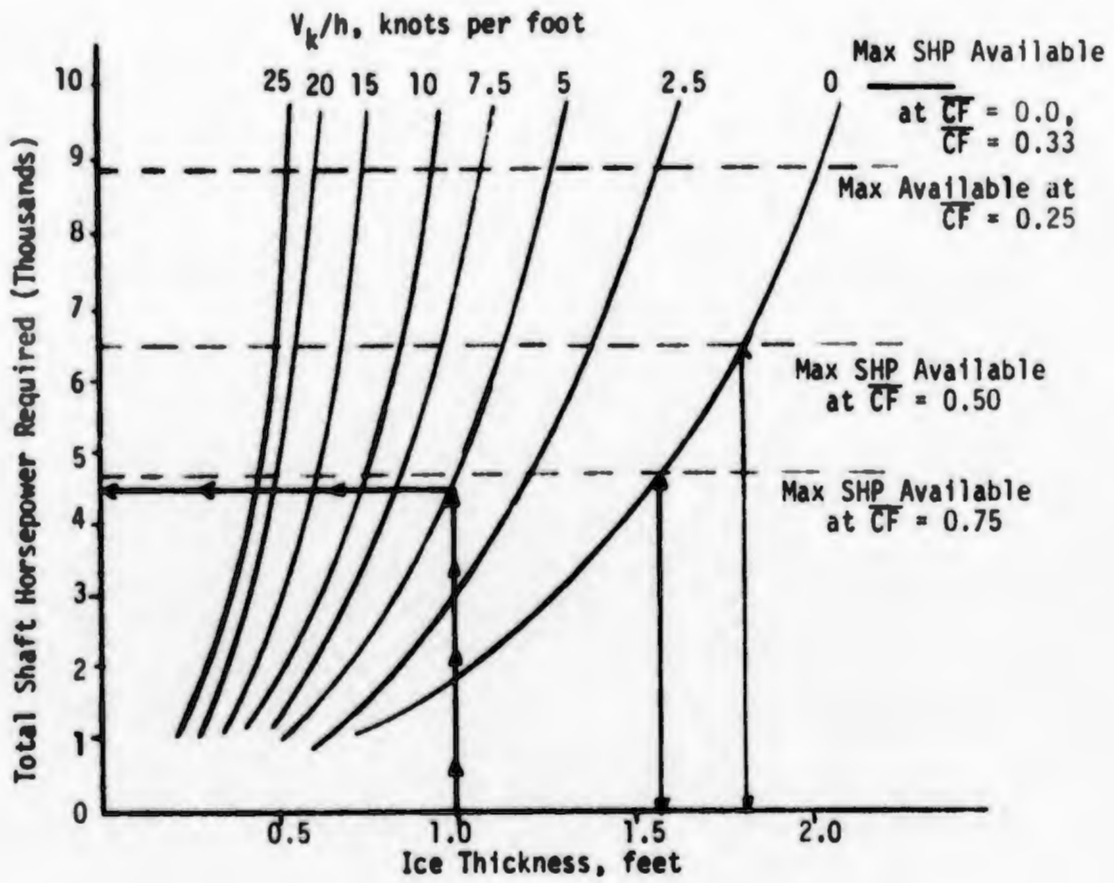
Figure II-2

Total Horsepower Required to Achieve a Desired V_k/h
in a Given Ice Thickness (for $\overline{CF}$'s of 0, 0.25, 0.33, and 0.75)

TABLE II-1

TEST SAMPLING PLAN

v_K/h	$\overline{CF}$					
	0.00	0.25	0.33	0.50	0.75	1.00
25	4*	4	4	3	--	--
20	4	4	4	3	2	--
15	3	3	3	3	2	2
10	2	2	2	2	1	1
5	2	2	2	2	1	1

*Numbers indicate relative density of sampling desired

horsepower required to attain a desired value of v_K/h in an ice field of a given thickness (h). Figure II-2 shows the restrictions imposed by variation in coupling on the feasible range of the experiment. The peculiarity of the electrical arrangement of the diesel generator sets restricts the total shaft horsepower such that, once a decision is made to use a non zero value of coupling factor, full rated total horsepower may be obtained only at a coupling factor of 0.333. Figure E-1 illustrates this situation very well.

In summary the experimental plan was formulated to provide uniform certainty in the determination of the function f_t over the range of its argument. A scheme for controlling the value of V (actually v_K/h for the MACKINAW experiment) by controlling developed horsepower was devised.

D. CONDUCTING THE EXPERIMENT

In general, conduct of the continuous ice resistance experiment consisted of:

1. Location and selection of uniform ice fields of various thickness to provide a wide range in v_K/h; and

2. Selection of the appropriate total horsepower and individual shaft horsepower to obtain the variation of $\overline{CF}$ and v_K/h stipulated in the test plan (Table II-1).

3. Running the icebreaker through the uniform ice field at different power levels and coupling factors while measuring and recording all of the variables delineated in Section B.

Location of large expanses of uniform ice was accomplished primarily by helicopter reconnaissance flights. The test director generally made these flights. In areas which appeared suitable, the helicopter landed and ice thickness measurements were made using a 1 1/2" auger and special measuring tape. Fixed wing reconnaissance flights provided occasional clues as to the location of suitable areas of uniform ice but for the most part contributed little toward the test effort. The helicopter reconnaissance service provided by Traverse City Air Station was timely and effective. It was an indispensable aid in conducting the experiment.

Once the USCGC MACKINAW was in position in a selected ice field, a preliminary ice thickness survey of the flow was made to determine if the area was truly uniform. In several areas, ice fields were discovered in which there were three distinct ice thickness levels. Prior knowledge of this permitted the test directo to take advantage of the variation and schedule changes in horsepower level along the run which produced additional data points. The results of the ice thickness survey were used by the test director to select the proper power level for the pro-peller shafts to obtain the selected value of $\overline{CF}$ and v_K/h. Control of the shaft horsepower levels was not accomplished easily.

Only under certain conditions can power be controlled directly on the MACKINAW or WIND Class ships. The bow propeller power was shown in Appendix E to be related to the rotational speed of the two generators normally connected to the bow propulsion motor. When all six propulsion generators drive the after propeller motors the same situation obtains. To avoid complications, however, a single scheme which would apply over

the full range of generator set-up combinations was settled upon. A
nomogram (see Figure II-3) which would permit rapid calculation of power
from motor voltage and current was constructed and the motor room
operating personnel were provided with copies of it. During the course
of the tests the motor room personnel were called upon to "control power"
by adjusting the generator excitation and speed so that the correct com-
bination of motor current and voltage was obtained on each propulsion
motor. This system did not prove satisfactory. Response of the personnel
to status changes requested by the test director was too slow. Overshoot and
undershoot occurred frequently. An alternative system was derived
which provided adequate control. This system consisted of maintaining
a plot of SHP vs. RPM for the bow and stern propellers. Ship speed was
plotted as a parameter. After data from several tests were plotted,
SHP could be selected by selecting a propeller speed based upon the
desired speed of advance. Figure II-4 shows the graph used with several
data points plotted on it. While the accuracy with which the proper
SHP could be selected was no better than 5 to 10 percent, the graph
proved a more reliable device for experimental control than the pre-
viously described system. In any future experiments power meters should
be temporarily installed in the electrical system and the power selected
directly. Once the levels of power to be used for the test were selected,
the test teams manned their respective stations. Table II-2 lists the
various test teams, briefly describes their tasks and lists the person-
nel assigned to them.

When all of the teams reported that they were on station and were ready, the following situation existed:

1. Communications between the respective stations had been established in accordance with the plan shown in Figure II-5.

2. The velocity team was on station ready to mark the passage of blocks past the sighting stations by depressing the remote marker switches. The block thrower had an adequate supply of numbered blocks to throw.

3. The motor room team was on station, ready to record main motor current and voltage and velocity block number whenever the forward velocity observer announced the passage of the block over the sound powered communication.

4. The instrument room team was on station. All recorders were warmed up and ready to be started. Calibration signals from the torque and thrust measuring systems on all propeller shafts were recorded.

5. The photographer was stationed on the ice, usually on a snow mobile ready to obtain motion pictures of the progress of the ship through the ice field.

6. The ice characteristics team was on the ice performing measurements of the ice characteristics.

7. The thickness measuring team was on the ice ready to follow the track of the ship. They measured the distance between the numbered blocks and the ice and snow thickness at each block.
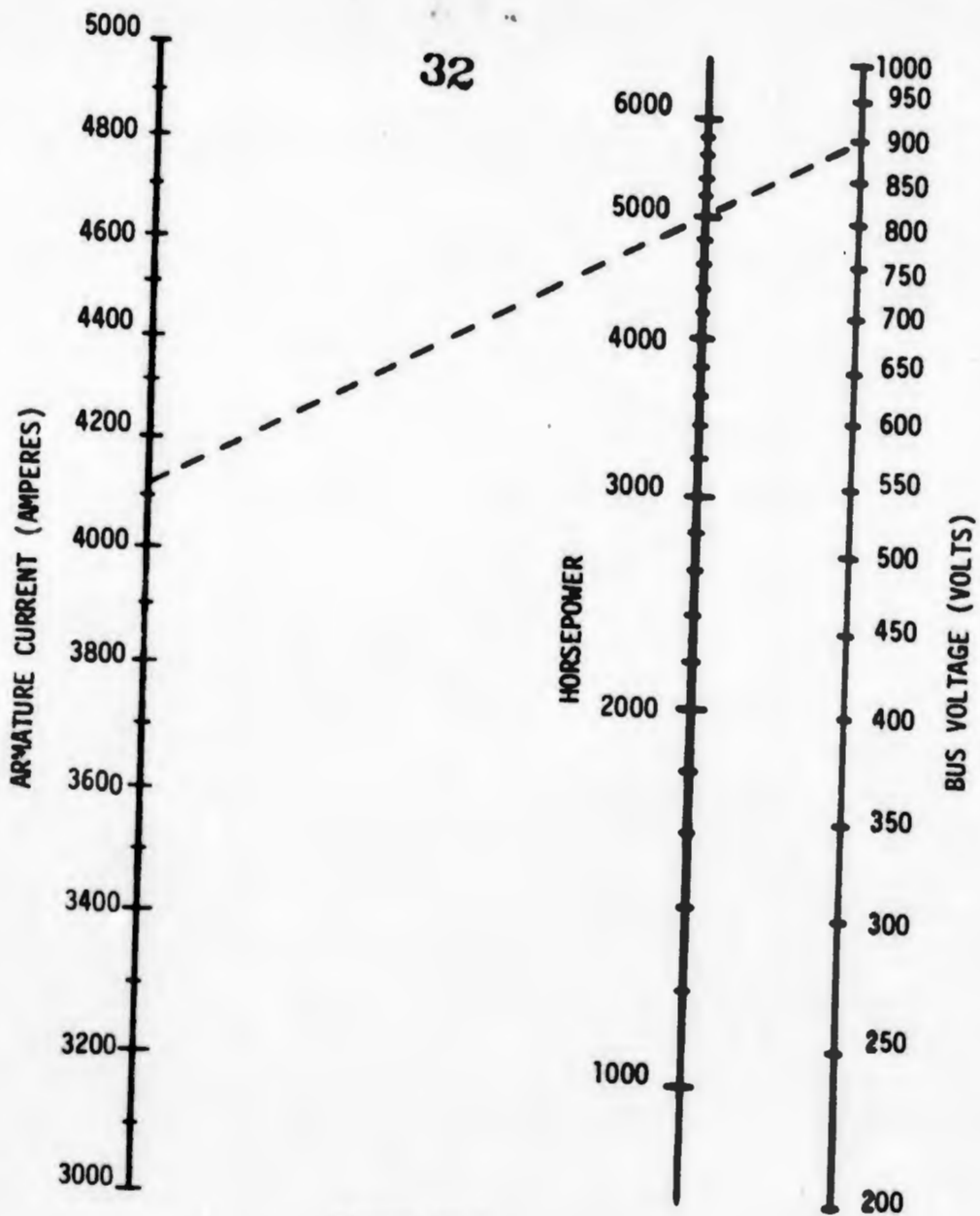
Figure II-3

NOMOGRAM FOR OBTAINING SHAFT HORSEPOWER
FROM MOTOR CURRENT AND VOLTAGE READINGS

FIGURE II-4

Shaft Horsepower vs. Propeller Speed

USCGC MACKINAW

Bow and Stern Screws

Subscripts - Velocity (ft/sec)

(Working plot for SHP Control)

Propeller Speed (RPM)

Shaft Horsepower
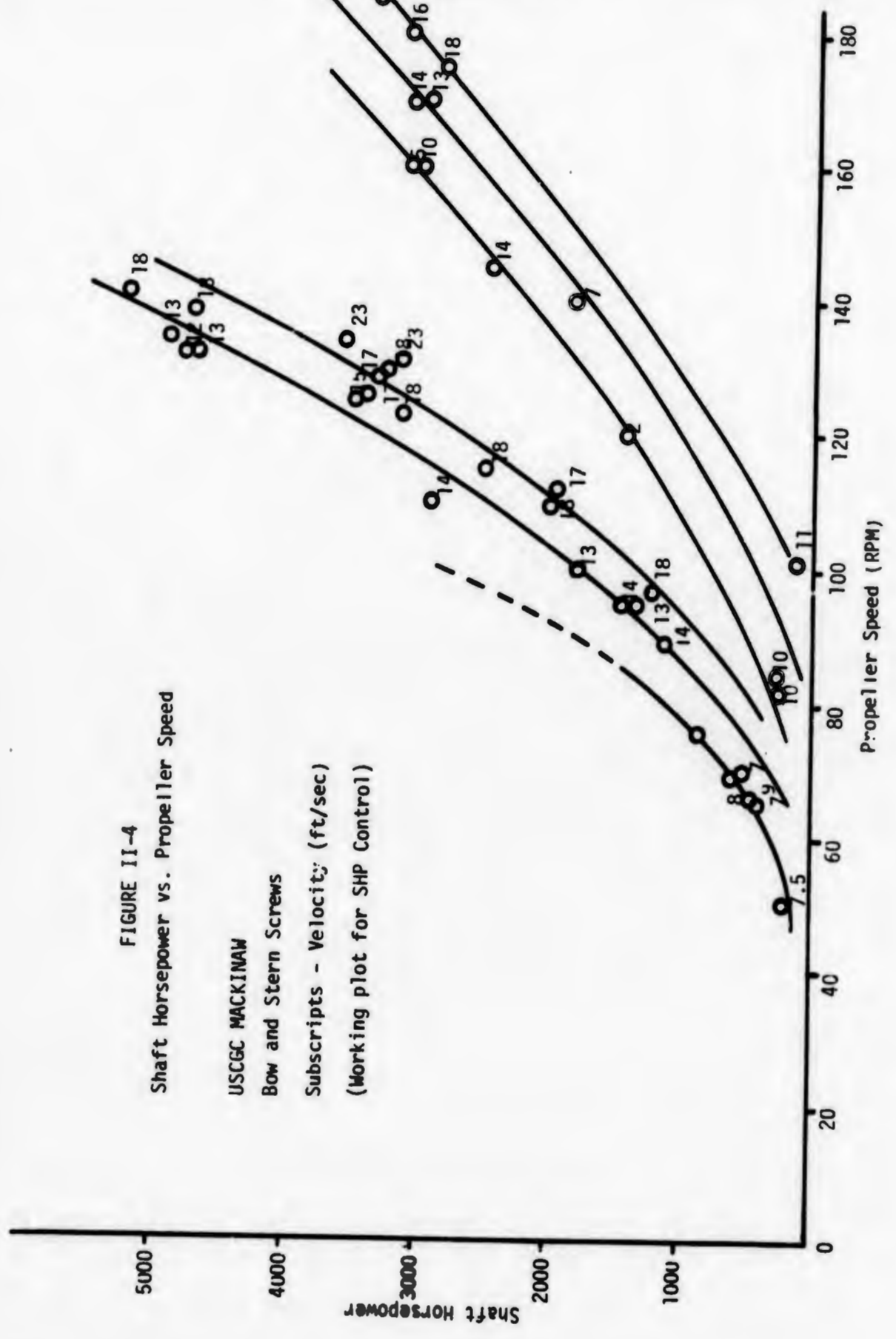
TABLE II-2

TEST TEAM ORGANIZATION

TEAM NAME	TASKS	PERSONNEL
Pilot House	1. Contr ... s with all stations 2. Comm ... 3. Reco ... eteorological data 4. Log and changes in ship status	1. Conning officer (L) 2. Normal bridge watch 3. Phone talker 4. Recorder
Motor Rooms (3)	1. Adjust power as ordered 2. Record values of main motor current and voltage when "mark" from forward velocity switch operator is heard on sound powered phones	1. P.O. in charge of watch (L) 2. Normal watch crew 3. Recorder/sound powered phone talker
Velocity Measuring	1. Throw numbered blocks onto the ice 2. Note passage of block by assigned station by pressing switch on cable at assigned station 3. Forward switch operator to say "mark" over s.p. phones when block passes his station	1. Block thrower 2. Forward switch operator (with sound powered phones) 3. After switch operator
Instrumentation	1. Maintain and control all instrument recording systems 2. Monitor velocity readings 3. Monitor and control T.V.	1. Engineer (TELEDYNE) 2. Technician (TELEDYNE) (with sound powered phones)
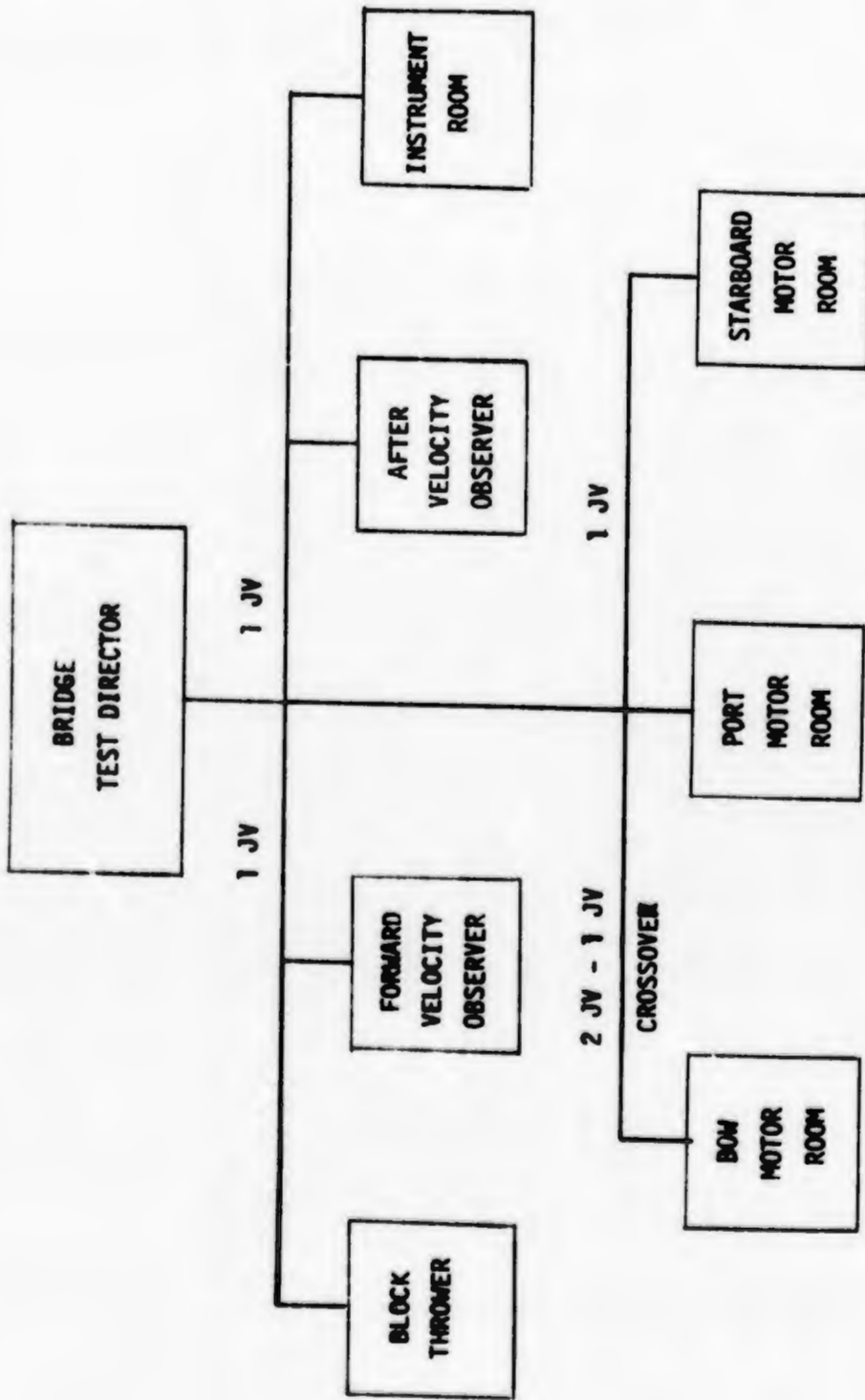
FIGURE II-5

SOUND POWERED COMMUNICATIONS PLAN

The test director, upon notification by all of the team leaders that they were ready, selected the appropriate power level by manipulating the bridge controls until he was maintaining a steady propeller speed on all shafts as stipulated in Figure II-4. As the ship accelerated the instrument room reported the elapsed time between passage of blocks to the test director. (A counter was remotely triggered by the velocity observers and was read out as elapsed time in seconds in the instrument room.) When the elapsed time remained steady over three to four "blocks", the test director selected the next power level in his plan for that particular run. This procedure was followed until the test was terminated due to lack of uniform ice ahead of the ship or to practical limitations on surveying the run. Few runs exceeded two miles. Upon termination of the run, calibration signals were recorded from all of the propeller thrust and torque gauges. Zero readings and calibration signals were placed on the hull strain gauge recording channels. Figure II-6 and II-7 are sketches showing the ship in the ice field before and after a test run.

The ship remained in position at the conclusion of the run and waited until the ice survey team completed the measurements of ice thickness, snow cover and distance between velocity blocks. While the ship was stopped, draft readings were recorded and friction experiments conducted. When the ice survey was completed, preparations for another test run were made. Whenever possible test runs were made without interfering with the team obtaining ice strength measurements. They were permitted to continue working without being recalled to the ship as long as the ship remained within a few miles of them in the same ice field.

III. INSTRUMENTATION SYSTEM

A. GENERAL

The instrumentation system consisted of transducers, cabling, a signal-conditioning system, monitoring and recording equipment, and a video recording system, as shown in the system diagram of Figure III-1. Layout of the system on the MACKINAW is shown in Figure III-2. Semiconductor strain gages were used both for measurements of propeller shaft thrust and torque and for hull strain measurements. The important components of the system are described in detail below.

B. TRANSDUCERS

1. Propeller Shaft Measurements

a. RPM

Shaft RPM was measured by using magnetic pickups which detected the passage of the teeth on the jacking gear. Sufficient assymmetry of the gear was present to provide a direct indication of a complete rotation of the shaft. The magnetic pickups were Model 3030, which are self-excited. The output voltage was applied to the signal-conditioning attenuators, and recorded directly on the CEC Model 5-134 Oscillograph, and on the Ampex FR 1300 FM tape recorder.

b. Thrust

Shaft thrust was measured using semiconductor strain gages connected in a full bridge as shown in the schematic of Figure III-3. It was necessary to use semiconductor gages having a gage factor of

-26-

FIGURE II-6
SHIP AND TEST TEAM DISPOSITION
PRIOR TO TEST

SUITABLE TEST FLOE

PRELIMINARY ICE THICKNESS
MEASUREMENTS

MOTION PICTURE TEAM
STANDING BY ON SNOWMOBILE

PLANNED TRACK

ICE CHARACTERISTICS PARTY

IN SITU BEAM BREAKING APPARATUS
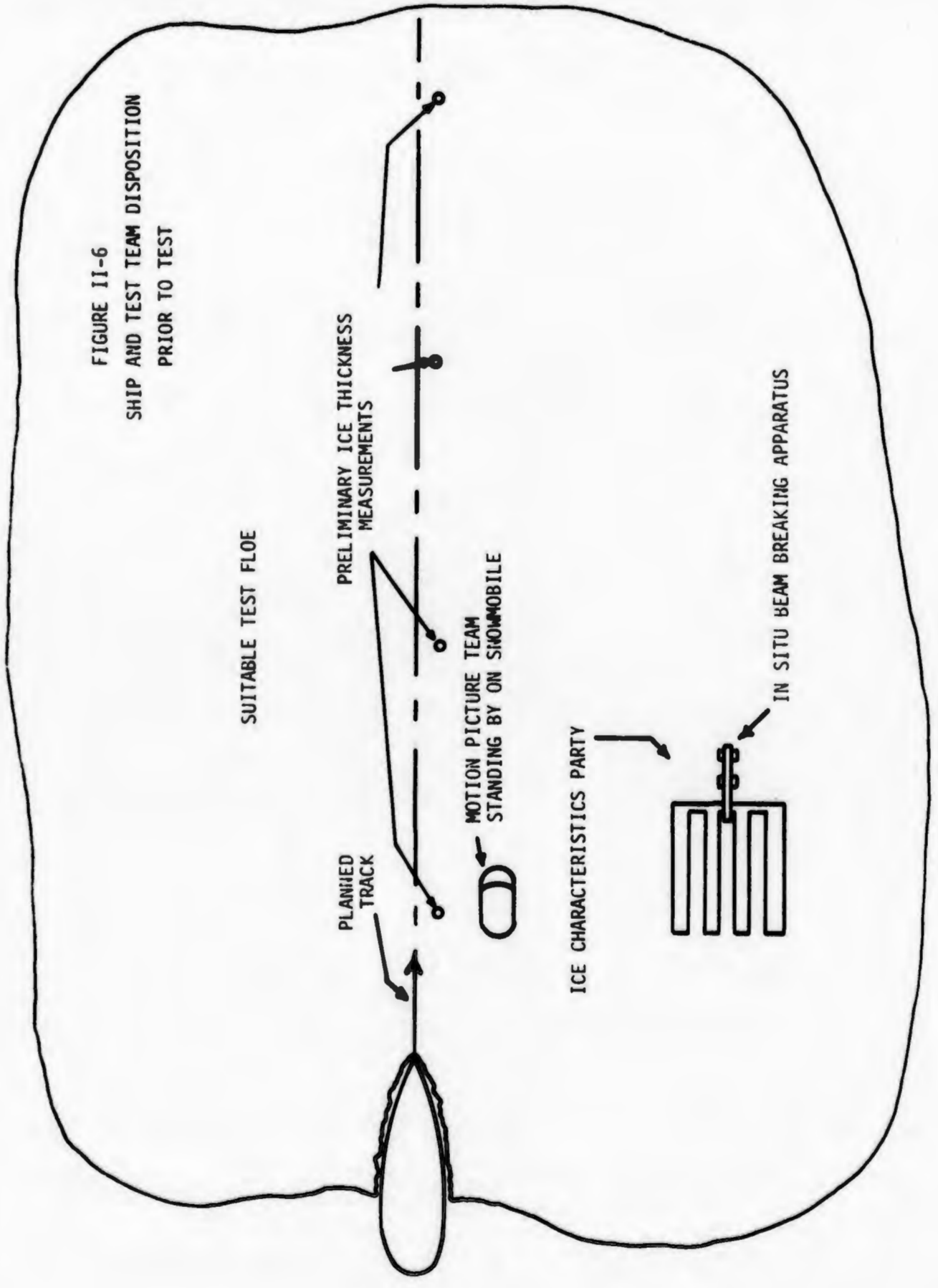
FIGURE II-7
SHIP AND TEST TEAM DISPOSITION
AFTER TEST
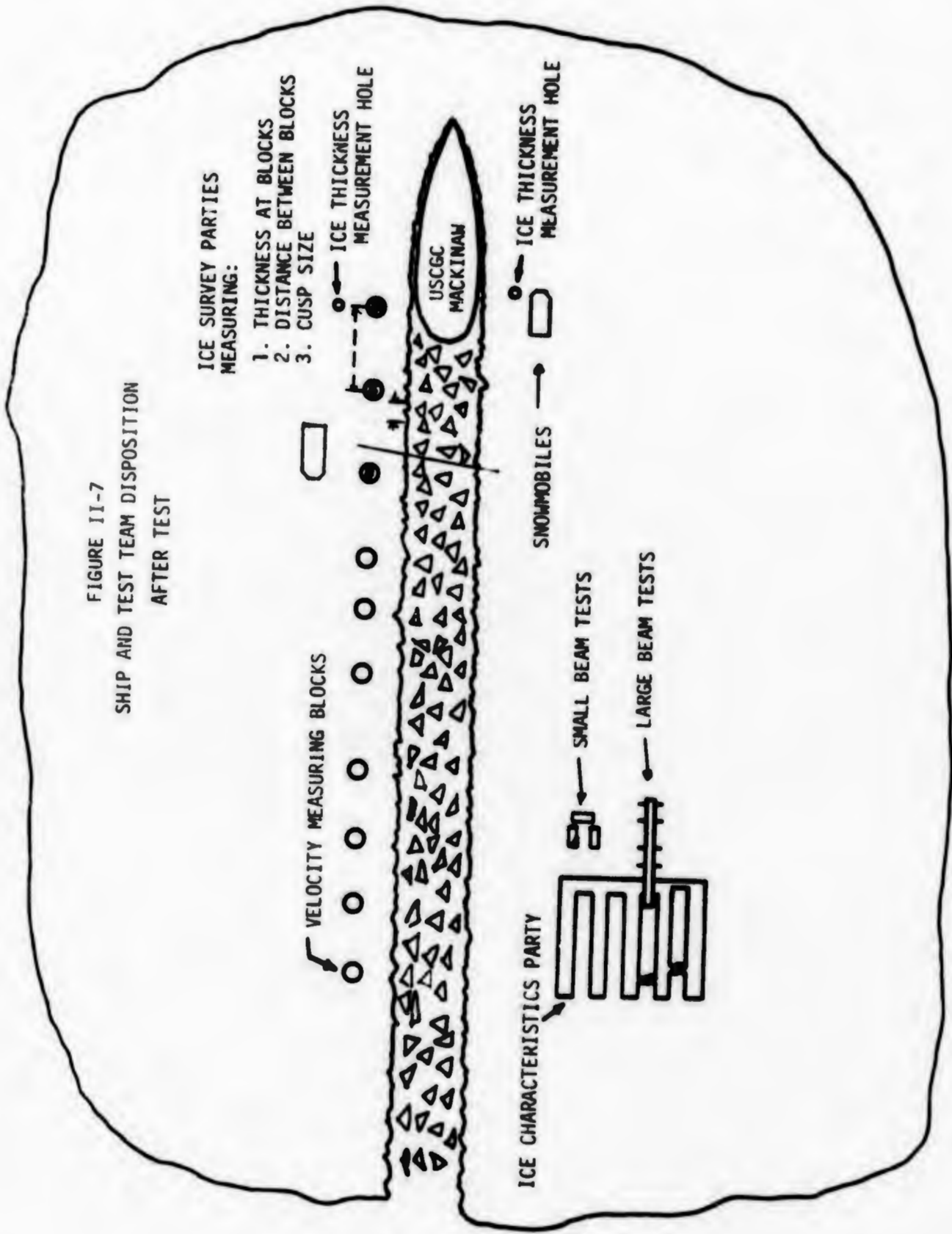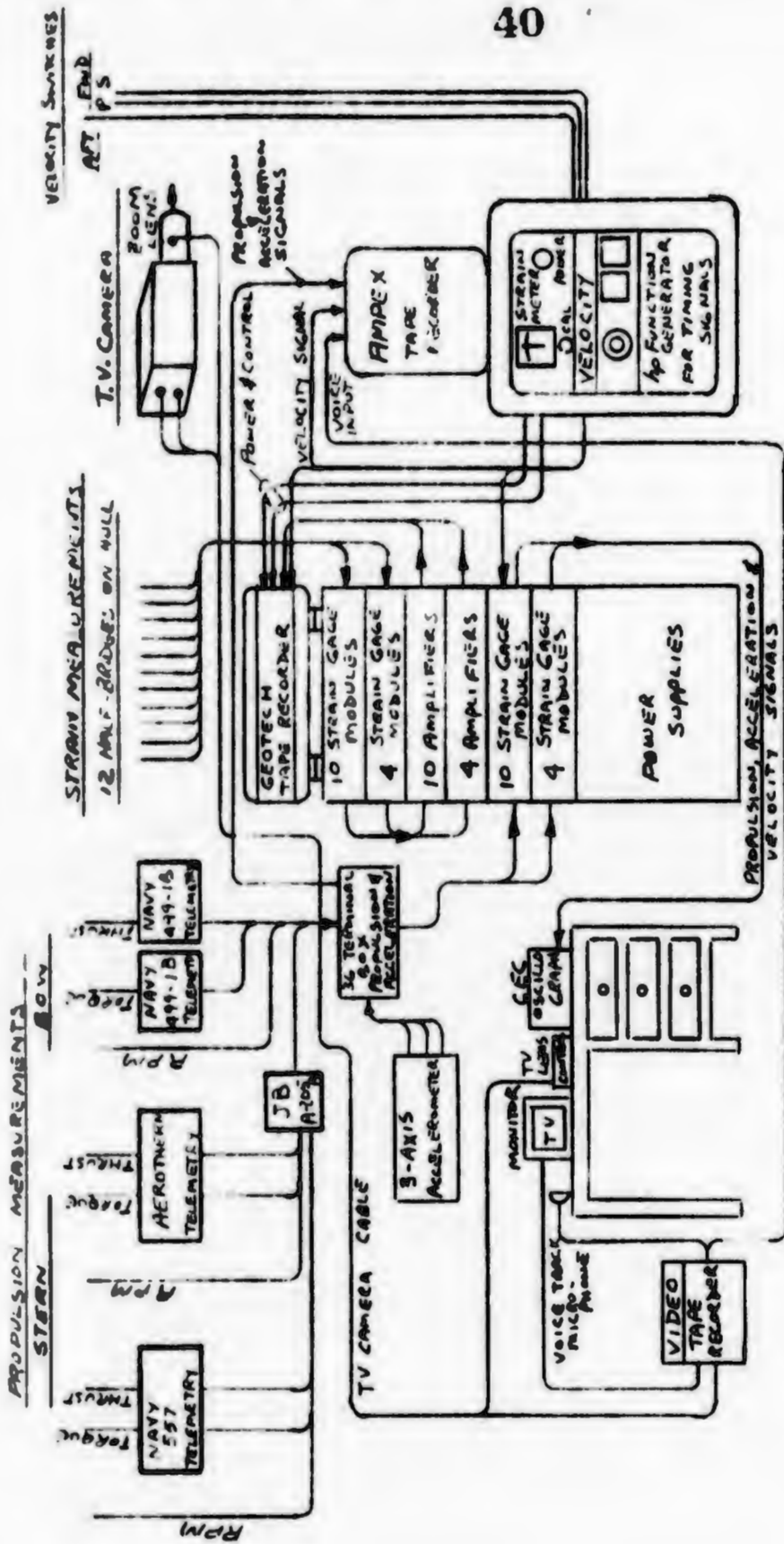
Figure III-1
Instrumentation System Diagram
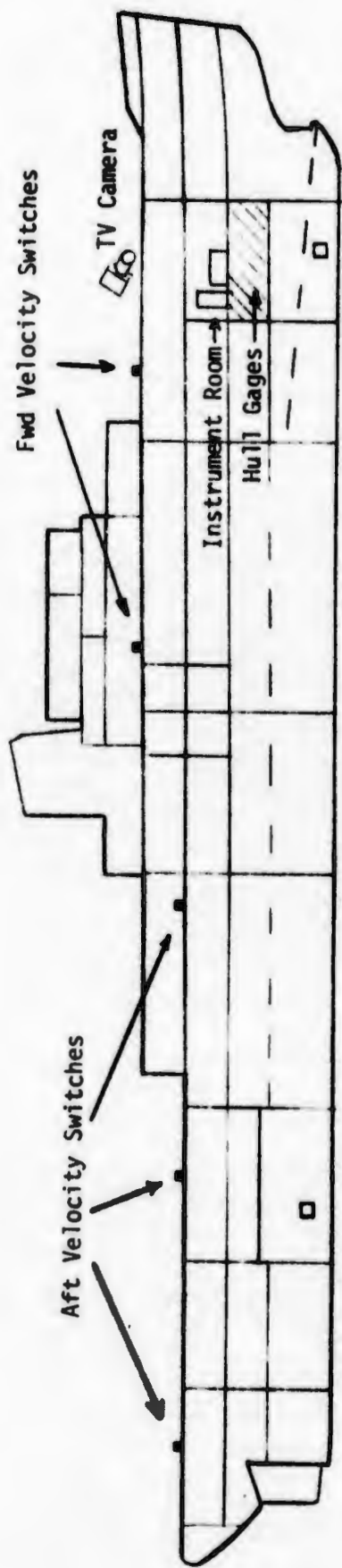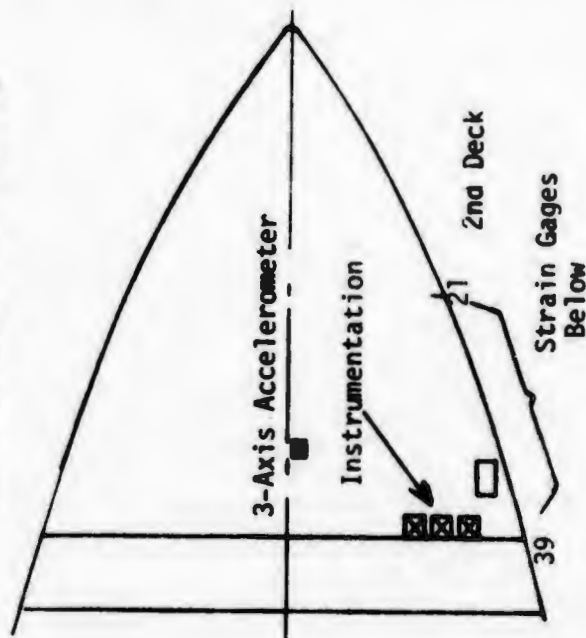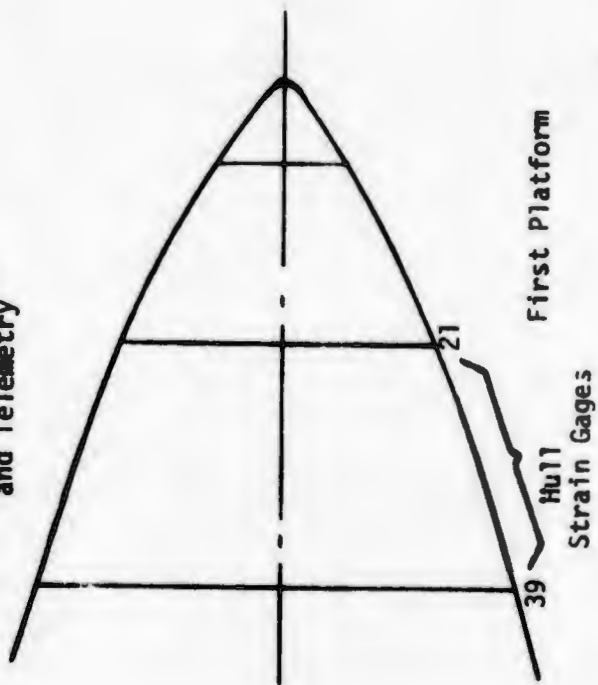
Figure III-2

Layout of Instrumentation
Aboard USCGC MACKINAW

TORQUE GAGE CONFIGURATION

THRUST GAGE CONFIGURATION
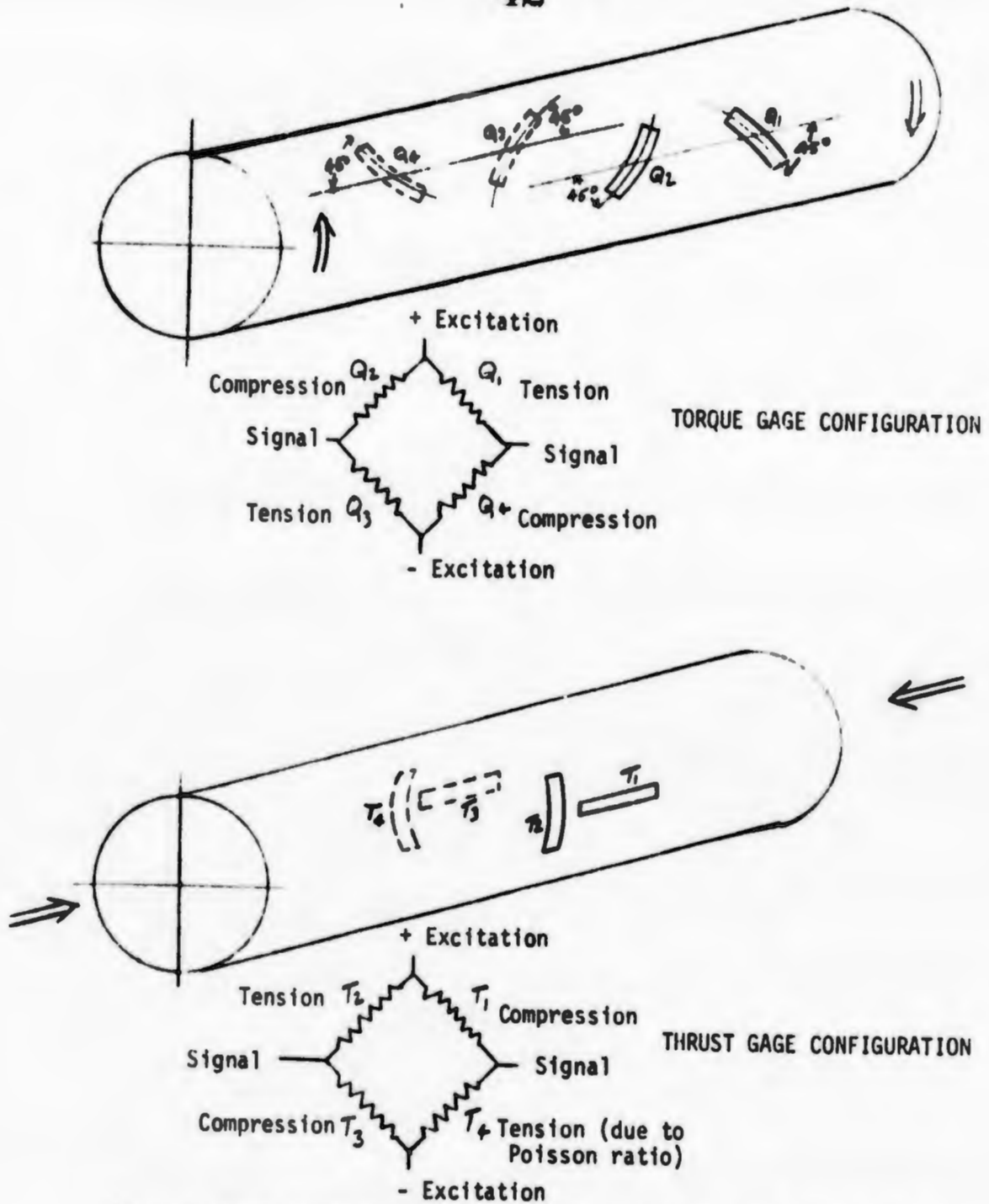
(Adapted from "Technical Instruction Manual for Dual Channel Shaft Telemetry System, NSRDC Type 557" by M. T. Casey and D. J. Plumpe)

Figure III-3
Propeller Shaft Strain Gage Configurations

+155 because the predicted axial thrust of these shafts produces a strain of only 20 microinches/inch at full thrust.

c. Torque

Torque from two of the three shafts was measured using similar semiconductor gages, but the torque from the Port shaft was detected using standard foil gages in a chevron configuration on antipodal locations of the shaft. These gages were used because their lower resistance (350 ohms vs. 1000) made them more compatible with the particular telemetry system used. The torque transducer systems are also shown in Figure III-3.

2. Telemetry Systems

To avoid the complications of slip-ring systems, radio telemetry techniques were used to couple the shaft thrust and torque strain-gage bridge signals to the signal conditioning equipment. On the bow shaft and on the (aft) Starboard shaft, Models 557 and 499 Telemetry systems developed by the Naval Ship Research and Development Center were used. These systems use millivolt-controlled-oscillators which radiate an FM signal on standard IRIG subcarrier frequencies. The receivers are essentially the subcarrier discriminators, with associated power supplies. The transmitting antenna system consists of a loop around the shaft (and insulated from it). The receiving antenna is an aluminum plate curved to fit the contour of the shaft, and spaced about one inch from it.

Since it was required to measure torque and thrust on three shafts, but only four channels of telemetry were available, two additional channels were purchased for this research program. The system

procured is manufactured by Aerotherm Corporation of Mountain View,
California. It operates in the 100 MHz region of the standard FM
broadcast band, and is considerably smaller than the Navy units.

Calibration of the Navy telemetry systems was accomplished
by substituting a regulated voltage to simulate full-scale input
from the bridge. The Aerotherm system, however, used shunt calibra-
tion of the bridges. In both cases, calibration could be accom-
plished only with the shafts at rest. Each transmitting system was
battery powered. The Navy systems were provided with rechargeable
batteries. The Aerotherm system used standard mercury cells, which
were replaced when convenient from an operational standpoint, since
the current drain is quite low. Table III-1 summarizes shaft gaging.

3. Velocity

The arrangement of numbered blocks and observers with switches
has been described above in Section II. The complete system is shown
schematically in Figure III-4. For real-time information for the
Test Director, the elapsed time between observations of each block
was read from the electronic counter. The basic information, however,
was also recorded on both the CEC oscillograph and the Ampex tape
recorder.

4. Hull Strain Gages

The selection of the hull strain gages was based on a predic-
tion from a mathematical model that the strain values would be very
low, on the order of 10 microstrain. The only gages available
capable of the required sensitivity were the semiconductor gages
already selected for the shaft gages.

TABLE III-1

Summary of Shaft Strain Gage Parameters

| Measurement | Gage | Calibration | | | Simulated Strain | Simulated Signal |
		Type	Series Resistor	Shunt Resistor		
Bow Torque	Kulite WUGP-1000-500	Voltage Substitution	29.7K	-	333 $\mu\epsilon$	304,000 ft-lbs
Bow Thrust	"	"	200 ohms	-	19.8 $\mu\epsilon$	87,300 lbs
Port (Stern) Torque	"	"	29.7K	-	200 $\mu\epsilon$	353,000 ft-lbs
Port (Stern) Thrust	"	"	1.1K	-	21 $\mu\epsilon$	134,500 lbs
*Stbd (Stern) Torque	BLH FABD-25-35S6	Shunt Resistance	-	422K	103.5 $\mu\epsilon$	183,000 ft-lbs
*Stbd (Stern) Thrust	Kulite WUGP-1000-500	"	-	120K	20.7 $\mu\epsilon$	132,600 lbs

*The values given apply to all tests after Test No. 4. Starboard Torque calibration resistor was 100K, producing 766,000 simulated foot-pounds for Tests 1 and 2. Starboard Thrust calibration resistor was 100K (159,000 lbs) for Tests 1 and 2, and 1 Megohm (15,900 lbs) for Tests 3 and 4.
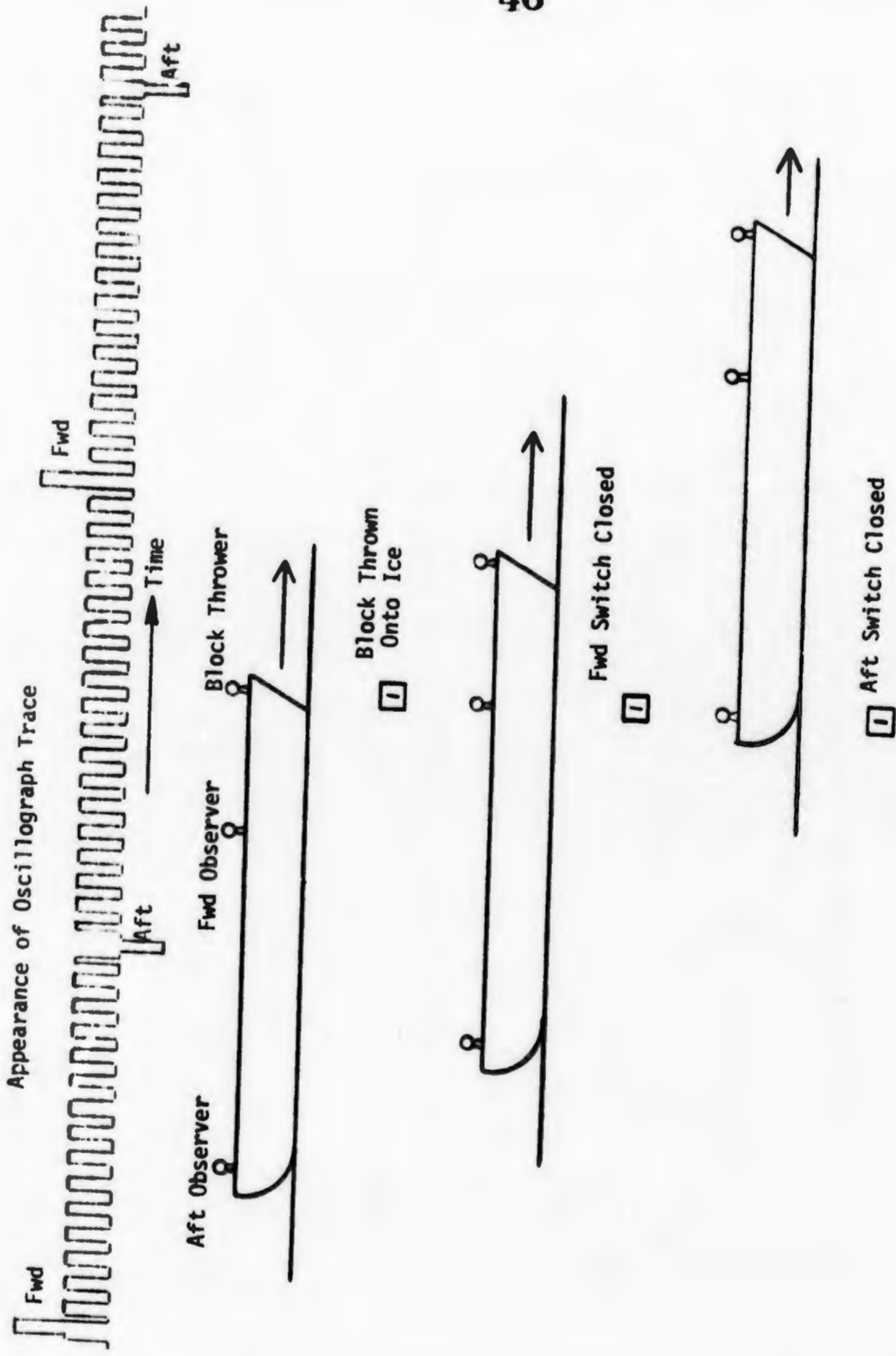
Figure III-4
Velocity Measuring System

The area of the hull to be instrumented was determined by considering the variation of normal force as a function of hull curvature. It was established that impact loads would be a maximum between Stations 1 and 3.

The gages were first applied to a row of seven alternate frames at the 19-foot design waterline in Compartment A-301A. During preliminary tests with the vessel underway, the outputs of these gages appeared to be quite similar; i.e., there appeared to be little variation with fore-and-aft location. Accordingly, the remaining gages were applied above and below the center row on the first four frames instrumented (28, 30, 32, and 34). Figure III-5 shows a profile of Frame 30, on which gages 2, 6, and 10 were installed. The gages were installed as half-bridges, with the vertical element sensing the strain due to ice impact, and the horizontal element sensing the transverse strain due to the Poisson effect, and providing temperature compensation. A schematic of the hull strain-gage installation, with various computations, is shown in Figure III-6.

5. Accelerometers

Three Kistler Model 305-T accelerometers were mounted orthogonally beneath the centerline girder in the instrument room and connected to their Model 515-T amplifiers, located adjacent to the accelerometers. Data were recorded on the Ampex tape recorder, and occasionally on the CEC oscillograph. Values recorded were generally low. Some failures of the transducers occurred, which limited the amount of data collected.

F   48

C. CABLING SYSTEM

With the cooperation of the ship's crew, a cabling system was
installed on the MACKINAW to provide connections from each trans-
ducer to the instrument room. Standard industrial multi-conductor
cable was used, pulled into existing wire racks. A common pair was
provided for portable sound-powered phones, which proved to be in-
valuable in performing calibrations from the shaft alleys.

D. SIGNAL CONDITIONING SYSTEM

A B & F Instruments, Model SY 165, 50-channel signal condition-
ing system was used to handle both high-level and low-level input
signals. High-level signals from the telemetry receivers, the RPM
pickups, the accelerometers, and the basic velocity signal square
wave were connected to channels having circuitry modified to per-
mit the "Balance" potentiometer to act as a voltage divider. Thus,
each high-level signal could be adjusted to provide the proper signal
to the CEC oscillograph. Adjustment of level for recording on the
tape recorder was accomplished by the sensitivity control on each
record oscillator.

The low-level outputs from each hull strain gage were applied to
standard channels containing precision 1000-ohm completion resistors,
plus calibration resistors and associated relays. The full-bridge
output was then connected through a built-in patchboard to twelve
DC amplifiers, and the amplifier outputs were in turn connected to
the record oscillators in the slow-speed Geotech FM tape recorder

-30-

TRANSVERSE FRAME NO. 30
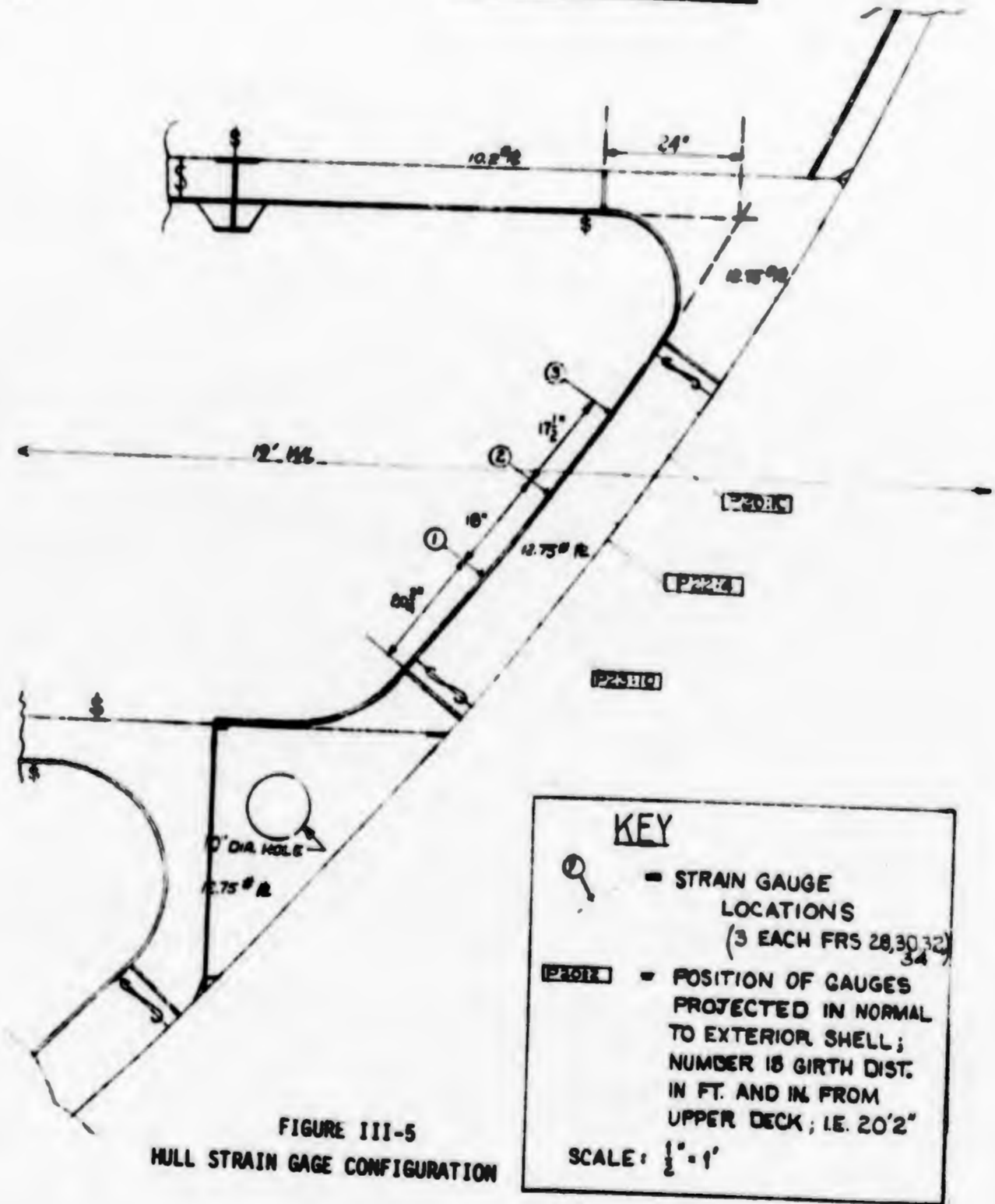
FIGURE III-5
HULL STRAIN GAGE CONFIGURATION

KEY

🔍 = STRAIN GAUGE
LOCATIONS
(3 EACH FRS 28, 30, 32,
34)

P-20-8 = POSITION OF GAUGES
PROJECTED IN NORMAL
TO EXTERIOR SHELL;
NUMBER IS GIRTH DIST.
IN FT. AND IN. FROM
UPPER DECK; I.E. 20'2"

SCALE: ½" = 1'

Typical Hull
Stiffener

If R_1 sees 10 με, R_2 will see -3με
due to Poisson effect. As wired,
effective output from 1 active arm
is 13με. Compute calibration resistor
by

$$R_{sh} = \frac{R_G \times 10^6}{k \; \epsilon_s}$$

where R_{sh} = value of calibration
resistor

K = gage factor, 155

ϵ_s = simulated strain (με)
= 13

R_G = gage resistance, 1000 ohms

Therefore, R_{sh} = 496,000 ohms for 10με
along axis of stiffener

+ excitation

R_1

bridge
completion
resistors

R_{cal}

Signal

R_2

to Amplifier
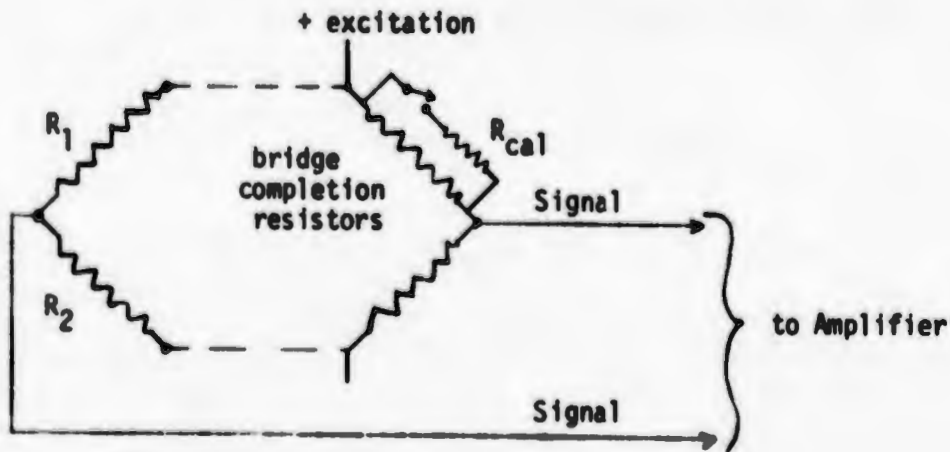
Signal

FIGURE III-6

HULL STRAIN GAGE
ELECTRICAL SCHEMATIC

used exclusively for the hull strain gages and velocity signal. A selector switch on the Geotech allowed any of the input signals to be measured by a meter, and examined on an oscilloscope.

E. MONITORING AND RECORDING EQUIPMENT

The primary recording medium was the CEC Model 5-134 lightbeam oscillograph. All of the shaft telemetry data plus the velocity signal (and usually at least one hull strain-gage signal) were recorded on this equipment. The principal advantage was that the data were available almost instantly, and could be spot-checked to provide guidance to the Test Director.

As a back-up to the oscillograph, and to provide more flexibility in future data reduction, an Ampex Model FR 1300 FM analog tape recorder was connected in parallel with the CEC oscillograph. This proved to an important consideration when the last spare lamp for the CEC failed after only two-thirds of the test runs had been made.

A Teledyne Geotech Model 19429 FM tape recorder was used for recording the hull strain-gage signals, with the velocity signal also recorded for synchronization and data reduction purposes.

F. VIDEO TAPE SYSTEM

A unique feature of the MACKINAW instrumentation system was the closed-circuit TV system which permitted the actual icebreaking process to be watched from the instrumentation room. The system is shown in Figure III-7. The camera was suspended from a telescoping

aluminum pole, held outboard off the starboard bow by a welded steel bracket. The focus, light sensitivity, and zoom position could be controlled remotely.

The TV pictures were found to be very helpful in monitoring the progress of the test runs, and in observing the general characteristics and thickness of the ice. Observed impacts of the point of a cusp of ice could be correlated with the sound recorded by a microphone in the instrument room. Tape recordings of the TV pictures were made using a Sony EVR-310 Videocorder.

Photographs of the main components of the instrumentation system during and after installation are shown in Figures III-8 through III-12.

TV Camera suspended off starboard
side of bow

Blocks of ice at waterline
visible on TV monitor

Close-up of ice-coated TV camera

Figure III-7

Television System

General View of Instrumentation

Close-up of Oscillograph
with Velocity Counter at
right and Video Tape Re-
Corder in Background

Figure III-8
Instrumentation System

55

Figure III-9
Installation of Strain Gages on Propeller Shafts

Starboard Shaft

Bow Shaft
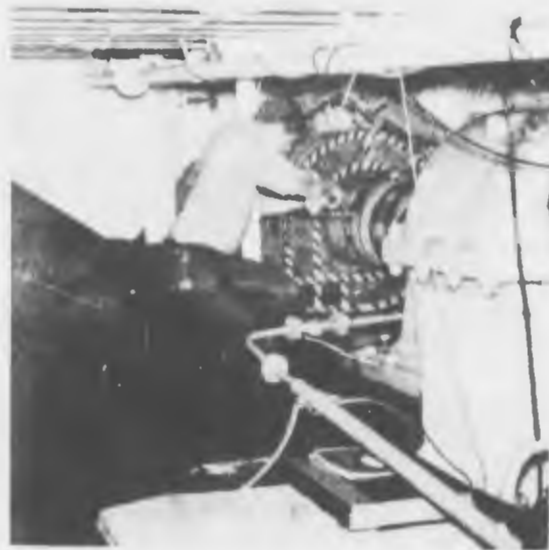
Installing Receiving Antenna,
Starboard Shaft

Figure III-10

Propeller Shaft Telemetry

Wiring Hull Strain Gages

Close-up of Hull Strain Gages
and Connector on Stiffener

General View of Array of 12 Hull Strain Gages

Figure III-11
Hull Strain Gage Installation

Figure III-12

Ice Team Cutting and Removing Samples

IV.   DATA REDUCTION AND ANALYSIS

A. Resistance

This section will describe the data obtained on the ship during the tests, the reduction of this data by computer, and the analysis of the resulting reduced data.

Thirty-five numbered tests were conducted, with a number of tests subdivided because of interruptions. Two tests (#24 and #27) could not be used because data was not recorded due to malfunction of the oscillograph recorder and communications system problems.

Three tests (Nos. 13, 17, and 27) were run in broken channels and, therefore, were not used for the determination of resistance in unbroken ice. The data were reduced as described in the following.

The following data was recorded on the ship: thrust and torque on all three shafts from strain gauges, rotational velocity on all three shafts, motor voltage and current for all three shafts, time that observers pass marker blocks, distance between blocks, ice thickness, snow cover, and hull deflection from strain gauges. In addition to being recorded on magnetic tape, the above data was recorded on a direct writing oscillograph. As block numbers were announced over the communication circuit, they were recorded by hand on the oscillograph tape. During subsequent data reduction, deflections were measured on the tape at each block number. Zero deflection and calibration deflection were used to convert to physical quantities. Data recorded on the oscillograph was in the form of a signal trace deflection which was proportional to voltage. Figure IV-1 shows a sample oscillograph record with just one signal trace for clarity and with

the time marker. A calibration deflection is shown, zero deflection, and typical data point.

This raw data was prepared for computer processing and placed on punched cards. Existing ARCTEC data reduction and analysis computer programs were modified to suit the form in which data was available and the fact that the ship had three propulsion shafts.

Calibration deflection and zero deflection values were recorded both before and after each test. A correction to these two values was applied assuming a linear variation with time. In general, the calibration values were consistant. There was, however, a zero drift caused by a temperature change in the propulsion shafts due to heating of the thrust bearings as the test progressed.

Shaft rotational velocity was determined as revolutions for a ten second period for the bow shaft and as a count of magnetic impulses from an 80 tooth gear affixed to the shaft for port and starboard after shafts. These were converted to rpm.

Measured values of motor voltage and current were converted to SHP (labeled "electrical") assuming 95 percent efficiency. This also determined an "electrical" torque

$$SHP_{electrical} = \frac{Volts * Amps}{746*0.95}$$

$$Q_{electrical} = \frac{33000*SHP_{electrical}}{2\pi*rpm}$$

It was found that the measured values of bow propulsion motor current were not accurate due to a defective ammeter. Therefore, for the bow motor,

-34-

FIGURE IV-1

SAMPLE OSCILLOGRAPH RECORD
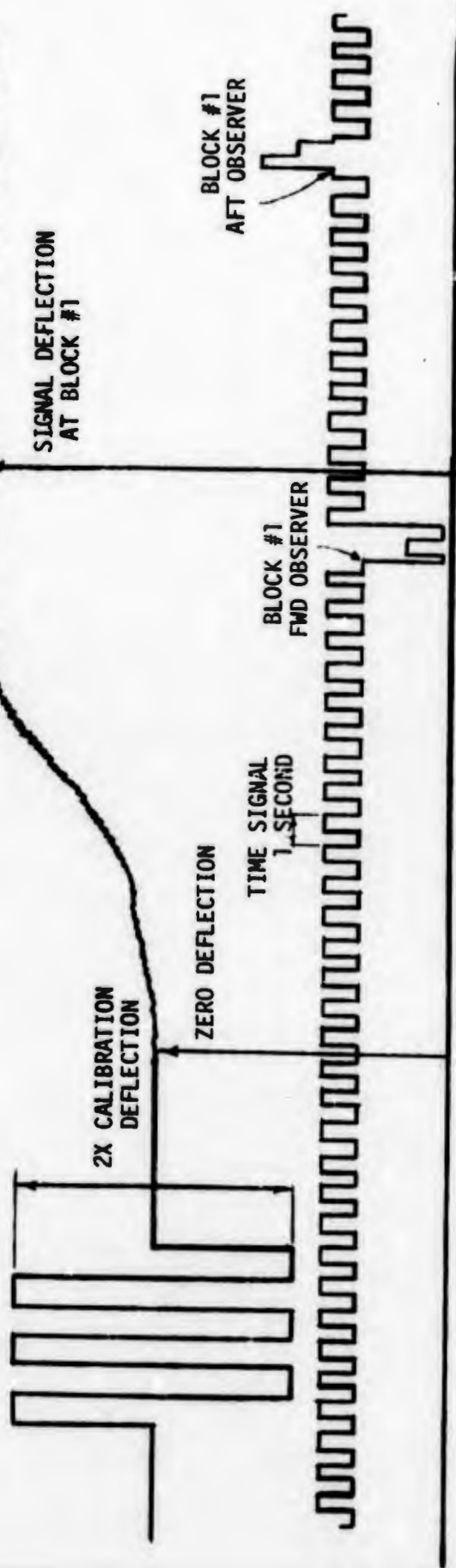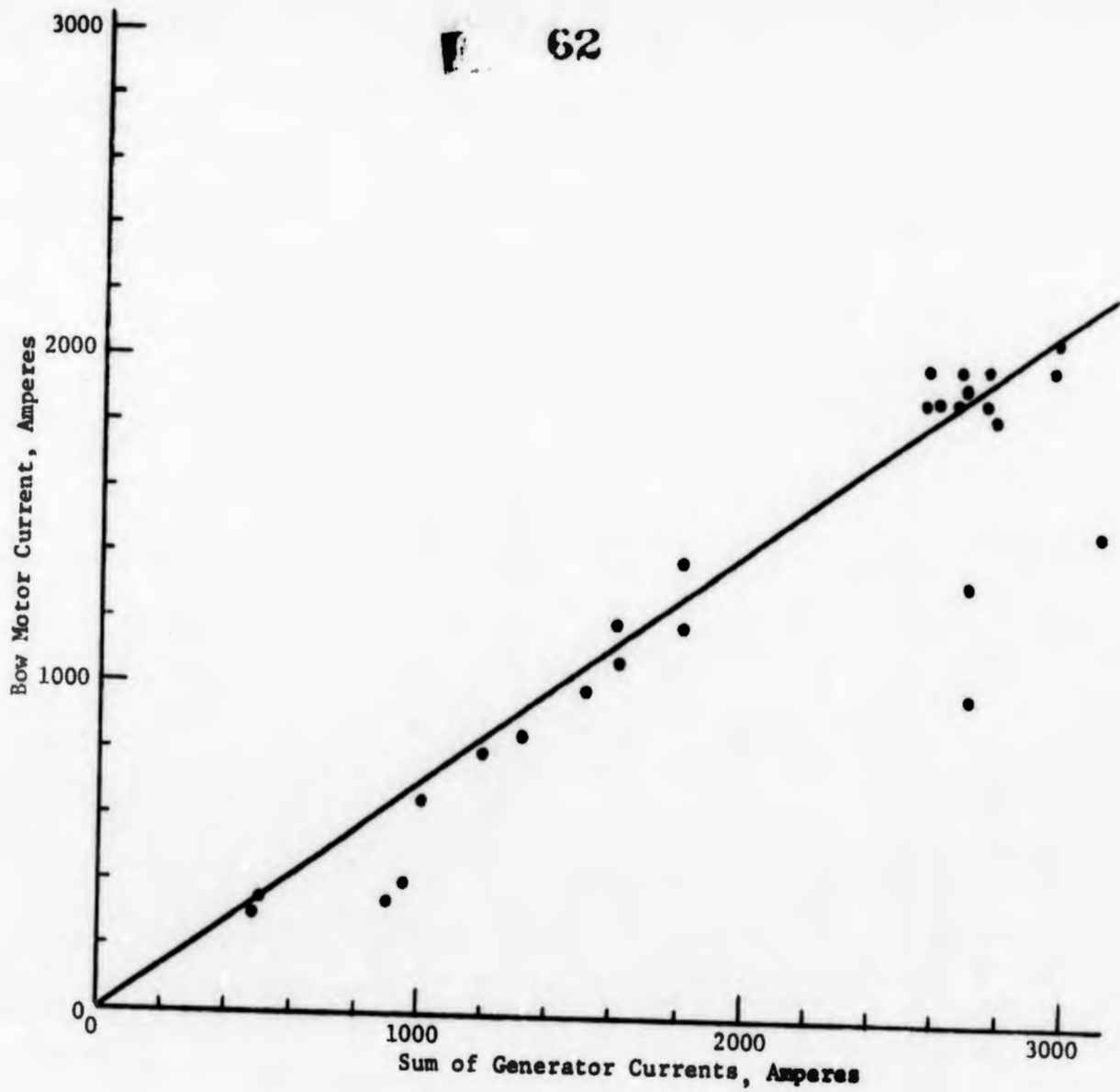
Figure IV-2

Bow Motor Current vs. Generator Current

current was determined to be the sum of the generator currents. For tests #3,#4,#5, and #6A, generator currents were not recorded. It was determined from data of later tests (Figure IV-2) that a factor of 1.4 applied to the bow motor current was a reasonable correction. It was also determined in a similar manner that the starboard motor current was 150 amps low.

Thrust and torque were both measured by means of strain gauges on the shafts. Using this torque and rpm a value of SHP was calculated and this was labeled "mechanical" SHP and the torque labeled "mechanical" torque.

Due to difficulty with the strain gauge thrust measurements a check was made using the propeller characteristic curves. A relationship was found between the propeller coefficients C_T and C_Q as shown in Figures IV-3 and IV-4. This data was taken from the model tests of the MACKINAW propellers. The propeller coefficients are defined as:

$$C_T = \frac{T}{n^2 P^2 D^2}$$

$$C_Q = \frac{Q}{n^2 P^3 D^2}$$

where

T = thrust in pounds

Q = torque in foot pounds

n = revolutions per second

P = pitch in feet

D = diameter in feet

A computer subroutine was setup to accept a torque, compute C_Q, interpolate linearly to find C_T, and return a calculated thrust.

Thrust could, therefore, be determined in three ways: as measured by strain gauge, as determined from the propeller curves using "electrical" torque, and as determined from the propeller curves using "mechanical" torque.

It was determined during the data reduction that "electrical" torque (and, therefore, "electrical" SHP) was most consistant and reliable. It was also determined that thrust determined from the propeller curves using "electrical" torque was best. Therefore, all dimensional and non-dimensional data was based on "electrical" torque and "electrical" thrust.

The basic method for determining ship velocity was by timing the passage of blocks of wood thrown off the bow as they passed two observers further aft. Knowing the distance between the two observers and knowing the distance between blocks (measured when ice was strong enough to support people) enabled us to determine three velocities from the three different time intervals which could be picked off the oscillograph records. These three time intervals were: (1) the time between the forward observer passing a block and the after observer passing the same block: (2) the time between the forward observer passing a block and the next block; and (3) the time between the after observer passing a block and the next block. When all three time intervals were available, the velocity was taken as the average. If any velocity was zero because of a missing time interval, the average excluded that value. While the absolute time at which these velocities were valid varied somewhat, all three velocities are theoretically identical during periods of constant speed.
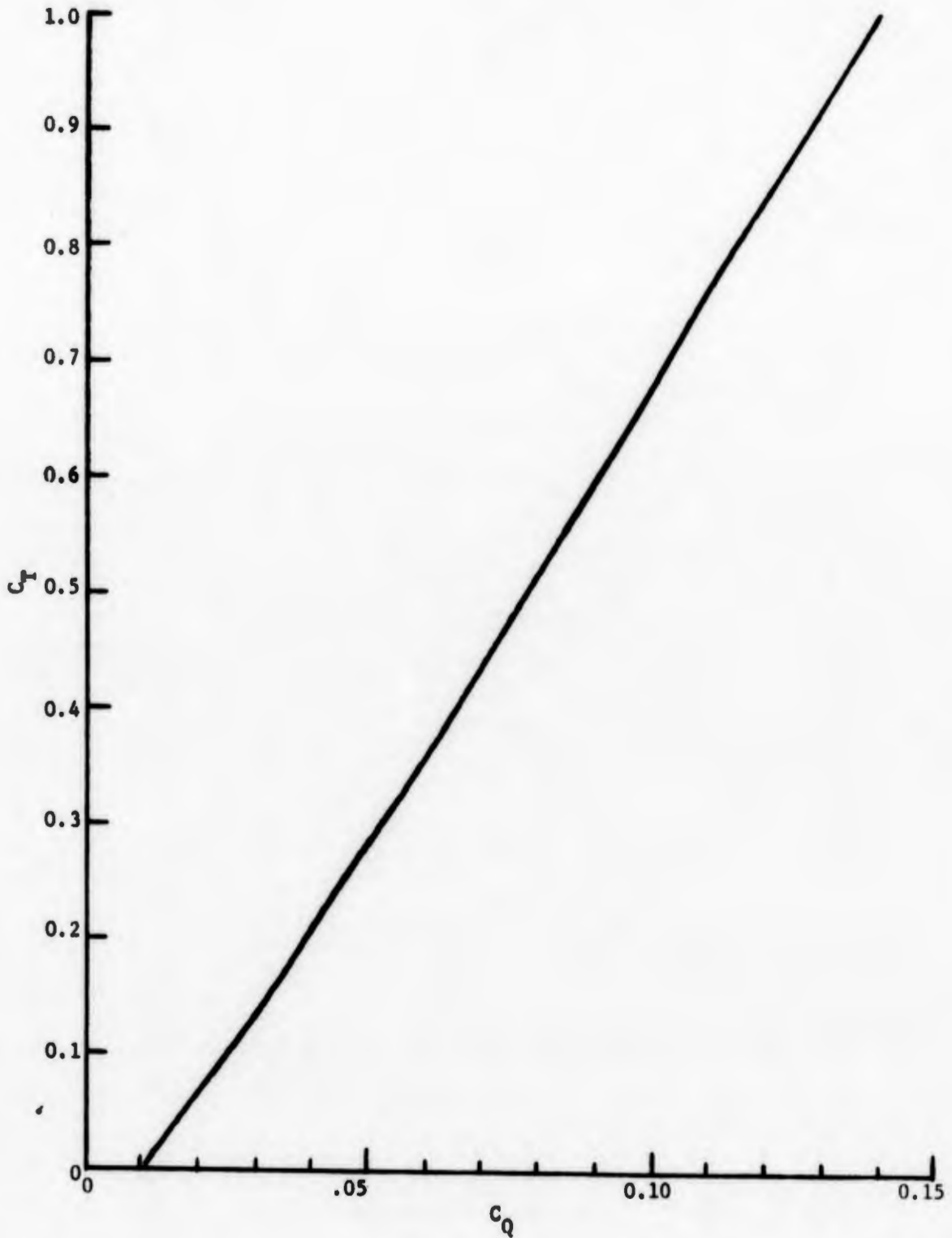
Figure IV-3

C_T vs. C_Q

Bow Propeller
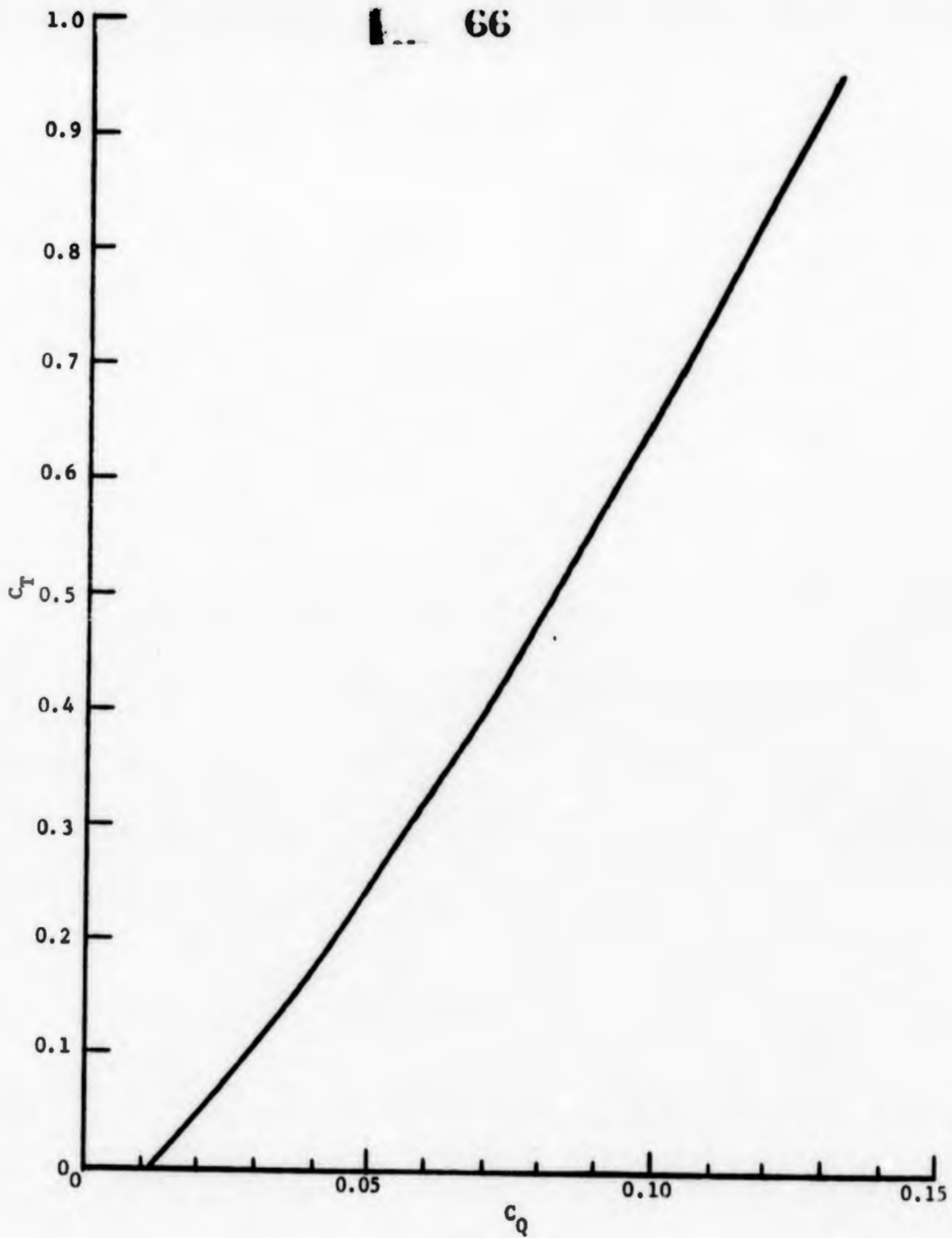
Figure IV-4

C_T vs. C_Q

Stern Propellers

Coupling factor was calculated and defined as being the ratio of bow SHP to total SHP.

Up to this point, the first stage data reduction program has provided us with meaningful raw data presented in the form of a time history of the test. This output was scanned to determine those periods of time in each test when the velocity, power, and ice thickness were reasonably constant. The second stage data reduction program determined the average value of each data item, excluding missing data, and calculated the various dimensionless parameters. Input to the second stage program consisted of velocity, thrusts, powers, coupling factors, ice thickness, and snow cover. The dimensionless parameters that were calculated are identified in Table IV-1.

A total of 136 data points representing the averages of data during periods of constant conditions were available from the results of the second stage program. These points are presented in Table IV-2. A standard statistical technique known as regression analysis was used to determine the significant combination of variables that would explain variations in the dependent variable.

The basic variables used in the regression analysis for thrust were:

$$h, v, \sigma_f, \overline{CF}, \overline{SC}, w, \theta$$

where

    h =   ice thickness in feet

    v =   ship speed in feet per second

    σ_f =   flexural strength of ice in pounds per inch^2 (SIGF)

    $\overline{CF}$ =   coupling factor = bow SHP/total SHP

TABLE IV-1

DIMENSIONLESS COEFFICIENTS

Dimensionless Loading Coefficient

$$XL \text{ or } \mathcal{L} = \frac{\frac{\Sigma T}{\rho_W \, g \, h^3}}{(1 - \frac{\rho_1}{\rho_W}) \, B/h}$$

Dimensionless Velocity Coefficient

$$V = \frac{v \, \mu_W}{\rho_W \, g \, h^2} \cdot \frac{1}{B/h}$$

Dimensionless Power Coefficient

$$S = \frac{SHP}{\rho_W \, (1 - \frac{\rho_1}{\rho_W}) \, g \, h^3 \, v} \cdot \frac{1}{B/h}$$

$$FVOL = \frac{B}{h} \frac{\rho_1 \, g \, h}{\sigma_f} \qquad\qquad SIGND = \frac{\sigma_f}{\rho_W \, g \, h}$$

$$FIN = \frac{B}{h} \frac{\rho_1 \, v^2}{\sigma_f} \qquad\qquad BND = B/h$$

$$RND = \frac{\Sigma T}{\sigma_f \, h^2} \qquad\qquad RHOR = \rho_1/\rho_W$$

$$VOLND = \frac{\Sigma T}{\rho_W \, g \, h^3} \qquad\qquad XMUND = \frac{\mu_W}{\rho_W \, \sqrt{g \, h^3}}$$

$$FR = \frac{v}{\sqrt{g \, h}}$$

TABLE IV-2
EXPERIMENTAL DATA
(Cont.)

T E S T	ICE THRUST LBS	SHIP THICK FT	SHIP VEL FPS	SNOW COVER FT	CE	XI	Y	S	SIGMO	DIR VEL

TABLE IV-2
EXPERIMENTAL DATA
Sheet 2

	SHIP THRUST TONS	ICE THICK FT	SHIP VEL FPS	Snow COVER FT	CE	XL	Y	S	SIGND DIK DEG	VEL

TABLE 1W2

EXPERIMENTAL DATA

T F S	SHIP	THRUST TONS	ICE T-ICK EI	SHIP VEL FPS	SNOW SIGE	COVER EI	CE	N	X	Y	Z	WIND DIR DEG	WIND VEL KNOTS
12		55.	1.5149	7.295	135.	.795	.000	128.5	0.4904	0.4815	205.24	18000	1300
12					135.			135.2			198.63	14000	1300
14		42.5	1.4929	6.403	135.	.1139	.0128	90.5	0.4437	0.3329	201.73	34500	800
14					135.			140.			185.22	34500	800
15			1.5714	11.407	135.	.795	.2714	154.4	0.7545	0.4347	205.00	34500	800
15					135.			175.5	1.8186	0.4261	212.63	34300	800
15		-11.		14.972	137.			-20.	0.9740	0.5926	205.64	34500	800
14				14.93	137.			21.1	0.9827	0.5608	218.00	34500	800
15		70.		14.125	139.	.197	.0444	154.	0.7501	0.5057	200.00	34200	800
15				14.596	137.			140.	0.5717	0.5417	207.	34200	800
15		7.40	0.674	13.766	137.	.0156	.0463	206.4	0.7163	0.5402	207.07	34500	800
15				13.030	135.	.144		174.	0.9227	0.4741	179.04	34500	800
15		56.		11.025	134.	0.1	.0456	169.2	0.7476	0.5076	186.04	34500	800
15				12.796	137.			175.4	0.8156	0.4854	197.04	34500	800
16		7.	1.54	15.359	137.	.7		10.	0.5334	0.4451	170.34	8300	705
16					137.								
			1.07-1	15.645	137.			155.	1.147	0.007	170.77	000	604
			1.095	16.148	139.								
			0.5699	20.250	137.			45.	0.542	0.000	157.04	7000	1000
				7.974	137.						034.	7000	1000
				45.716	137.			375.3	3.554	0.083	164.	9000	1000
								672.	3.672	1.683	74.	9000	1000
		15.71		.744	137.			555.5	2.0463	10.591	52.018	9000	1000
			0.6740	17.040	137.			25.76	6.361	5.046	114.	9000	1000
		.91	0.411	16.460	137.			455.	4.447	6.4166	770.93	9000	1000
				17.715	137.								
1			0.57	16.459	137.			1024.9	3.0306	1.9605	757.	35000	1000
1		17.5		16.544	137.			817.	.5866	0.346	72.	28000	1000
2		.70		.259	137.			659.3	2.5526	0.5268	854.	28000	1000
				6.514	137.			534.			28.	28000	1000
1			1.7	.7	128.	.16.9		811.	0.5617	0.7736	176.	22000	900
2		7.40		.6	137.	.7		175.7	0.7	0.5522	157.	22000	900
								245.5	1.5-5	0.5220	137.	22000	900

TABLE IV-2
EXPERIMENTAL DATA

I	I	H.P.	THRUST LBS	ICE THICK FT	SHIP VEL FPS	SIZE	COVER FT	CF	X	Y	Y	S		DIR DEG	WIND VEL knots
26	2	2757.	55.25	1.4950	2.525	128.00	0.1200	0.2500	150.3	0.1754	1.3264	197.53		185.0	9.0
26	1			1.4600	5.166	128.00	0.1200		106.8		0.5126	202.27		185.0	8.0
26	4	2847.	57.97	1.5249	40.649	128.00	0.1299	0.1000	99.2	0.3166	0.5139	193.65		185.0	9.0
28	1	365.		0.8350	5.552	126.00			158.3						
28	2	1252.	33.14		10.775	126.00	0.0000	0.0000	272.5	1.3012	0.6312	338.02		250.0	11.0
28	3	1652.	3.27	0.9700		126.00			215.1	1.1253	0.5087	299.69		250.0	11.0
2?	2	3427.	40.35	0.9400	16.240	126.00			319.2	1.7943	0.6484	309.25		250.0	11.0
2?	3	3374.	45.23	0.9400	16.135	126.00			318.2	1.7827	0.6466	309.25		250.0	11.0
?	?	4401.	46.41	1.0200	16.195	126.00	0.0000	0.0000	268.1	1.6499	0.5428	283.61		250.0	11.0
?	?	4522.	5.61	0.7466	17.43	126.00			328.1	1.8627	0.6428	329.62		300.0	10.0
20	2	5620.	64.37	0.8259	19.965	146.00	0.0000		526.6	2.5104	0.1527	354.04		90.0	10.0
3?	1	7790.	78.16	0.8439	22.11	126.00			667.3	2.7208	0.1428	270.0		270.0	7.5
30	2	8624.	80.94	0.5471	23.127	128.00	0.0000		719.5	2.9038	1.4799	351.45		270.0	7.5
3?	3	9511.	3.17	0.8700		126.00			726.7	2.8405		336.16		270.0	7.5
31	1	5623.	61.47	1.0366	14.403	128.00	0.0266		341.6	1.4463	0.8653	286.42		620.0	7.5
31	2	5066.		0.8835	15.125	126.00	5.35		655.6		1.7663			650.0	7.5
31	3	3777.	47.01	0.9500	13.555	126.00	0.2450	289.2	289.2	1.6573	0.8552	342.00		650.0	7.5
31	4	2537.	63.65	0.3133	12.979	126.00		0.1333	318.1		0.71??			620.0	7.5
31	5	5921.	67.72	0.9474	15.661	126.00	0.0000	0.0599	450.6	2.0407	0.9446	300.01		650.0	7.5
?	?	1759.	26.44	0.5339	7.445	127.20			176.4			257.63		500.0	5.0
?	2	2747.	43.45	0.9299	12.264	167.20	0.0000		300.2	1.3096	0.7006	262.94		250.0	5.0
32	3	6192.	65.03	0.8866	22.053	167.20			546.8	2.6502	1.2273	274.96		250.0	5.0
33	1	1770.	33.00	0.8700	9.420	56.00	0.2700	0.2700	266.7	1.1245	0.6620	145.50		115.0	5.0
33	2	2623.	34.22	0.8700	11.152	56.00		0.192	270.1	1.0312	0.6392	148.54		115.0	5.0
34	1	1207.	1.67	0.8700	4.420	56.00	1.0000	1.0000	147.3	0.5276	0.9642	148.30		0.0	7.5
34	2	1977.	12.31	0.9470	5.717	56.00			198.7	0.6825	0.6162	168.34		0.0	7.5
35	1	2317.	27.44	0.6700	6.746	56.00	0.0000	1.0000	219.7	0.8053	1.2102	148.50		180.0	7.0
35	2	29.44	3.42	0.8707	7.523	58.00			257.5	0.9981	1.3601	148.50		180.0	7.0
35	3	77.9.	74.15	0.8700	20.893	56.00		0.3733	824.4	2.4941	1.3134	148.50		180.0	7.0
35	4	45.6.	7.02	0.8770	17.060	56.00		.555	659.7	1.0819	0.9305	148.50		180.0	7.0
35	5	4-08.	57.13	0.8700	16.037	56.00		0.5750	451.3	1.9144	1.0605	148.50		180.0	7.0
35	6	4318.	51.63	0.8713	15.435	56.00		0.2150	4.45.5	1.8768	0.9769	148.50		180.0	7.0

$\overline{SC}$ = snow cover in feet

w = relative wind velocity in feet per second

θ = angle on the bow of the relative wind

The variables w and θ were combined into two variables which were included in the regression analysis as first order terms only with no cross products:

$$w^2 \sin\theta$$

$$w^2 \cos\theta$$

The basic variables for the regression analysis of the dimensionless loading factor, were:

$$V, \overline{SC}/h, \overline{CF}, \overline{SIGND}$$

For both, all second order terms (squares and cross products) except as mentioned above, were initially included. Only those variables which produced a statistically significant (at the 95 percent confidence level) reduction in the sum of the squares were retained in the final equation.

A correction for the resistance of the ship in water was applied to the total measured thrust. Figure IV-5 shows the resistance of the ship in smooth, open water in terms of EHP. The resistance due to water can be found from:

$$R_{water}(tons) = \frac{550\ EHP}{2240\ v}$$

where v is the ship speed in feet per second. The ice resistance can then be defined as:

$$R_{ice} = \Sigma T - R_{water} \text{ (in tons of 2240 pounds)}$$

The regression equation developed for thrust included terms for the effect of wind. These terms can be used to correct measured thrust to conditions of no wind.

For purposes of the regression analysis of the dimensionless data, the total thrust was corrected for wind effects and also for both wind and water resistance effects. Note that all data showing the dimensionless velocity, V, has been increased by the factor 10^7.

B. Ice Loads on the Hull

During each of the experimental runs the Geotech FM tape recorder was recording the twelve strain gage signals and the velocity signal. A typical set of data is shown in the oscillograph record of Figure IV-6, which shows the instantaneous strain impulses on Frame 30 (Gages 2, 6, and 10) as a result of the pressure of a cusp of unbroken ice, or the grinding or crushing of an already broken piece. Each trace also contains, although not shown in the figure, a calibration signal equivalent to 10 microstrain from which the strain amplitudes can be scaled.

Because of the great quantity of data, and because it was assumed that for any steady-state condition an average of RMS number would properly represent the behavior of any particular set of gages, the first approach to data reduction and analysis was statistical. A small computer called a "Probability Analyzer" was used to measure the amplitude of each sequential strain pulse, classify each into one of sixteen possible amplitude ranges, and present the data automatically on punched cards. An IBM 1130 computer program then computed average, maximum, and RMS values, the total number of data points, and presented the data in histogram form. In addition, a summary was prepared for each "interval", or group of blocks representing steady-state conditions for each test. The output (for Experiment No. 30) is shown as Table IV-3.

Examination of the results in terms of the geometrical patterns observed during the calibration (see Appendix A) showed very poor correlation to expected behavior. The reason for this soon became apparent. In order to prevent overloading the capacity of the Probability Analyzer, the low-level strains had been suppressed electrically so that only the significant strains were counted and measured. This resulted, however, in an unequal bias in the results from the three gages on the frame, since the lower gage always showed lower values consistently. Eliminating the lowest values resulted in higher average values from the lower gage than the real data warranted. If the equipment available had been able to absorb all of the small strain variations from each gage, the statistical approach would probably have produced very useful results.

The other, and successful, approach was to examine a reasonable number of instantaneous events from each steady-state interval. To do this, one set of gages (2, 6, and 10) was played back onto an oscillographic recorder with the velocity signal as a fourth track for identification purposes. In each interval, the five highest-amplitude strains from Gage 2 were selected, and measurements made of the response of all three gages to each of the five events. Figure IV-6 is a reproduction of a typical oscillograph record, showing two of the five strains selected for measurement during Experiment 4, Interval 5. Also shown, are the two distinctive signals created by the velocity block observers at the bow and stern of the ship.

Of the total number of steady-state data points from all experiments shown in Table IV-2, thirty-three were selected as being most significant

Speed (Knots)
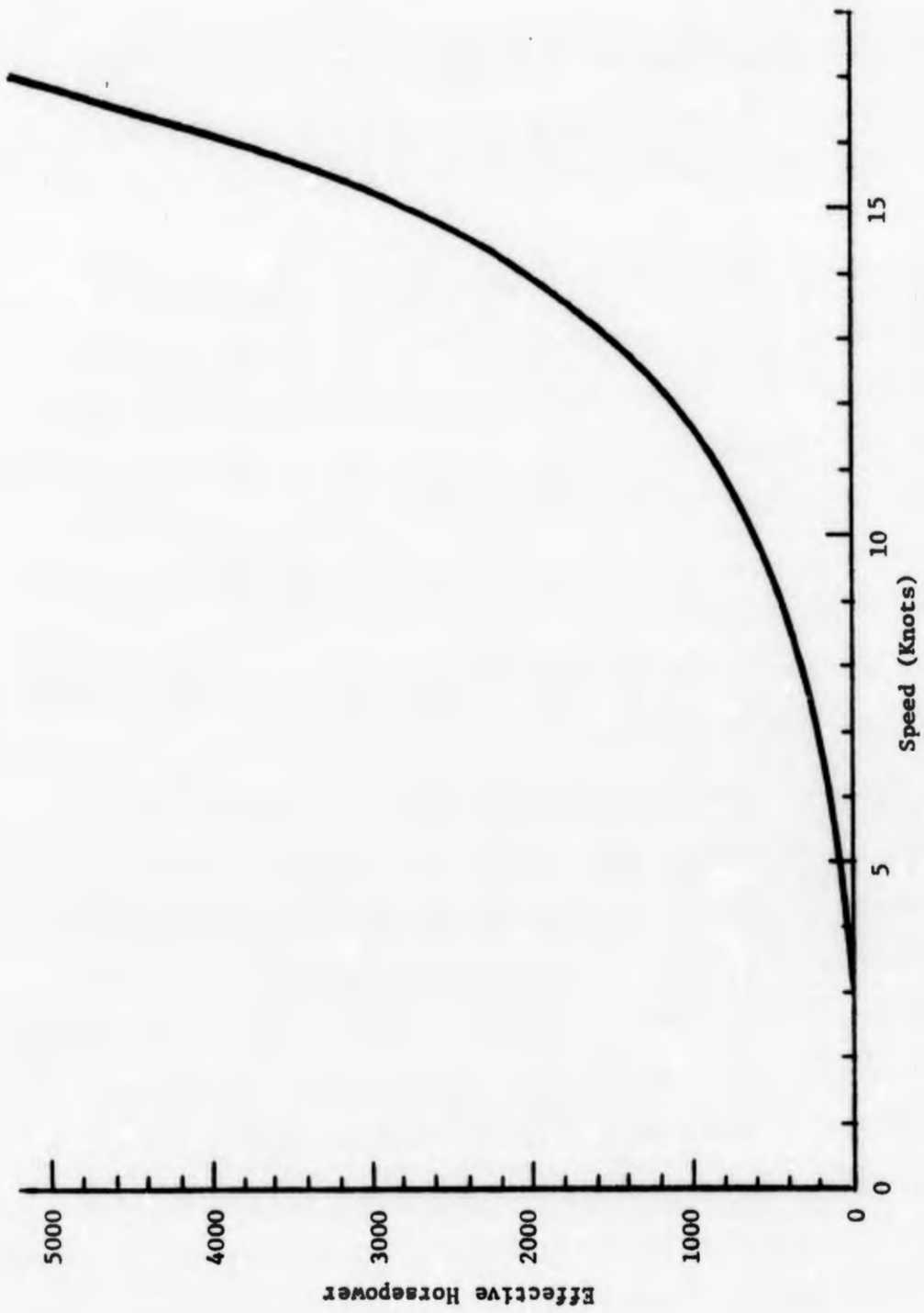
Figure IV-5

Resistance in Open Water

Effective Horsepower
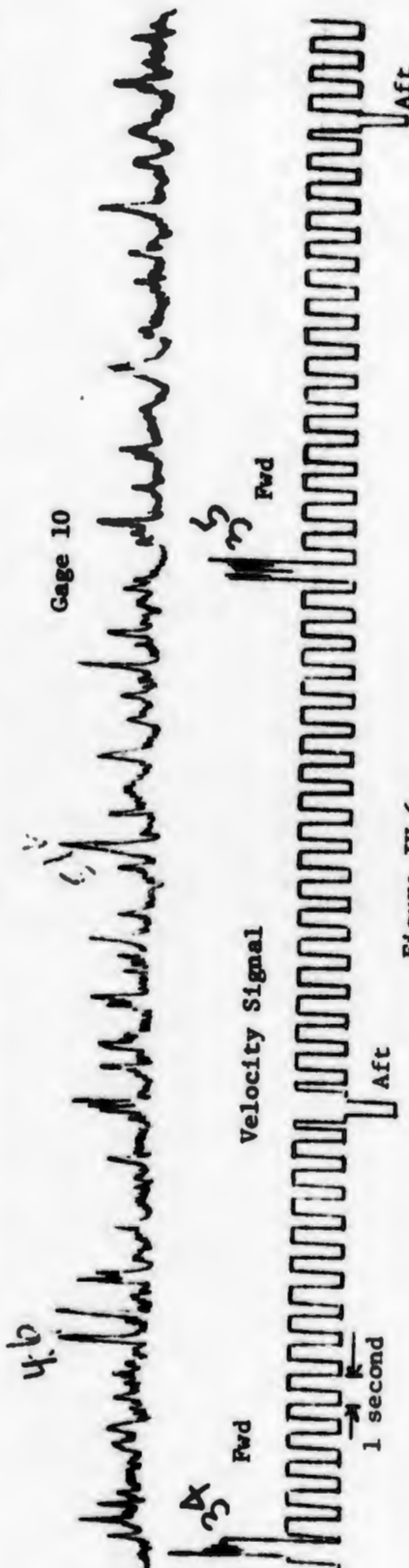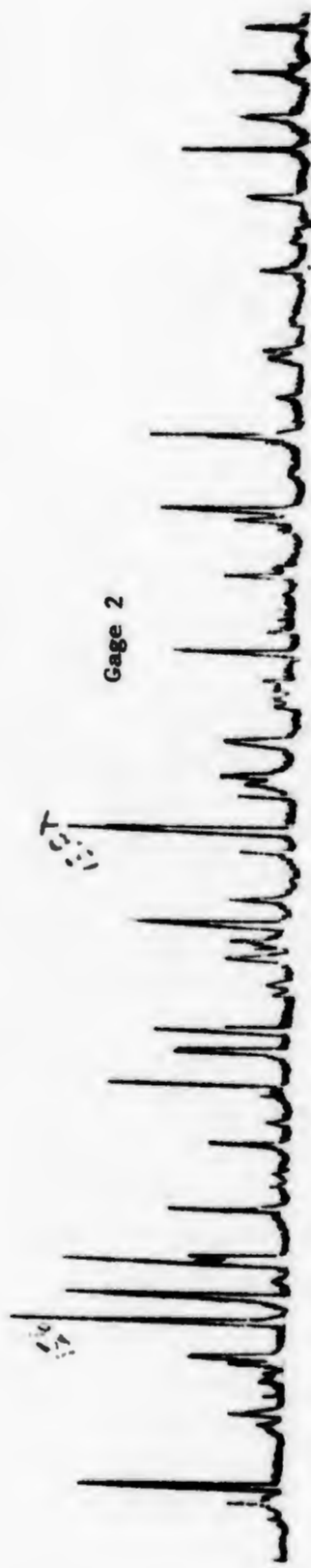
Figure IV-6

Strains on Frame 30 Due to Ice Loads

Experiment 4, Blocks 34-35

TABLE IV-3A

MACKINAW HULL STRAIN GAGE ANALYSIS
TEST 30

------ TELEDYNE MATERIALS RESEARCH ------
MAY 26,1971

GAGE 1 TAPE CAL= 5.0 OSC DIV =10 MICROSTRAIN PA CAL= 23.5 OSC DIV = 31 COUNTS TOT CARDS= 6 SF=MS/COUNT
CAL T30 G 1   5.0   23.5 10 6 001 000 156 000 000 000 000 000 000 000 000 000 000 031

				STRAIN LEVEL REGISTERS - COUNTS													MICROSTRAIN				
		1	2	3	4	5	6	7	8	9	10	11	12	13	14	15	16	MAX	AVE	RMS	SUMN	SF
BLOCKS 02-06 CARDS	1- 2	59	93	38	8	1	0	0	0	0	0	0	0	0	0	0	80	27.	31.	199.	1.5
BLOCKS 08-12 CARDS	3- 4	77	87	12	2	4	0	0	0	1	0	0	0	0	0	0	163	23.	31.	184.	1.5
BLOCKS 14-18 CARDS	5- 6	115	126	24	3	0	1	1	0	0	0	0	0	0	0	0	116	22.	26.	268.	1.5

GAGE 2 TAPE CAL= 6.0 OSC DIV =10 MICROSTRAIN PA CAL= 23.5 OSC DIV = 31 COUNTS TOT CARDS= 6 SF=MS/COUNT
CAL T30 G 2   6.0   23.5 10 6 000 001 156 000 000 000 000 000 000 000 000 000 000 031

				STRAIN LEVEL REGISTERS - COUNTS													MICROSTRAIN				
		1	2	3	4	5	6	7	8	9	10	11	12	13	14	15	16	MAX	AVE	RMS	SUMN	SF
BLOCKS 02-06 CARDS	1- 2	141	98	34	20	1	1	0	0	0	0	0	0	0	0	0	92	20.	25.	299.	1.2
BLOCKS 08-12 CARDS	3- 4	217	107	27	19	8	0	0	0	0	0	0	0	0	0	0	66	17.	22.	378.	1.2
BLOCKS 14-18 CARDS	5- 6	262	136	28	20	5	1	3	0	0	0	0	0	0	0	0	94	17.	23.	455.	1.2

GAGE 3 TAPE CAL= 5.7 OSC DIV =10 MICROSTRAIN PA CAL= 23.5 OSC DIV = 30 COUNTS TOT CARDS= 6 SF=MS/COUNT
CAL T30 G 3   5.7   23.5 10 6 000 001 155 000 000 000 000 000 000 000 000 000 000 030

				STRAIN LEVEL REGISTERS - COUNTS													MICROSTRAIN				
		1	2	3	4	5	6	7	8	9	10	11	12	13	14	15	16	MAX	AVE	RMS	SUMN	SF
BLOCKS 02-06 CARDS	1- 2	119	91	25	5	1	0	0	0	0	0	0	0	0	0	0	56	19.	23.	241.	1.3
BLOCKS 08-12 CARDS	3- 4	91	97	16	6	2	1	0	0	0	0	0	0	0	0	0	103	20.	25.	212.	1.3
BLOCKS 14-18 CARDS	5- 6	130	93	21	10	1	2	1	1	0	0	0	0	0	0	0	125	20.	26.	259.	1.3

TABLE IV-3B

GAGE 4 TAPE CAL= 5.6 OSC DIV =10 MICROSTRAIN PA CAL= 23.5 OSC DIV = 31 COUNTS TOT CARDS= 6 SF=MS/COUNT
CAL T30 G 4   5.6   23.5 10 6 000 001 155 000 000 000 000 000 000 000 000 000 000 31

	STRAIN LEVEL REGISTERS - COUNTS																MICROSTRAIN			
	1	2	3	4	5	6	7	8	9	10	11	12	13	14	15	16	MAX	AVE	RMS	SUMN	SF
BLOCKS 02-06 CARDS 1- 2	156	99	28	3	0	0	0	0	0	0	0	0	0	0	0	0	43	17.	20.	286.	1.3
BLOCKS 08-12 CARDS 3- 4	115	79	10	5	4	0	0	0	0	0	0	0	0	0	0	0	87	18.	23.	213.	1.3
BLOCKS 14-18 CARDS 5- 6	155	104	19	0	0	0	0	1	1	0	0	0	0	0	0	0	132	17.	22.	278.	1.3

GAGE 5 TAPE CAL= 5.8 OSC DIV =10 MICROSTRAIN PA CAL= 23.5 OSC DIV = 31 COUNTS TOT CARDS= 6 SF=MS/COUNT
CAL T30 G 5   5.8   23.5 10 6 000 001 155 000 000 000 000 000 000 000 000 000 000 31

	STRAIN LEVEL REGISTERS - COUNTS																MICROSTRAIN			
	1	2	3	4	5	6	7	8	9	10	11	12	13	14	15	16	MAX	AVE	RMS	SUMN	SF
BLOCKS 02-06 CARDS 1- 2	186	106	15	2	0	0	0	0	0	0	0	0	0	0	0	0	58	15.	17.	309.	1.3
BLOCKS 08-12 CARDS 3- 4	148	68	3	1	0	0	0	0	0	0	0	0	0	0	0	0	47	13.	15.	220.	1.3
BLOCKS 14-18 CARDS 5- 6	222	80	5	1	0	0	0	0	0	0	0	0	0	0	0	0	62	12.	15.	309.	1.3

GAGE 6 TAPE CAL= 5.0 OSC DIV =10 MICROSTRAIN PA CAL= 23.5 OSC DIV = 31 COUNTS TOT CARDS= 6 SF=MS/COUNT
CAL T30 G 6   5.0   23.5 10 6 000 001 156 000 000 000 000 000 000 000 000 000 000 31

	STRAIN LEVEL REGISTERS - COUNTS																MICROSTRAIN			
	1	2	3	4	5	6	7	8	9	10	11	12	13	14	15	16	MAX	AVE	RMS	SUMN	SF
BLOCKS 02-06 CARDS 1- 2	170	134	21	0	1	1	0	0	0	0	0	0	0	0	0	0	95	19.	23.	327.	1.5
BLOCKS 08-12 CARDS 3- 4	177	96	15	5	1	0	0	0	0	0	0	0	0	0	0	0	80	17.	21.	291.	1.5
BLOCKS 14-18 CARDS 5- 6	275	112	9	3	1	0	0	0	0	0	0	0	0	0	0	0	72	15.	18.	400.	1.5

GAGE 7 TAPE CAL= 6.3 OSC DIV =10 MICROSTRAIN PA CAL= 23.5 OSC DIV = 30 COUNTS TOT CARDS= 6 SF=MS/COUNT
CAL T30 G 7   6.3   23.5 10 6 001 001 156 000 000 000 000 000 000 000 000 000 000 30

	STRAIN LEVEL REGISTERS - COUNTS																MICROSTRAIN			
	1	2	3	4	5	6	7	8	9	10	11	12	13	14	15	16	MAX	AVE	RMS	SUMN	SF
BLOCKS 02-06 CARDS 1- 2	215	147	66	4	3	0	0	0	0	0	0	0	0	0	0	0	80	18.	23.	446.	1.2
BLOCKS 08-12 CARDS 3- 4	216	122	71	4	3	0	0	0	0	0	0	0	0	0	0	0	65	15.	19.	369.	1.2
BLOCKS 14-18 CARDS 5- 6	324	152	7	4	2	0	0	0	0	0	0	0	0	0	0	0	59	13.	17.	489.	1.2

GAGE 9 TAPE CAL= 5.7 OSC DIV =10 MICROSTRAIN PA CAL= 23.5 OSC DIV = 31 COUNTS TOT CARDS= 6 SF=MS/COUNT
CAL T30 G 9   5.7   23.5 10 6 001 000 155 000 000 000 000 000 000 000 000 000 000 31

	STRAIN LEVEL REGISTERS - COUNTS																MICROSTRAIN			
	1	2	3	4	5	6	7	8	9	10	11	12	13	14	15	16	MAX	AVE	RMS	SUMN	SF
BLOCKS 02-06 CARDS 1- 2	73	4	0	0	0	0	0	0	0	0	0	0	0	0	0	0	25	12.	14.	105.	1.3
BLOCKS 08-12 CARDS 3- 4	19	13	0	0	0	0	0	0	0	0	0	0	0	0	0	0	26	14.	16.	32.	1.3
BLOCKS 14-18 CARDS 5- 6	79	19	0	0	0	0	0	0	0	0	0	0	0	0	0	0	29	11.	12.	98.	1.3

TABLE IV-3C

80

GAGE 10 TAPE CAL= 5.6 OSC DIV =10 MICROSTRAIN PA CAL= 23.5 OSC DIV = 30 COUNTS TOT CARDS= 6 SF=MS/COUNT
CAL T30 G10   5.6   23.5 10 6   000 001 156 000 000 000 000 000 000 000 000 30
STRAIN LEVEL REGISTERS - COUNTS   MICROSTRAIN

	1- 2	3	4	5	6	7	8	9	10	11	12	13	14	15	16	MAX	AVE	RMS	SUMN	SF
BLOCKS 07-08 CARDS	33	27	0	0	0	0	0	0	0	0	0	0	0	0	0	39	16.	19.	62.	1.3
BLOCKS 09-12 CARDS	17	15	0	0	0	0	0	0	0	0	0	0	0	0	0	32	16.	18.	32.	1.3
BLOCKS 14-18 CARDS	40	20	0	0	0	0	0	0	0	0	0	0	0	0	0	26	13.	14.	60.	1.3

GAGE 11 TAPE CAL= 5.9 OSC DIV =10 MICROSTRAIN PA CAL= 23.5 OSC DIV = 30 COUNTS TOT CARDS= 6 SF=MS/COUNT
CAL T30 G11   5.9   23.5 10 6   000 001 155 000 000 000 000 000 000 000 000 30
STRAIN LEVEL REGISTERS - COUNTS   MICROSTRAIN

	1- 2	3	4	5	6	7	8	9	10	11	12	13	14	15	16	MAX	AVE	RMS	SUMN	SF
BLOCKS 07-06 CARDS	81	27	0	0	0	0	0	0	0	0	0	0	0	0	0	26	11.	13.	108.	1.3
BLOCKS 08-12 CARDS	27	20	1	0	0	0	0	0	0	0	0	0	0	0	0	31	15.	17.	48.	1.3
BLOCKS 14-18 CARDS	70	14	0	0	0	0	0	0	0	0	0	0	0	0	0	22	10.	12.	84.	1.3

GAGE 12 TAPE CAL= 5.0 OSC DIV =10 MICROSTRAIN PA CAL= 23.5 OSC DIV = 30 COUNTS TOT CARDS= 6 SF=MS/COUNT
CAL T30 G12   5.0   23.5 10 6   000 001 156 000 000 000 000 000 000 000 000 30
STRAIN LEVEL REGISTERS - COUNTS   MICROSTRAIN

	1- 2	3	4	5	6	7	8	9	10	11	12	13	14	15	16	MAX	AVE	RMS	SUMN	SF
BLOCKS 02-06 CARDS	37	35	0	0	0	0	0	0	0	0	0	0	0	0	0	31	18.	20.	72.	1.5
BLOCKS 08-12 CARDS	11	25	0	0	0	0	0	0	0	0	0	0	0	0	0	29	22.	24.	36.	1.5
BLOCKS 14-18 CARDS	6	20	0	0	0	0	0	0	0	0	0	0	0	0	0	29	23.	25.	26.	1.5

SUMMARY BY BLOCKS

TEST90

GAGE

	1	2	3	4	5	6	7	8	9	10	11	12	AVG1-4	AVG5-8	AVG9-12
BLOCKS 02-06															
MAX	80	92	56	43	58	95	80	0.	25	39	26	31	58.	30.
AVG	27.	20.	19.	17.	15.	15.	18.	0.	12.	16.	11.	16.	13.	15.
RMS	31.	23.	23.	20.	17.	23.	23.	0.	14.	19.	13.	20.	16.	17.
SUMN	199.	299.	241.	286.	309.	327.	446.		105.	62.	108.	72.	270.	86.
BLOCKS 08-12															
MAX	163	66	103	87	47	80	65	0	26	32	31	29	104.	29.
AVG	23.	17.	20.	18.	13.	17.	15.	0.	14.	16.	15.	22.	20.	17.
RMS	31.	22.	25.	23.	15.	21.	19.	0.	16.	18.	17.	24.	26.	19.
SUMN	184.	378.	212.	213.	220.	291.	369.		32.	32.	48.	36.	246.	37.
BLOCKS 14-18															
MAX	116	94	125	132	62	72	50	0.	22	26	22	22	116.	26.
AVG	22.	17.	20.	17.	12.	15.	15.	0.	11.	16.	16.	23.	18.	15.
RMS	26.	23.	26.	22.	15.	18.	17.	0.	13.	16.	12.	25.	24.	16.
SUMN	268.	455.	259.	278.	309.	600.	480.		96.	60.	64.	315.	299.	67.

from the standpoint of desirable combinations of ice thickness, ship velocity, coupling factor, and other parameters. These thirty-three intervals were identified on the FM magnetic tape, and played back as shown in Figure IV-6. The signal amplitudes measured were converted to microstrain by scaling against the recorded calibration signal.

At this point strain responses were known, but neither the location nor the effective area of the ice load could be determined. Considerable thought was given to the results of the calibration of the hull (Appendix A), and to ways in which the calibration data could enable the recorded experimental strains to be related to forces on the hull.

One approach which was attempted was to relate the zero crossing of the Gage 6--Gage 10 line to the load location. A rather weak relationship was established, and trials with the real data did not produce consistent results.

Examining Figure A-9 of Appendix A, it seemed apparent that some boundaries or limitations could be put on the gage responses to known loads. It seemed evident that there is an upper limit on the strain sensitivity immediately under the load. This limit is approximately 15 microstrain per ton, and shows a tendency to decrease towards the upper end of the panel, probably due to changing characteristics as the Second Deck is approached. The tests with varying load area (Cases 10, 11, and 12) indicate a definite area effect, but with a

quite probable upper limit as shown by Case 12, since it is unlikely that significant forces would be developed by pieces of ice as small as six square inches in contact area.

Another boundary on the response characteristics is the fact that the icebreaking function is confined to a fairly narrow range about the waterline. Referring to Figure A-9, the design waterline is 19 feet, which is at 0.575 distance from the Second Deck to the Platform Deck. The 18-foot waterline is at 0.70. Thus, the calibration Cases 2, 10, 11, and 12 are located in the general area where icebreaking occurs.

Considering all of these factors, including the symmetrical appearance of the lines for Cases 2, 10, 11, and 12, it seemed that to make an assumption that the triangles were isosceles would not lead to any significant errors. This procedure was first tested on the calibration data, with results as shown in Figure IV-7. The effect is to change the magnitude and location of apparent applied load to some extent, but not so much as to change the overall picture.

Reviewing the extrapolated sensitivities under the loads from the calibration data again, it seemed that a conservative upper limit of 18 microstrain per ton could be set. In other words, based on the calibration cases where the load was applied nearest to a strain gage, and on the same frame, no ice impact would produce a response of greater than 18 microstrain for each ton of applied load.

With these assumptions, the data measured from the thirty-three intervals were plotted graphically in the same manner as the calibration data previously examined in Figure IV-7. Typical results are
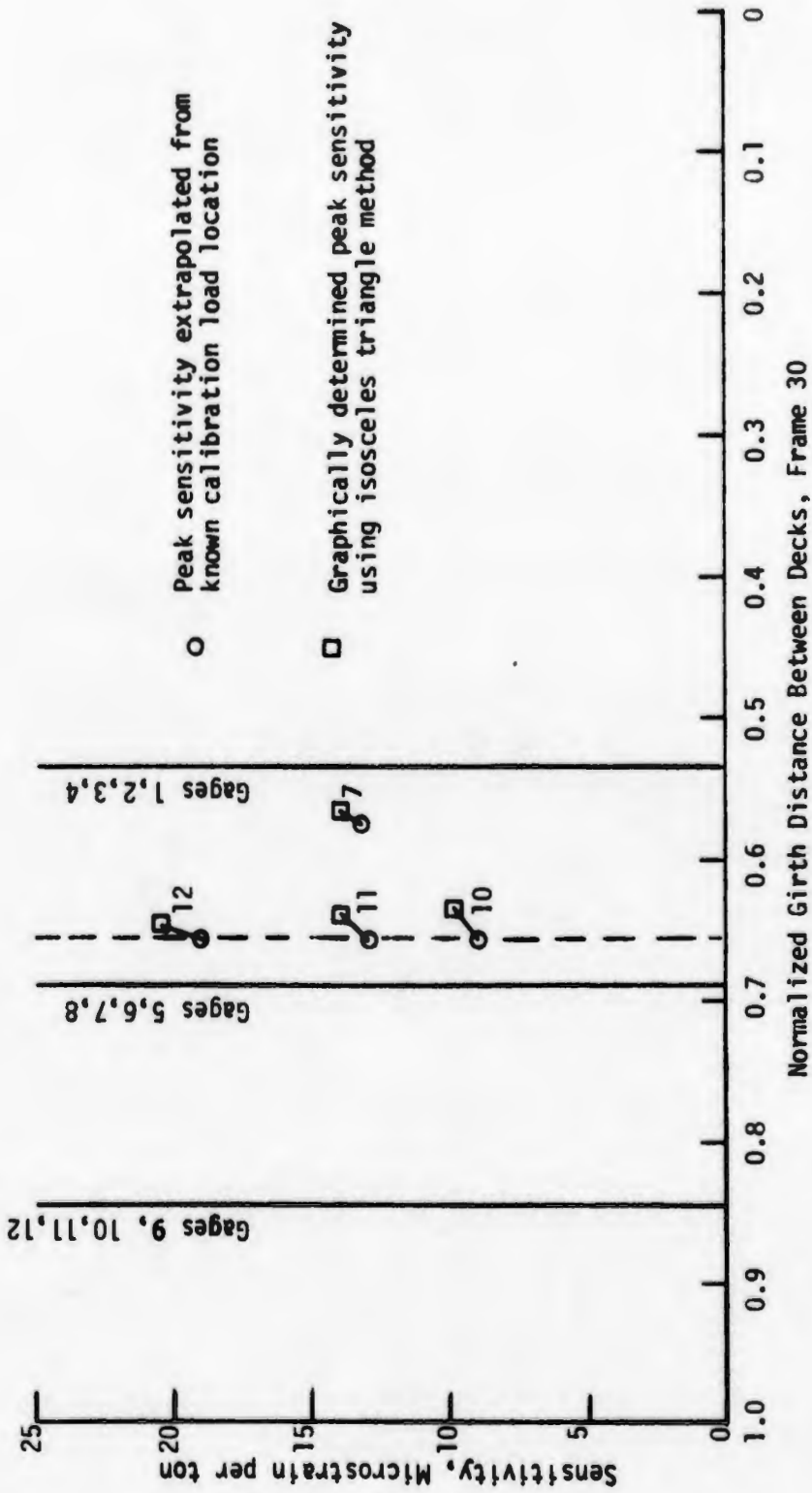
-42-

Figure IV-7

Test of Isosceles Triangle Method

Figure IV-8
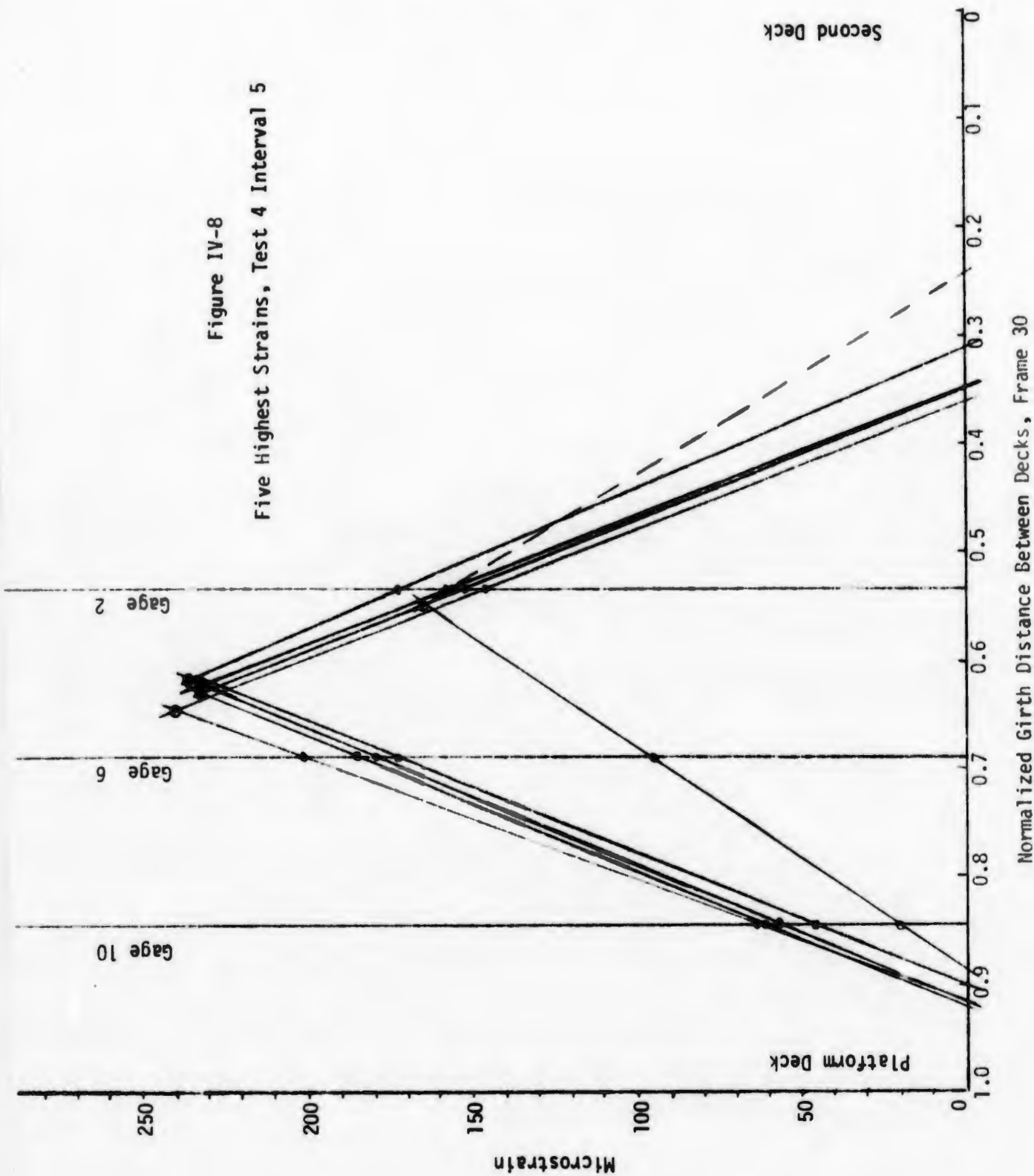Five Highest Strains, Test 4 Interval 5

Figure IV-9

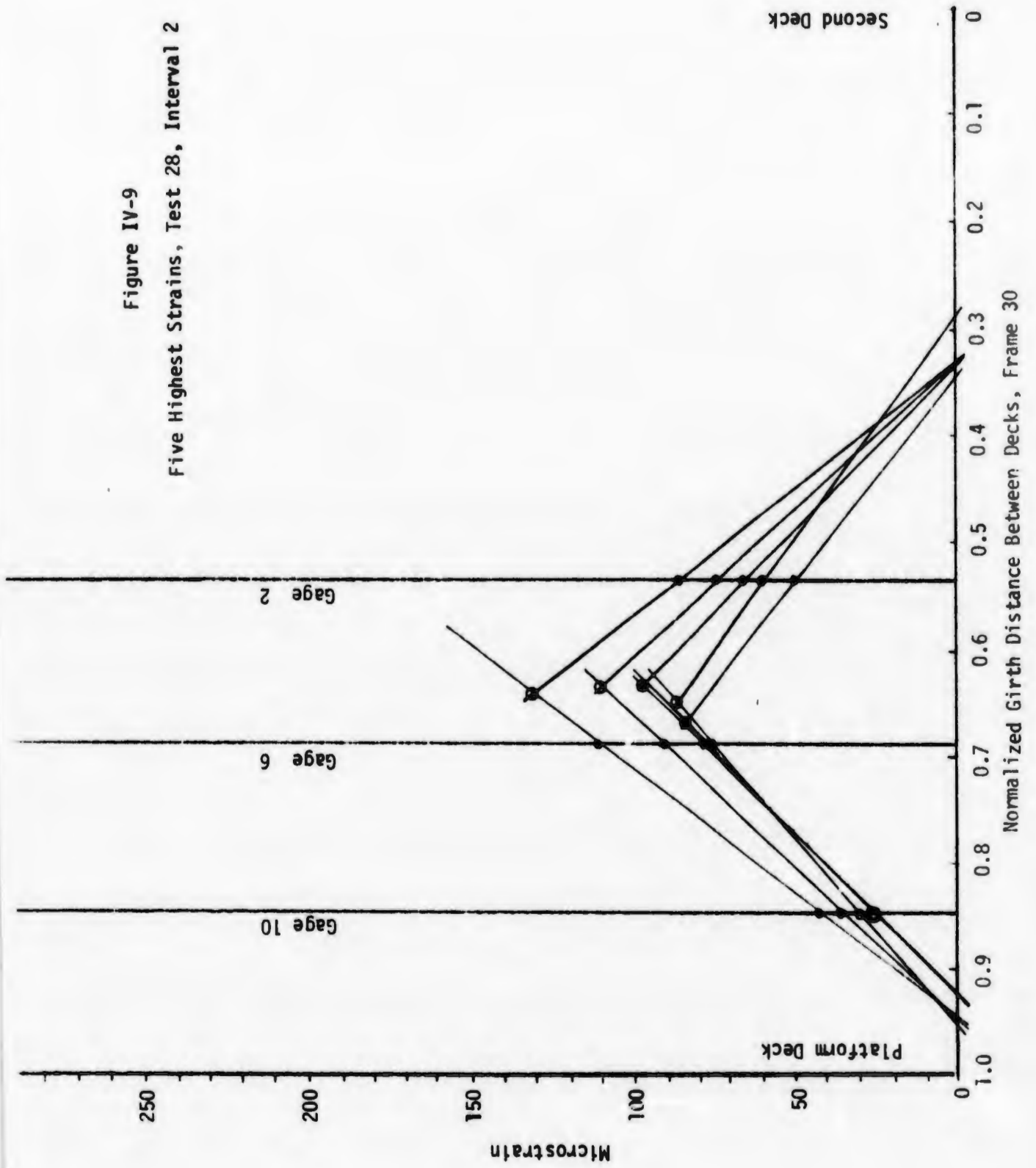Five Highest Strains, Test 28, Interval 2

Figure IV-10

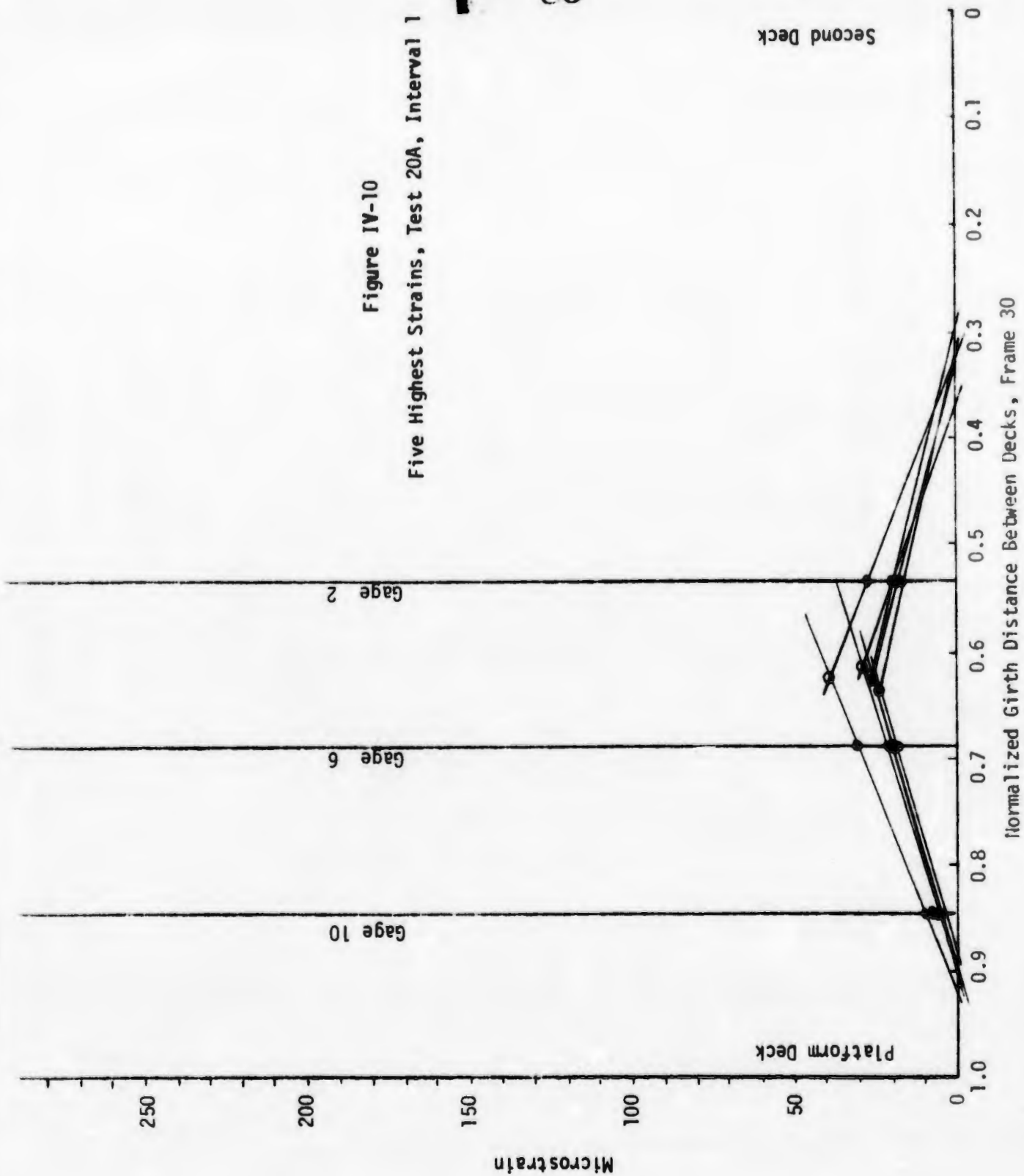Five Highest Strains, Test 20A, Interval 1

TABLE IV-4

HULL FORCE DATA, FRAME 30

Test	Interval	Microstrain		Force, Tons	
		Maximum	Avg. 5 Highest	Maximum	Avg. 5 Highest
2	2	200	149	11.1	8.3
3	4	210	200	11.6	11.1
4	4	244	201	13.5	11.1
4	5	240	235	13.3	13.0
5	2	37	35	2.0	1.9
5	3	262	250	14.5	13.9
5	4	151	108	8.4	6.0
5	5	188	169	10.4	9.4
5	6	220	180	12.2	10.0
6A	4	181	161	10.0	9.0
6A	6	155	140	8.6	7.8
6B	1	123	74	6.8	4.1
6B	2	175	160	9.7	8.9
7A	1	77	64	4.3	3.5
9A	1	46	38	2.5	2.1
18A	1	40	32	2.2	1.8
18A	3	38	30	2.0	1.7
18A	4	57	40	3.2	2.2
19	1	74	55	4.1	3.1
20A	1	38	28	2.0	1.5
25	1	137	115	7.6	6.4
26	3	134	95	7.4	5.3
28	2	131	102	7.3	5.7
29	1	136	120	7.6	6.7
29	2	103	84	5.7	4.7
30	1	180	117	10	6.5
30	2	68	64	3.8	3.5
30	3	320	186	17.8	10.4
31	5	125	107	7.0	6.0
32	3	119	79	6.6	4.4
33	1	164	122	9.1	6.8
34	1	90	69	5.0	3.8
35	7	102	92	5.7	5.1

shown in Figures IV-8 through IV-10. The data showed an extremely consistent pattern of linearity, and the extrapolated load positions and amplitudes, for the most part, clustered together very well. (In selecting the five highest strains for examination, some of them were much lower than others.)

The amplitudes of the extrapolated loads were recorded, converted to force, and a table was prepared (Table IV-4) showing the maximum value and the average value (of the five highest) for each interval. These data were then processed by graphical techniques to establish the relationships between the force data and the steady-state parameters which pertained during the interval.

it was very difficult to locate thin ice or ice without snow cover. As a result the majority of the data was derived from runs in thick, snow-covered ice.

Generally, the equipment performed adequately. However, the CEC 5-134 oscillograph was delivered with a defective light source (mercury vapor lamp). Three of these $57.00 items were consumed in the period 1 February through 9 March. The last one failed on 9 March prior to test #25. The remaining ten tests were recorded on the Ampex tape recorder only. These tests required a considerable amount of additional time (two weeks) to reduce, since the reduction effort was geared to the use of oscillograph records rather than to the use of magnetic tape. As mentioned above, the shaft thrust measurements were unsatis-factory. The gauges were placed in the vicinity of the thrust bearings. These bearings became extremely hot with the result that the thrust bridges exhibited significant zero shift and calibration drift during test runs. This situation had not been observed previously by the investigators in similar tests. Once the problem was diagnosed, careful calibration before and after each test run was accomplished. A pro-vision was made in the data reduction program to accept a time-dependent zero value and calibration factor. However, even these precautions did not improve the quality of the thrust data to the extent that it was acceptable for use in the analysis phase. However, other alternative techniques for determining resistance from torque and electrical horse-power were employed and they appear to have produced good results.

All but one of the accelerometers malfunctioned during the test. Replacements were not available at the time. However, observing the

output of these devices during the tests it is doubtful that even data from the one which functioned correctly will serve any useful purpose. The accelerometer trace did provide qualitative evidence of the following:

a. Lateral accelerations appear to be the most significant of the three components.

b. Large lateral accelerations coincide with large strain levels in the strain gauged panel.

c. These lateral accelerations are a combination of rigid body acceleration of the ship and to some extent deformation of the hull girder laterally due to the load on the hull.

The velocity measuring system performed well as did the hull strain sensing system. All strain gauges in the 12-gauge array functioned adequately during the entire project. The use of semiconductor gauges provided more than adequate sensitivity. Calibration of the hull panel demonstrated that the strain gauged panel provided repeatable response to known loads applied to the hull. The electrical power data, velocity data, ice thickness data and meteorological data was acquired by shipboard test teams. The teams were supervised by senior shipboard personnel. In general, their performance was excellent.

The accuracy of measurement of the principal variables is worthy of mention. The theoretical velocity measurement accuracy has been computed in Appendix E. Appendix E indicates that velocity error can be quite high, $\approx$ 10 percent under certain conditions. In fact, the velocity

in any single interval is the average of three independent measurements of velocity, i.e.

$$v_1 = \frac{\text{Distance Between Observers}}{\Delta t}$$

$$v_2 = \frac{\text{Distance Between Blocks}}{\Delta t_1}$$

$$v_3 = \frac{\text{Distance Between Blocks}}{\Delta t_2}$$

where

Δt = time required for block to "travel" between forward and aft observers

Δt_1 = time between passage of successive blocks past forward observers

Δt_2 = time between passage of successive blocks past the aft observer

In addition to this averaging effect, the mean of these values was usually taken over several intervals to arrive at an estimate of the steady state velocity. Several intervals were checked at random. The worst case obtained was an interval with three blocks. The sample mean was 14.3 ft/sec. The sample standard deviation was .135 ft/sec. The 95 percent confidence limits were ± 0.33 ft/sec. This is equivalent to a 2.3 percent error.

The ice thickness is assumed to be a random variable with some population mean and standard deviation (unless it is obvious that the data comes from an ice field where there is a gradient

in the ice thickness). Intervals which were used as data points and analyzed in Section IV were selected at random out of the printout folder. The sample mean, standard deviation, t value, and confidence limits were computed. The standard deviation appeared to be a function of thickness with a typical value of 0.07 ft. Ninety-five percent confidence intervals range between $\pm$ .09 and $\pm$ .11 ft. The 95 percent confidence interval divided by the mean may be used as percent error. The resulting error in the low thickness range .3 - .8 ft. is approximately 7 percent. The total error in measuring dimensionless velocity (V) in the high speed, low ice thickness range may be estimated as follows:

$$W_V = \sqrt{W_v^2 + W_h^2} \qquad [V-1]$$

where

W_V = percent error in dimensionless velocity (V)

W_v = percent error in velocity (v)

W_h = percent error in thickness

W_V = 7.3 percent

Using a similar technique, the error in $\mathcal{L}$, (R/h²) due to the uncertainty of knowing h could be as high as 9.5 percent. The error in measuring hull strain has not been theoretically estimated. The power supply and signal conditioning equipment are 1 percent systems. The method shown in Appendix E for estimating errors in thrust measurement may be applied to the strain measurements. The errors in measuring strain will in all probability not exceed 2 percent. The uncertainty in estimating force from strain observations is complicated by the complex static and dynamic response of the entire panel to exterior loads (see Appendix A).

B. Resistance Experiments

1. Regression analysis of dimensional data. The dimensional, experimental and calculated data is shown in Table IV-2. The results of a stepwise regression analysis of the data is shown in Table V-1. The resulting regression equation is:

$$\Sigma T = 4.59 + 3.61\ h \cdot v + 134.14\ \overline{SC} - 0.644\ \sigma_f \cdot \overline{SC} - 32.71\ \overline{SC} \cdot \overline{CF}$$
$$+ 0.00313\ W^2 \cos\theta + .00611\ W^2 \sin\theta \qquad\qquad [V-2]$$

where

ΣT	=	sum of the calculated thrusts of the three propellers (tons)
n	=	ice thickness (ft.)
σ_f	=	flexural strength of the ice (psi)
v	=	ship speed (ft/sec)
$\overline{SC}$	=	snow cover depth (ft)
$\overline{CF}$	=	coupling factor (SHP_{bow}/ SHP)
W	=	wind velocity (ft/sec)
	=	angle on the bow of the relative wind

Examining Table V-1 and equation [V-2], it may be seen that the most significant term in the regression analysis is h·v, the product of ship speed and ice thickness. The relative magnitude of the computed t value shown in Table V-1 is a good gauge of the importance of a variable in the regression. The t value shown in Table V-1 is part of a test to determine whether the regression coefficient for the variable under consideration could be zero. For example, if a table of the distribution of t is entered with the number of degrees of freedom (number of observations less number of variables + 1) i.e., 129 in our case, a value of t = 3.3 would be extracted for p = .001. Our computed value

is 34.36 indicating that it is highly unlikely that the coefficient
of h·v is zero. Another way of examining the validity of the regression
coefficient is to determine the confidence limits on the coefficient.
We assume that the true regression coefficient, β_i, is a normally dis-
tributed random variable of which b_i, the sample regression coefficient,
(those shown in equation [V-2]) is an unbiased estimator. We seek to
know how good an estimator b_i is of β_i. Snedecor and Cochran (8) show
that $(b-\beta)/s_b$ follows the "t" distribution. (s_b is the sample stan-
dard error of the regression coefficient shown in Table V-1.) The
"t" distribution is a two-tailed distribution which is quite similar
to the normal distribution for large values of the number of degrees
of freedom. Given the number of degrees of freedom and a value of t,
we can obtain a probability that a value of t can be found which is
greater than t or less than -t.

Conversely, a value of $\pm$ t may be found corresponding to the
desired probability and the number of degrees of freedom. We have
arbitrarily set 95 percent as our confidence limits. For 129 degrees
of freedom at the 95 percent level t = $\pm$ 1.98. Hence,

$$\frac{b - \beta}{s_b} \geq \pm 1.98 \qquad\qquad [V-3]$$

and

$$b - 1.98 \, s_b \leq \beta \leq b + 1.98 \, s_b \qquad\qquad [V-4]$$

Table V-1 lists the 95 percent confidence limits on each of the
regression coefficients in the right hand column. Figure V-1 is a plot
of ΣT vs. h·v. Superimposed on the data is a curve corresponding to

TABLE V-1

RESULTS OF REGRESSION ANALYSIS

UNCORRECTED TOTAL CALCULATED THRUST VS DIMENSIONAL TEST VARIABLES

VARIABLE	MEAN	STANDARD DEVIATION	CORRELATION X VS Y	REGRESSION COEFFICIENT	STD. ERROR OF REG. COEF.	COMPUTED t VALUE	95% CONFIDENCE LIMITS ON REGRESSION COEFFICIENTS	
							HIGH	LOW
hv	13.55928	7.20546	0.92194	3.60684	0.10496	34.36245	3.39904	-3.81464
$\overline{SC}$	0.16508	0.17784	0.18301	134.13705	18.38439	7.29624	97.73700	-170.53900
$\sigma_f \cdot \overline{SC}$	22.69537	25.94865	0.13147	-0.64477	0.13111	-4.91766	-0.90470	-.38470
$\overline{SC} \cdot \overline{CF}$	0.05832	0.11499	-0.09840	-32.71479	9.12325	-3.58586	-50.76500	-24.66500
$w^2 \cos\theta$	-261.51001	730.19848	-0.07566	0.00313	0.00113	2.75598	0.00089	.00537
$w^2 \sin\theta$	295.35968	322.74084	0.15277	0.00611	0.00256	2.38353	0.00105	.01117
DEPENDENT								
ΣT	60.08351	29.03997						

Intercept   4.58792

Multiple Correlation   0.95752

Std. Error of Estimate   8.56640

ANALYSIS OF VARIANCE FOR THE REGRESSION

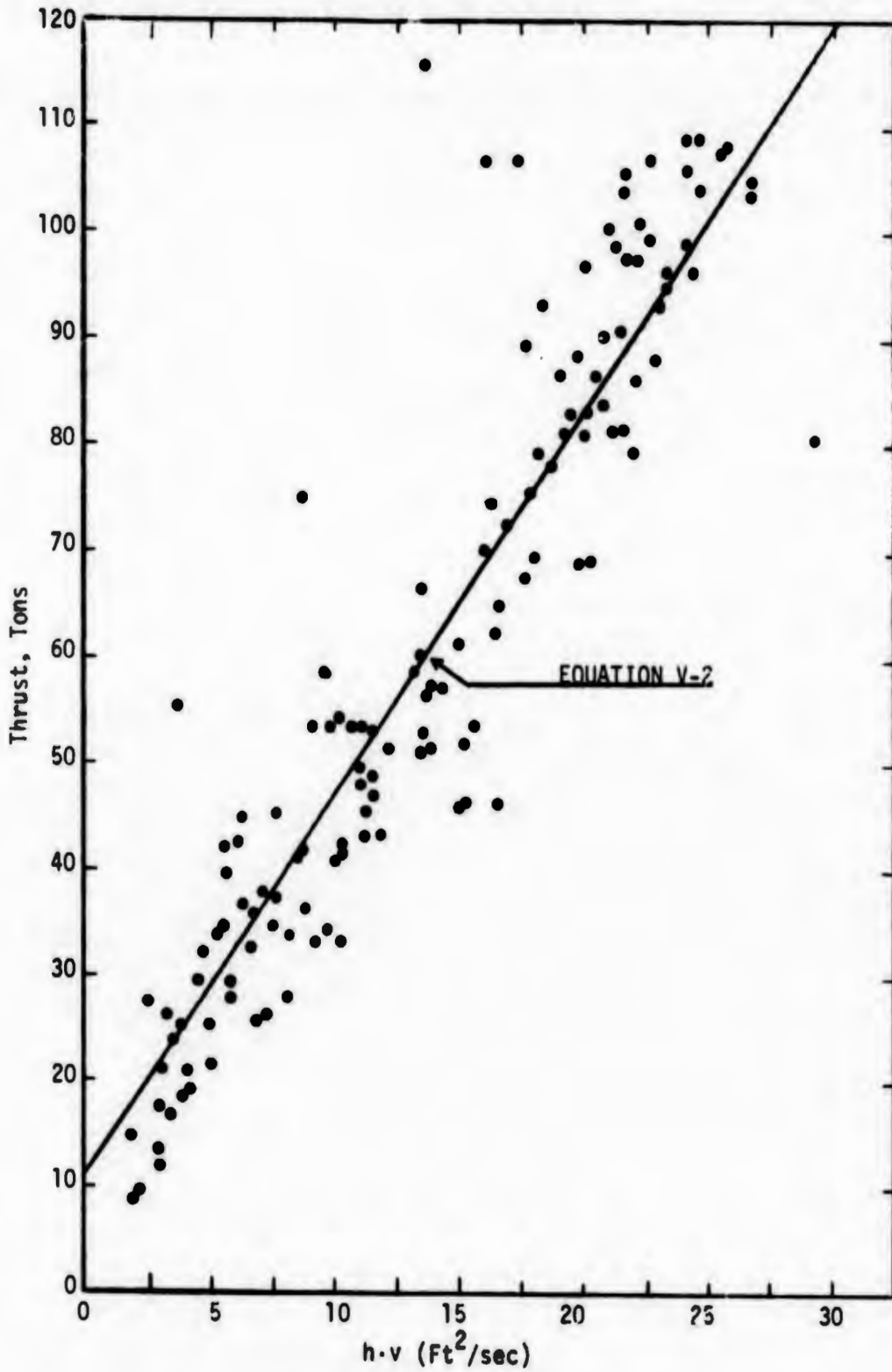| SOURCE OF VARIATION	DEGREES OF FREEDOM	SUM OF SQUARES	MEAN SQUARES	F VALUE
Attributable to Regression	6	104381.75021	17396.95708	237.06991
Deviation from Regression	129	9466.43947	73.38323	
TOTAL	135	113848.18768		

Figure V-1

Total Thrust (Tons) vs. the Product of
Ice Thickness and Velocity

equation [V-2] with all variables except h·v held at their mean value. The physical meaning of the second order regression terms was not considered in their selection. However, several terms in the regression are worth discussing. The product of velocity and ice thickness appears because both are significant parameters in determining resistance and because low velocity is associated with high ice thickness and vice versa. Snow cover depth appears in the regression with a large coefficient indicating a strong dependence of resistance upon snow cover. The term which includes the product of snow cover depth and ice strength is difficult to explain. The product of snow cover and coupling factor is significant in the regression. There is a possibility that this reflects the fact that the bow propeller's effect is more noticeable when there is snow cover. The two terms involving wind and the bow angle reflect the effect on resistance caused by wind resistance. The cosine term is the component of wind resistance due to drag while the sine term includes the effect of the frictional forces caused by the wind force tending to push the ship against the lee side of the channel. These terms are barely significant at the 95 percent level. Nonetheless, the fact that the sine term appears in the regression indicates that wind can cause an augmentation in resistance in ice even for a ship with as low a profile as USCGC MACKINAW. This term could be expected to be significant for ore carriers whose surface area is so much greater, particularly when they are in ballast.

The values of ΣT were corrected by subtracting the water resistance as estimated from model EHP tests. These corrected values of total thrust

were treated as a new variable -- pure ice resistance, R_{ice}, and were submitted to regression analysis using a procedure identical to that used for the uncorrected thrust data. The resulting regression equation was,

$$R_{ice} = 2.63022 + 3.142\ h \cdot v - 31.4848\ \overline{SC} \cdot \overline{CF} + .00334\ W^2\ \cos\theta$$
$$+ 149.5749\ \overline{SC} - 0.6511\ \sigma_f \cdot \overline{SC} + .0075\ W^2\ \sin\theta + 9.669\ h$$

$$[V-5]$$

Table V-2 lists the results of the regression analysis. Two terms appearing in Table V-2 have been omitted from equation [V-5]; the product of h and $\overline{SC}$ and the product of velocity and ice strength. The computed value of t is much less than 1.98 ($t_{.05}$, 126 d.f.). Hence, the hypothesis that the coefficients of these two terms are zero cannot be rejected. The equation should be relatively similar to equation [V-2]. One may compare the coefficients of similar terms of the two equations in Table V-3. Essentially, the same comments apply to the variables in this regression as to the regression of uncorrected total thrust. It should be noted that placing the variables in the order of increasing computed value results in the same order for both equations. That order is shown in Table V-3.

TABLE V-2

RESULTS OF REGRESSION ANALYSIS

TOTAL THRUST LESS WATER RESISTANCE VS DIMENSIONAL TEST VARIABLES

VARIABLE	MEAN	STANDARD DEVIATION	CORRELATION X VS Y	REGRESSION COEFFICIENT	STD. ERROR OF REG. COEF.	COMPUTED t VALUE	95% CONFIDENCE LIMITS ON REGRESSION COEFFICIENTS HIGH	
$h\,v$	13.55928	7.20546	0.90396	3.14261	0.22995	13.66615	3.59780	2.68740
$h \cdot \overline{SC}$	0.21556	0.23275	0.34671	-15.11824	10.92148	-1.38426		
$\overline{SC} \cdot \overline{CF}$	0.05832	0.11499	-0.06782	-31.48479	9.67331	-3.25481	-12.33164	-50.63794
$w^2 \cos\theta$	-261.51001	730.19848	-0.08145	0.00334	0.00111	3.00417	.00553	.00115
$v \cdot \sigma_f$	1521.89404	743.28833	0.39273	-0.00099	0.00186	-0.53101		
$\overline{SC}$	0.16508	0.17784	0.22040	149.57495	26.10217	5.73036	201.25829	97.89160
$\sigma_f \cdot \overline{SC}$	22.69537	25.94865	0.16290	-0.65114	0.15908	-4.31270	-.35220	-.95008
$w^2 \sin\theta$	295.35968	322.74084	0.16074	0.00748	0.00254	2.94225	.01250	.00246
h	1.16181	0.44096	0.67893	9.66958	3.68144	2.62657	16.95883	2.38033

DEPENDENT

$\Sigma T - R_{water}$	55.86540	27.73479

Intercept	-2.63022
Multiple Correlation	0.95699
Std. Error of Estimate	8.32805

ANALYSIS OF VARIANCE FOR THE REGRESSION

SOURCE OF VARIATION	DEGREES OF FREEDOM	SUM OF SQUARES	MEAN SQUARES	F VALUE
Attributable to Regression	9	95105.64083	10567.29299	152.36190
Deviation from Regression	126	8738.92385	69.35653	
	135	103844.56268		

TABLE V-3

COMPARISON OF COEFFICIENTS IN
EQUATIONS [V-2] AND [V-5]

	ΣT	$\Sigma T - R_{water}$
$v \cdot h$	3.61	3.14
$\overline{SC}$	134.14	149.57
$\overline{SC} \cdot \overline{CF}$	-31.48	-32.71
$\sigma_f \cdot \overline{SC}$	-.644	-.651
$W^2 \cos\theta$	.00313	.00334
$W^2 \sin\theta$	.00611	.00748
h	0.	9.669

2. <u>Regression analysis of dimensionless data points</u>. The dimnesional variables have been incorporated into a series of dimensionless variables as described in Section IV. The dependent dimensionless variable was $\mathcal{L}$. Two $\mathcal{L}$'s were developed and will be discussed in this section. They are listed below:

$$\mathcal{L}_{T-R_{wi}} = \frac{\Sigma T - R_{wind}}{\rho_w \left(1 - \frac{\rho_1}{\rho_w}\right) g B h^2} \qquad [V-6]$$

$$\mathcal{L}_{T-RWA-R_{wi}} = \frac{(\Sigma T - R_{water} - R_{wind})}{\rho_w \left(1 - \frac{\rho_1}{\rho_w}\right) g B h^2} \qquad [V-7]$$

The regression analysis was restricted to first and second degree combinations of V, $\overline{CF}$, $\overline{SC}/h$ and $\overline{SIGND}$. The result of the regression of $\mathcal{L}_{T-R_{wi}}$ against the above variables is shown in equation [V-8] below:

$$\begin{aligned}
\mathcal{L}_{T-R_{wi}} = \; & 58.812 + 57.659 \, V^2 + 94.41 \, V + 297.967 \, \overline{SC}/h \\
& - 0.187 \, V \cdot \overline{SIGND} + 92.633 \, V \cdot \overline{CF} + .00028 \, \overline{SIGND}^2 \\
& - 266.456 \, \overline{CF} \cdot \overline{SC}/h \qquad\qquad [V-8]
\end{aligned}$$

Note that equation [V-8] does not include two of the variables shown in Table V-4, $\overline{CF}$ and $V \cdot \overline{SC}/h$. Upon addition of the last term, $\overline{SC}/h \cdot \overline{CF}$, both $\overline{CF}$ and $V \cdot \overline{SC}/h$ became insignificant in the regression; i.e., t tests of the coefficients of these terms revealed that the hypothesis that they could be zero could not be rejected at the 95 percent confidence level. Table V-4 shows the regression analysis results. Figure V-2 shows

equation [V-8] superimposed on a plot of $\alpha_{T-R_{wi}}$ vs V. All other terms in equation [V-8] containing variables have been evaluated at the mean value of those variables.

Commenting on the meaning of the many variables in this regression equation is difficult. The most significant and meaningful terms in equation [V-8] are V, V² and $\overline{SC}/h$. Appendix E contains an adequate explanation of the derivation of V. $\overline{SC}/h$ is a dimensionless number which is a result of dimensional analysis. The physical meaning of $\overline{SC}/h$ is not apparent, nonetheless $\overline{SC}/h$ appears to materially improve the regression. The product of V · $\overline{SIGND}$ also is significant in the regression analysis. Again, the physical significance of this product term is obscure. The two terms involving coupling factor are barely significant in the regression analysis. The term comprised of V · $\overline{CF}$ has a positive regression coefficient indicating an increase in required thrust with increase in $\overline{CF}$ and V. Given a value of $\overline{CF}$, its effect is small and beneficial at small V and small but detrimental at large V. In addition, the term containing $\overline{SC}/h$ · $\overline{CF}$ would cause a reduction in resistance noticeable only if there is snow cover. All of these explanations are plausible. Nonetheless they are second order effects. <u>Dimensionless load depends primarily upon dimensionless velocity and the ratio of snow cover to ice thickness</u>.

It was considered important to artifically deduct the water resistance from the total thrust and to form a new set of dimensionless variables based upon ΣT less wind resistance and water resistance. The result of this regression analysis is presented in Table V-5 and in
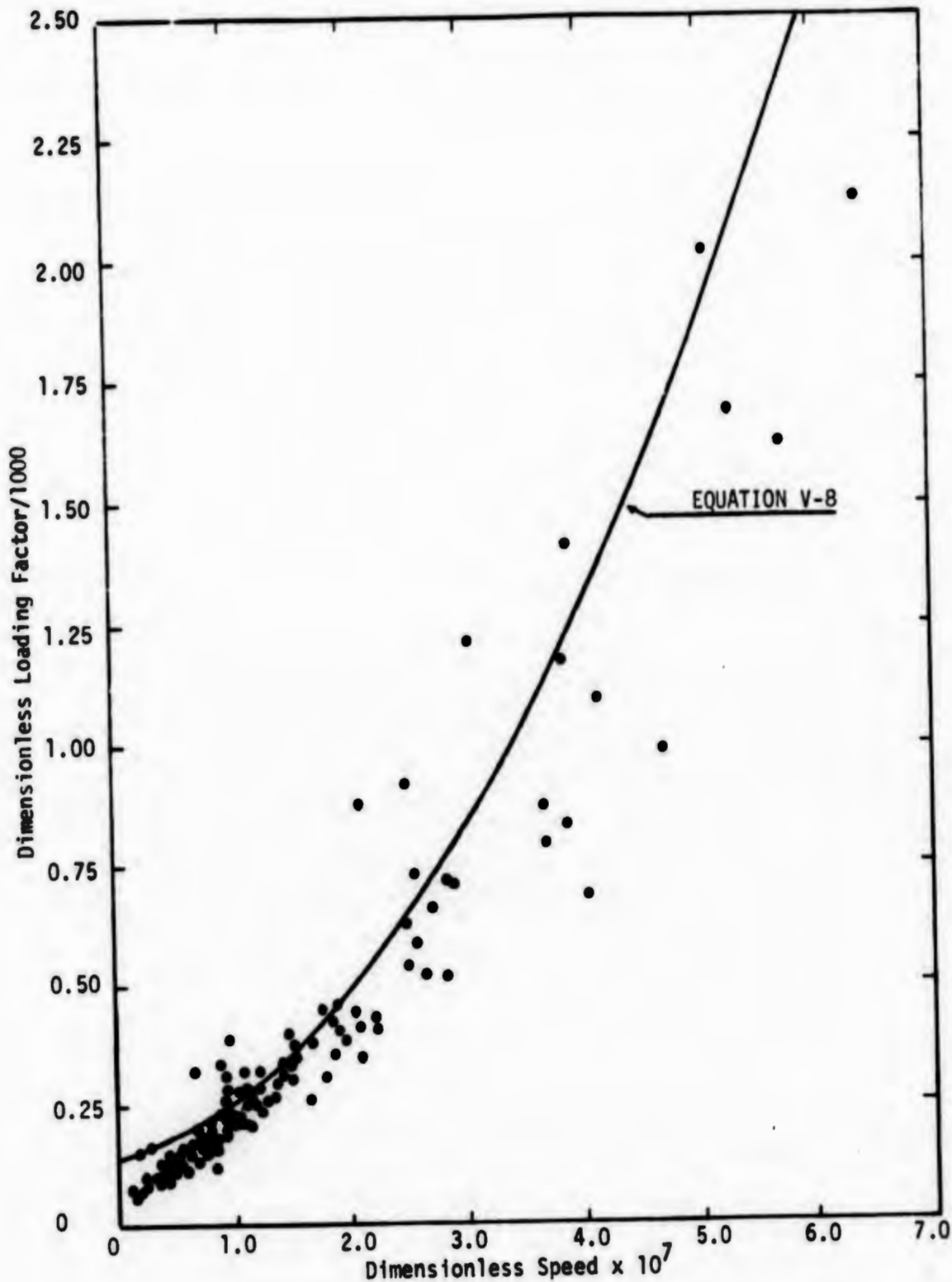
Figure V-2
Dimensionless Load (based on $\Sigma T-R_{wind}$)
vs. Dimensionless Velocity

TABLE V-5

RESULTS OF REGRESSION ANALYSIS

$$\mathcal{L}_{T-R_w-R_{wa}} \text{ VS DIMENSIONLESS TEST VARIABLES}$$

VARIABLE	MEAN	STANDARD DEVIATION	CORRELATION X VS Y	REGRESSION COEFFICIENT	STD. ERROR OF REG. COEF.	COMPUTED t VALUE	95% CONFIDENCE LIMITS ON REGRESSION COEFFICIENTS HIGH	LOW
V	1.42694	1.19693	0.91568	85.71389	20.52636	4.17579	126.35608	45.07170
V·SC/h	0.24079	0.72727	0.61080	70.36949	21.73712	3.23729	113.40898	27.33000
V²	3.45828	6.36768	0.90211	27.97838	4.13841	6.76065	36.17243	19.78433
V·CF	0.27041	0.34213	-0.03870	133.73443	30.35502	4.40567	193.83736	73.63150
CF	0.28181	0.30530	-0.31068	-114.82191	35.71617	-3.21484	-44.10390	-185.53992
SC/h	0.15127	C.23420	0.35424	176.36166	64.29295	2.74309	303.66170	49.06162
V·SIGND	704.68762	1208.22021	0.86287	-0.04268	0.01674	-2.54973	-.00954	-.07582

DEPENDENT

$$\mathcal{L}_{T-R_w-R_{wa}} \quad 313.42175 \quad 281.58245$$

Intercept 77.00556

Multiple Correlation 0.97042

Std. Error of Estimate 69.80564

ANALYSIS OF VARIANCE FOR THE REGRESSION

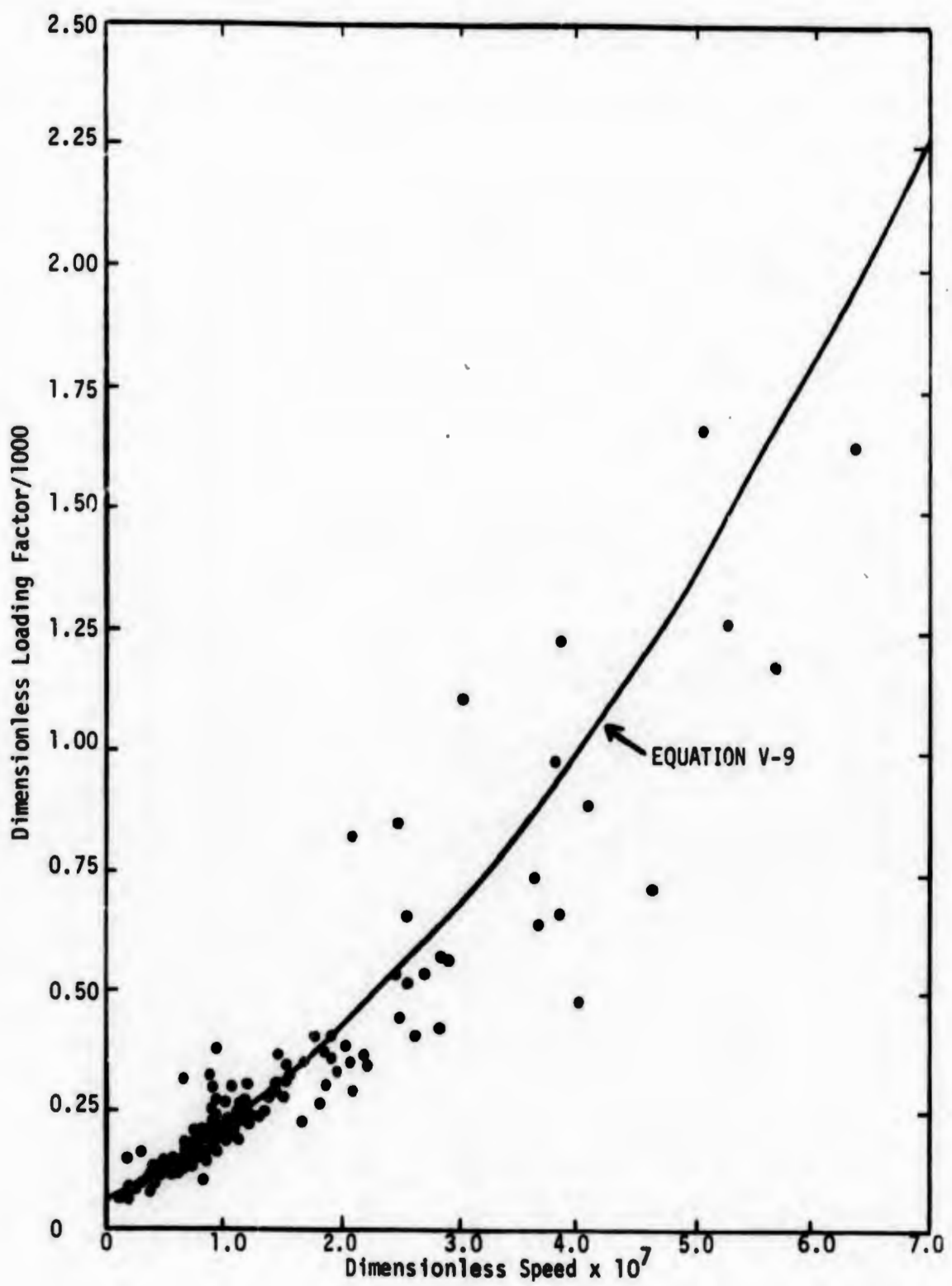| SOURCE OF VARIATION	DEGREES OF FREEDOM	SUM OF SQUARES	MEAN SQUARES	F VALUE
Attributable to Regression	7	10080252.02734	1440035.75292	295.52356
Deviation from Regression	128	623722.12670	4872.82911	
TOTAL	135			

Figure V-3
Dimensionless Load ($X_{T-R_{wi}-R_{wa}}$)
vs. Dimensionless Velocity

equation [V-9] below:

$$\alpha_{T-R_{wi}-R_{wa}} = 77.005 + 85.714\ V + 27.978\ V^2 + 70.369\ V \cdot \overline{SC}/h$$
$$+ 133.734\ V \cdot \overline{CF} - 114.822\ \overline{CF} + 176.362\ \overline{SC}/h$$
$$- .0427\ V \cdot \overline{SIGND} \qquad\qquad [V-9]$$

Figure V-3 shows this relationship plotted on a graph of $\alpha_{T-R_w-R_{wa}}$ vs. V. Variables other than V were set to their mean values for the purpose of calculating the coordinates of the curve. The removal of water resistance appears to have reduced the coefficient of V^2. This is certainly reasonable. The other coefficients of the two regression equations have changed somewhat. $V \cdot \overline{SC}/h$ is significant in this regression equation but not in equation [V-8], while $\overline{SC}/h \cdot \overline{CF}$ appears in equation [V-8] but not in [V-9]. The magnitude of the difference between the coefficients of the terms which appear in common in the two equations is not large. Examining the confidence limits on the coefficients of the common terms in both equations, one can see that a noticeable difference may be observed only in the V^2 term. Despite the replacement of the $\overline{SC}/h \cdot \overline{CF}$ term in equation [V-8] with $\overline{CF}$ in equation [V-9] there still exists in equation [V-9] a set of terms including coupling factor which indicate that coupling factor is detrimental at high speeds. Extracting these terms from equation [V-9] and hypothesizing a term called coupling-dependent dimensionless load, we have:

$$\alpha_{\overline{CF}} = \overline{CF}\ (133.734\ V - 114.822) \qquad\qquad [V-10]$$

The transition value of V at which $\alpha_{\overline{CF}}$ becomes positive is 0.868. This is perhaps tenuous evidence upon which to base the evaluation of the bow propeller; nonetheless, it is all that is available. There is a clear indication from the regression analysis that the bow propeller has a small beneficial effect at low V which becomes a small detrimental effect at high values of V. Equation [V-9] contains two terms which include snow cover. Both the dimensional and dimensionless data demonstrate that resistance to motion in ice fields is strongly dependent upon snow cover.

In an attempt to demonstrate graphically the fit of the regression equation to the data, the dimensional regression equation [V-2] was used to correct the resistance for the effect of snow cover and coupling factor. Table V-6 lists the dimensional thrust data, the wind and water resistance corrective terms and the values of corrected thrust data. The corrected resistance values were used to form the dimensionless number α which was then regressed against first and second order combinations of V and $\overline{SIGND}$. The resulting regression equation was

$$\alpha = 77.008 + 85.7108 \ V + 27.979 \ V^2 - .0427 \ V \cdot \overline{SIGND} \qquad [V-11]$$

This equation is almost exactly the same as equation [V-9] with $\overline{SC}$ and $\overline{CF}$ set to zero. Table V-7 shows the particulars of the regression analysis. Figure V-4 is a plot of the corrected α vs V. Equation [V-11] is plotted in this figure.

3. <u>Comparison with WIND Class full scale data</u>. The WIND Class full scale dimensional data from Lewis and Edwards (6) has been converted

TABLE V-6   109

THRUST CORRECTION DATA

T E S T	I N T	T	R WATER	R WIND	T-RWIND	T-RWIND -RWATER
1	1	13.30	1.45	4.19	9.10	7.65
1	2	34.67	8.54	4.19	30.47	21.93
1	3	45.28	11.38	4.19	41.08	29.70
2	1	115.93	1.77	5.00	110.92	109.14
2	2	103.83	3.14	5.00	98.82	95.67
2	3	106.77	3.01	5.00	101.76	98.75
3	1	36.20	2.11	6.97	29.22	27.11
3	2	41.60	0.94	6.97	34.62	33.67
3	3	96.68	4.97	6.97	89.70	84.73
3	4	104.03	6.00	6.97	97.05	91.04
3	5	105.61	5.16	6.97	98.63	92.47
4	1	41.30	1.55	4.38	36.91	35.36
4	2	86.48	4.80	4.38	82.09	77.28
4	3	100.90	6.10	4.38	96.51	90.40
4	4	80.47	5.78	4.38	76.08	70.30
4	5	74.33	1.82	4.38	69.94	68.11
5	1	25.35	1.83	1.28	24.06	22.22
5	2	44.75	7.68	1.28	43.46	35.78
5	3	106.79	4.39	1.28	105.50	101.11
5	4	36.57	0.46	1.28	35.28	34.82
5	5	66.44	1.57	1.28	65.15	63.57
5	6	83.10	3.19	1.28	81.81	78.61
5	7	100.45	5.02	1.28	99.16	94.14
6	1	29.13	0.71	-5.56	34.69	33.98
6	2	58.64	2.35	-5.56	64.20	61.85
6	3	56.64	2.63	-5.56	62.20	59.57
6	4	64.91	4.29	-5.56	70.47	66.18
6	5	69.06	4.77	-5.56	74.62	69.85
6	6	87.97	7.87	-5.56	93.53	85.65
6	1	42.50	0.47	-5.56	48.06	47.59
6	2	93.01	8.73	-5.56	98.57	89.84
7	1	14.74	0.08	2.93	11.80	11.71
7	2	53.18	2.09	2.93	50.24	48.14
7	3	89.32	3.63	2.93	86.38	82.74
7	4	106.11	6.12	2.93	103.17	97.05
7	1	74.99	0.76	2.93	72.05	71.28
7	2	106.83	3.68	2.93	103.89	100.20
8	1	21.03	0.23	0.47	20.55	20.32
8	2	23.65	0.30	0.47	23.17	22.87
8	3	29.39	0.55	0.47	28.91	28.36
8	4	34.30	0.70	0.47	33.82	33.12
8	5	54.20	1.60	0.47	53.72	52.12
8	6	41.55	1.36	0.47	41.07	39.71
8	7	72.45	4.10	0.47	71.97	67.86
8	8	92.99	6.31	0.47	92.51	86.20
8	9	86.58	7.41	0.47	86.10	78.69

T E S T	I N T	T	R WATER	R WIND	T-RWIND	T-RWIND -RWATER
9	1	26.04	1.54	1.16	24.87	23.32
9	2	41.85	3.69	1.16	40.68	36.99
9	3	39.45	5.02	1.16	38.28	33.26
9	4	53.47	8.74	1.16	52.30	43.56
9	1	58.54	14.44	1.16	57.37	42.92
10	1	33.91	0.72	-0.23	34.14	33.41
10	2	97.50	6.09	-0.23	97.73	91.63
10	3	98.73	7.73	-0.23	98.96	91.23
11	1	70.06	2.26	0.73	69.32	67.05
11	2	97.44	5.05	0.73	96.70	91.64
11	3	51.52	1.57	0.73	50.78	49.20
11	1	27.45	0.10	0.68	26.77	26.67
11	2	45.37	1.40	0.68	44.68	43.28
11	3	48.00	1.44	0.68	47.31	45.87
11	4	109.00	5.70	0.68	108.31	102.61
11	5	107.65	6.69	0.68	106.96	100.27
11	1	48.84	1.45	0.62	48.21	46.75
11	2	49.62	1.36	0.62	48.99	47.62
11	3	41.18	1.14	0.62	40.55	39.40
12	1	108.78	6.60	-1.50	110.28	103.67
12	2	103.55	7.70	-1.50	105.05	97.35
12	3	53.49	1.37	-1.50	54.99	53.62
12	4	81.47	4.41	-1.50	82.97	78.56
14	1	42.25	1.14	0.47	41.77	40.63
14	2	57.01	1.60	0.47	56.53	54.93
14	3	69.49	2.80	0.47	69.01	66.21
14	4	80.81	3.65	0.47	80.33	76.68
14	5	99.35	5.05	0.47	98.87	93.82
14	6	94.93	5.26	0.47	94.45	89.19
14	7	86.05	4.67	0.47	85.57	80.90
15	1	96.06	5.15	0.47	95.58	90.42
15	2	90.74	4.42	0.47	90.26	85.83
15	3	81.49	4.02	0.47	81.01	76.99
15	4	82.94	3.09	0.47	82.46	79.37
15	5	83.86	3.81	0.47	83.38	79.57
16	1	79.32	4.17	1.63	77.68	73.50
16	2	99.11	5.32	1.63	97.47	92.14
16	3	104.99	5.85	1.63	103.35	97.49
16	4	108.18	6.35	1.63	106.54	100.19
18	1	8.85	1.00	1.74	7.10	6.10
18	2	12.06	1.52	1.74	10.31	8.78
18	3	16.61	2.32	1.74	14.86	12.54
18	4	19.04	3.32	1.74	17.29	13.96
18	5	25.71	4.41	1.74	23.96	19.55
18	1	32.00	7.10	1.74	30.25	23.14
18	2	35.91	6.53	1.74	34.16	27.62

TABLE V-6 (cont.)

TEST	INT	T	R WATER	R WIND	T-RWIND	T-RWIND -RWATER
18	3	28.00	7.88	1.74	26.25	18.37
19	1	20.63	3.41	3.82	16.80	13.38
20	1	17.50	1.58	1.87	15.62	14.03
20	2	16.72	1.72	1.87	14.84	13.12
20	1	9.52	1.20	1.87	7.64	6.44
25	1	53.48	1.11	0.48	52.99	51.88
25	2	53.36	1.17	0.48	52.87	51.69
25	3	75.42	2.90	0.48	74.93	72.02
25	4	88.24	3.89	0.48	87.75	83.85
25	5	96.36	6.06	0.48	95.87	89.80
26	1	51.23	1.60	-0.59	51.82	50.22
26	2	55.25	0.25	-0.59	55.84	55.59
26	3	37.45	0.83	-0.59	38.04	37.21
26	4	37.97	0.71	-0.59	38.56	37.85
28	1	21.46	0.92	1.61	19.84	18.92
28	2	33.14	2.35	1.61	31.52	29.17
28	3	33.27	2.22	1.61	31.65	29.43
28	4	46.38	6.43	1.61	44.76	38.33
28	5	46.23	6.33	1.61	44.61	38.27
28	6	46.31	6.39	1.61	44.69	38.30
29	1	53.81	7.24	1.74	52.06	44.82
29	2	62.37	10.75	1.74	60.62	49.87
30	1	78.16	14.28	0.98	77.17	62.89
30	2	80.94	16.32	0.98	79.95	63.62
30	3	90.19	17.93	0.98	89.20	71.27
31	1	61.47	4.91	1.10	60.36	55.45
31	2	60.42	5.50	1.10	59.31	53.80
31	3	47.10	4.32	1.10	45.99	41.67
31	4	43.46	3.95	1.10	42.35	38.40
31	5	67.72	8.93	1.10	66.61	57.68
32	1	26.44	1.41	0.33	26.10	24.68
32	2	43.48	3.39	0.33	43.14	39.75
32	3	69.08	15.36	0.33	68.74	53.37
33	1	33.80	1.78	0.30	33.49	31.71
33	2	34.22	2.57	0.30	33.91	31.34
34	1	18.67	0.66	0.50	18.16	17.50
34	2	25.31	0.96	0.50	24.80	23.84
35	1	27.84	1.23	-0.43	28.27	27.04
35	2	32.62	1.42	-0.43	33.05	31.62
35	3	79.13	12.12	-0.43	79.56	67.44
35	4	51.92	7.58	-0.43	52.35	44.77
35	5	57.19	6.24	-0.43	57.62	51.37
35	6	52.94	5.86	-0.43	53.37	47.51
35	7	51.52	6.16	-0.43	51.95	45.79

TABLE V-7

RESULTS OF REGRESSION ANALYSIS

$\mathcal{L}$ (BASED UPON $\Sigma T-R_{wind}-R_{water}-R_{CF}-R_{SC}$)

VS V AND $\overline{SIGND}$

VARIABLE	MEAN	STANDARD DEVIATION	CORRELATION X VS Y	REGRESSION COEFFICIENT	STD. ERROR OF REG. COEF.	COMPUTED t VALUE	95% CONFIDENCE LIMITS ON REGRESSION COEFFICIENTS HIGH	LOW
V²	3.45828	6.36768	0.94846	27.97963	3.65258	7.66022	35.21173	20.74753
V	1.42694	1.19693	0.93748	85.71081	15.82510	5.41613	117.04450	54.37712
V·$\overline{SIGND}$	704.68762	1208.22021	0.88912	-0.04268	0.01601	-2.66532	-.01099	-.07437

DEPENDENT

$\mathcal{L}$* : 265.99249   238.65966

Intercept   77.00825

Multiple Correlation   0.95858

Std. Error of Estimate   68.73786

ANALYSIS OF VARIANCE FOR THE REGRESSION

SOURCE OF VARIATION	DEGREES OF FREEDOM	SUM OF SQUARES	MEAN SQUARES	F VALUE
Attributable to Regression	3	7065705.01367	2355235.00683	498.47357
Deviation from Regression	132	623686.12646	4724.89454	
TOTAL	135	7689391.01171		
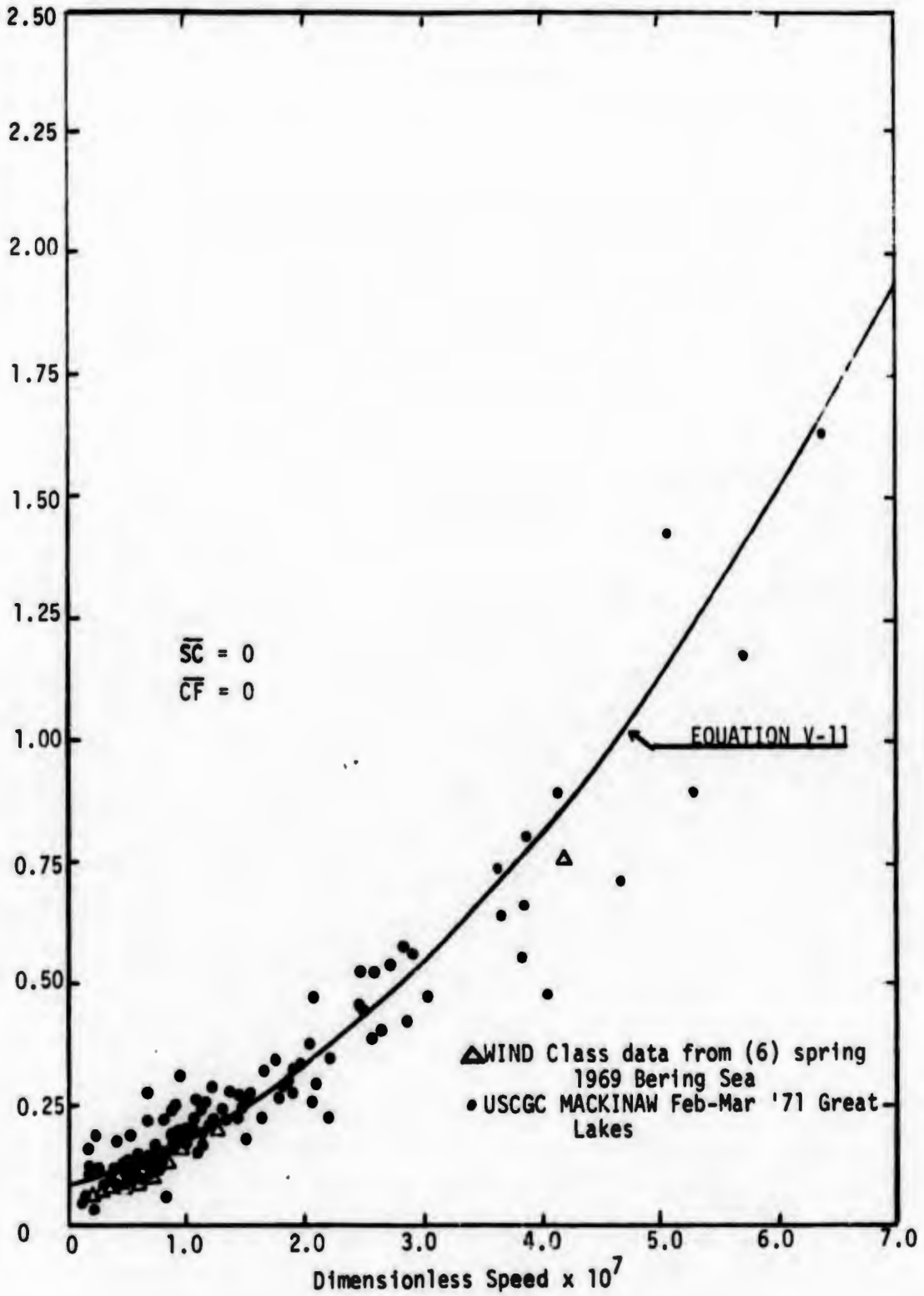
Figure V-4

Dimensionless Load (based upon $\Sigma T - R_{wind} - R_{water} - R_{SC} - R_{CF}$)
vs. Dimensionless Velocity
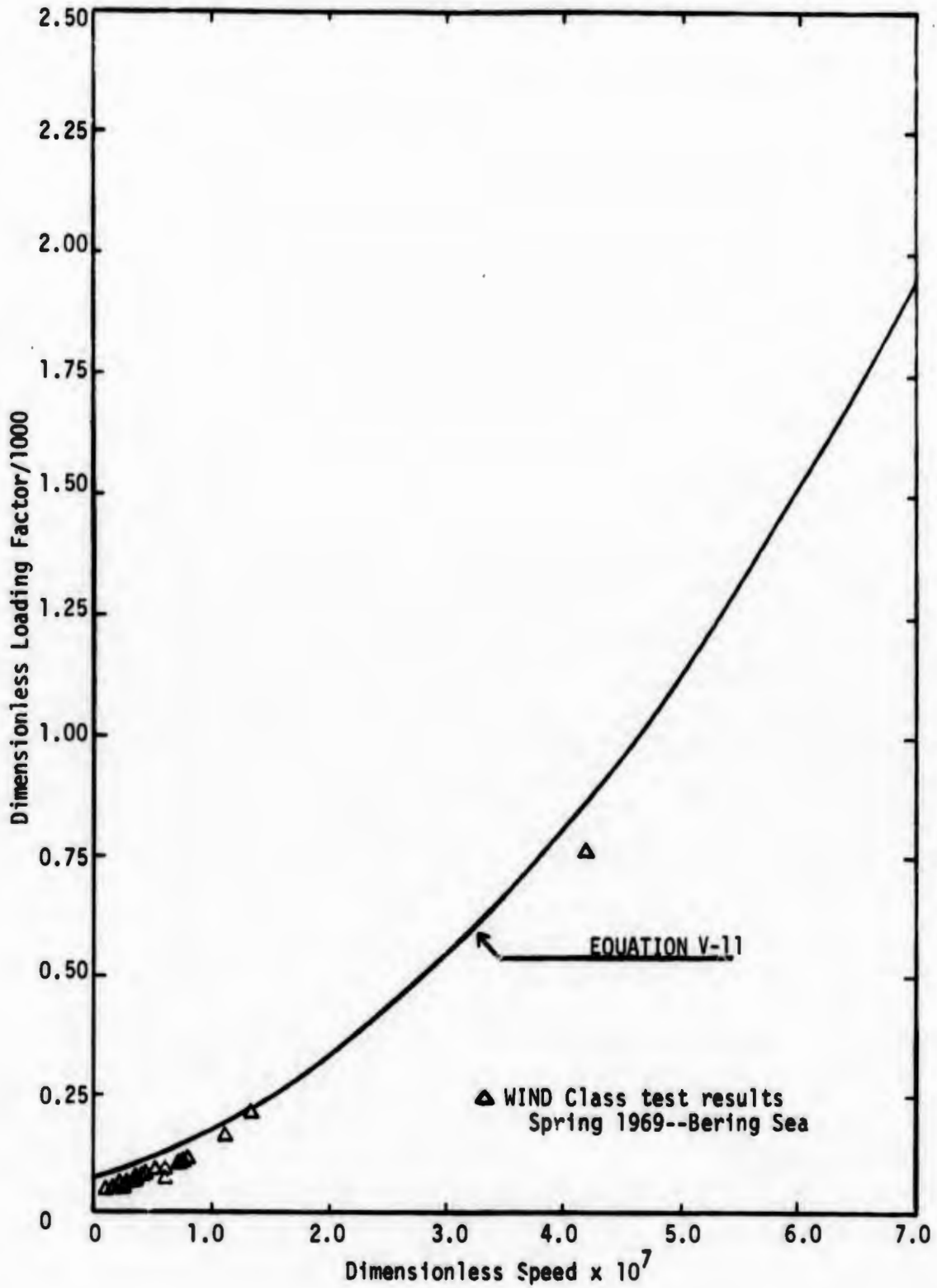
Figure V-5

Dimensionless Load vs. Dimensionless Velocity

to dimensionless numbers ($\mathcal{L}$, V, and $\overline{\text{SIGND}}$). The resulting data have been plotted on Figure V-4. The plot indicates that the dimensionless load ($\mathcal{L}$) for the WIND Class Icebreaker is almost identical to that of the USCGC MACKINAW for similar values of V. The data for both the MACKINAW and WIND Class full scale tests which is plotted in this figure, are for identical situations (zero snow cover and zero power on the bow propeller) except for forebody shape and ice strength. The mean value of ice flexural strength for the WIND Class tests was 3.4 kg/cm^2, while the mean value for the MACKINAW trails was 9.04 kg/cm^2. It is apparent that despite the fact that the MACKINAW trials were conducted in ice 2.6 times as strong as the ice in which the WIND Class Icebreaker was tested, the dimensionless load as a function of V is almost identical for both ships. Figure V-5 shows WIND Class results plotted with equation [V-11] for clarity.

The difference in the shape of the two ships is quantified by Lewis and Edwards (7). The shape factors for zero speed resistance taken from (7) for the USCGC MACKINAW and WIND Class are respectively 1.52 and 1.65. This fact suggests that the low speed resistance of USCGC MACKINAW should be 7 percent lower than the WIND Class resistance (at equal values of beam). The effects of ice strength and shape cannot be determined from the experiments conducted on the USCGC MACKINAW and USCGC STATEN ISLAND. These effects fall within the limits of experimental accuracy. Nonetheless, the hypothesis that the resistance of an icebreaker is substantially dependent on the product of strength and ice thickness squared can be rejected on the basis of these experiments. The hypothesis of Kashteljan (4) and Lewis and Edwards (6) that the effect of strength is small seems to be supported by this experiment.

-57-

C. Resistance to Motion in a Broken Channel

Three test runs (13, 17, and 27) were made in the channel produced during previous continuous icebreaking tests (12, 16, and 26). The ship speed and powering data were accumulated in a manner similar to that of the continuous icebreaking tests. Table V-8 lists the results of these tests. The channel breadth and percent ice coverage in the channel were the same for each test. Figures V-6 through V-8 show the results of the tests. Figure V-6 is a plot of the propeller thrust (estimated from the electrical propulsion performance parameters) versus ship speed. The continuous icebreaking thrust and the open water appendaged hull resistance are shown in Figure V-6 for comparison.

Figure V-7 shows the icebreaking propeller thrust multiplied by the thrust deduction factor obtained in model open water tests. The open water resistance from model tests is again plotted to permit a comparison to be made. Figure V-8 is a plot of "pure" ice resistance versus speed of advance, where pure ice resistance is the aggregate propeller thrust multiplied by open water thrust deduction factor and from which open water resistance has been subtracted. The plot exhibits a leveling off at high speeds. This may be illusory since the open water resistance may also behave in a peculiar manner in a narrow channel. Theoretically, the ship should be run in a clear narrow channel and the resistance obtained from such a test deducted from the total resistance in the broken channel.

Only three broken channel tests were conducted. The only variable which was changed appreciably was ship speed; hence, dimensionless analysis of the data was not undertaken.

-58-

TABLE V-8

BROKEN CHANNEL RESISTANCE DATA

Date 1971	Run No.	Inter. No.	Total SHP (Elec.)	Thrust (lbs), T	Ship Speed (ft/sec)	Ice Thick. (ft.)	$1-t$	$T(1-t)$ (lbs.)	Open Water Resist. R_{ow} (lbs.)	$T - R_{ow}$ (lbs)	$T(1-t)-R_{ow}$ (lbs)
03-02	13	1	1401	59,449	11.40	1.52	0.85	50,500	9,649	49,800	40,851
		2	4288	112,706	19.70		0.79	89,037	27,835	84,871	61,202
		3	5774	129,481	22.20		0.76	98,405	38,400	91,087	60,008
		4	7749	155,680	25.20		0.76	118,316	60,019	95,600	58,297
		5	10019	180,118	29.60		0.76	136,889	117,060	63,057	19,825
03-03	17	1	1211	53,155	7.67	1.64	0.85	45,181	3,505	49,570	41,596
		2	2147	70,768	11.64		0.85	60,152	9,649	61,119	50,503
		3	5544	126,000	16.75		0.82	103,320	24,700	101,300	78,620
		4	8094	161,011	18.97		0.80	128,808	30,555	130,456	98,253
03-09	27	1	643	35,757	7.62	1.51	0.85	30,393	3,585	32,172	26,808
		2	6940	155,259	24.54		0.76	117,996	53,789	101,470	64,207
		3	9700	186,420	27.20		0.76	141,679	79,871	106,549	61,808

Coupling Factor = 0

Percent Coverage = 75

FIGURE V-6 TOTAL PROPELLER THRUST VS. SPEED OF ADVANCE

USCGC MACKINAW Proceeding Through Broken Channel (75% Ice Particle Coverage

OPEN WATER RESISTANCE (Reference 10)

CONTINUOUS ICEBREAKING RESISTANCE (h = 1.5')

Run No. 13 h = 1.52'
Run No. 17 h = 1.64'
Run No. 27 h = 1.51'

Coupling Factor = 0

SHIP SPEED (ft/sec)

TOTAL PROPELLER THRUST (lbs × 10⁻³)
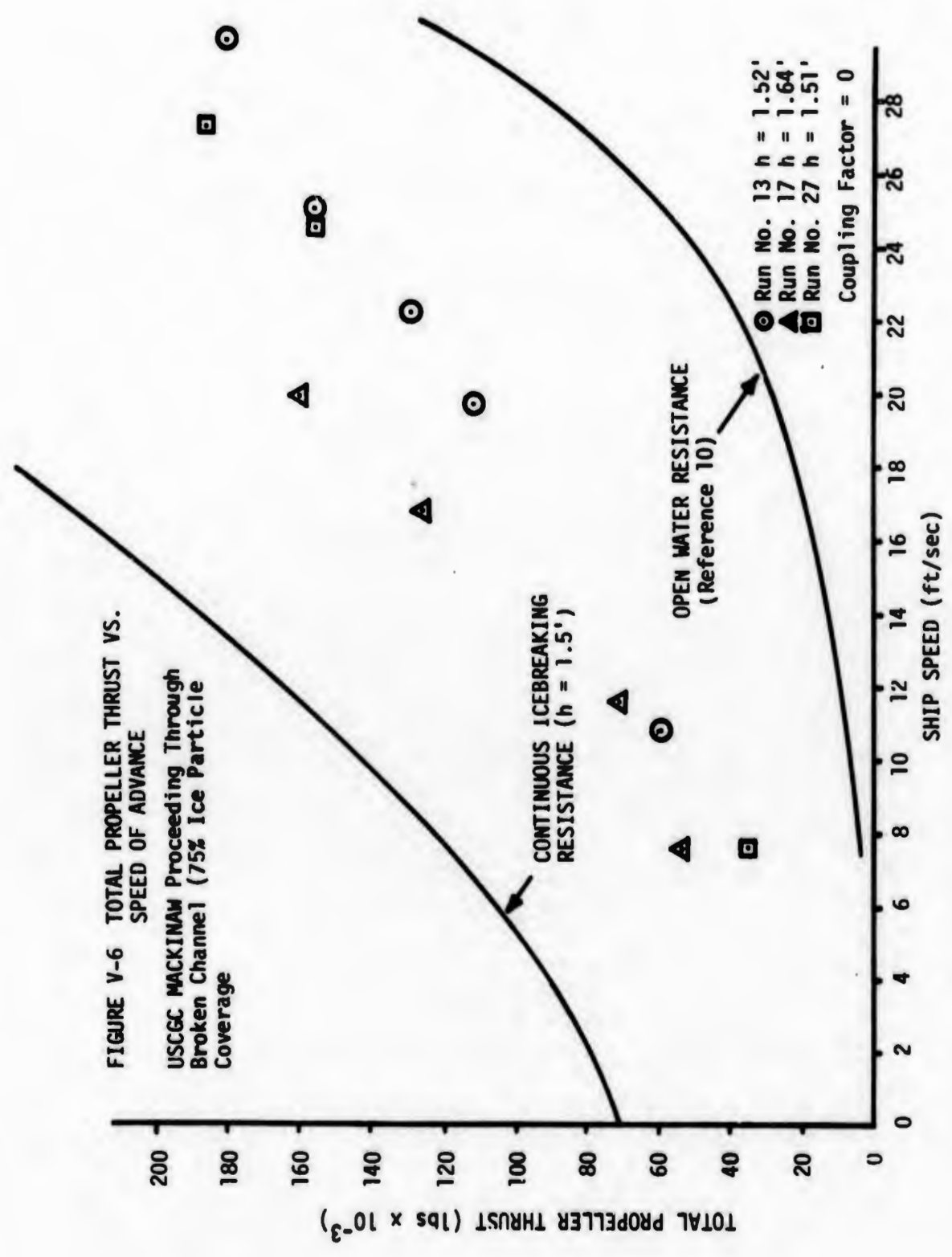
FIGURE V-7 PROPELLER THRUST x THRUST DEDUCTION FACTOR
VS. SHIP SPEED

USCGC MACKINAW Proceeding Through a Broken Channel
(75% Ice Particle Coverage)

OPEN WATER RESISTANCE
(Reference 10)

⊙ Run No. 13 h = 1.52'
▲ Run No. 17 h = 1.64'
▣ Run No. 27 h = 1.51'

Coupling Factor = 0

SHIP SPEED (ft/sec)

$T (1-t) (lbs \times 10^{-3})$

FIGURE V-8 TOTAL BROKEN CHANNEL RESISTANCE
LESS OPEN WATER RESISTANCE
VS.
SHIP SPEED
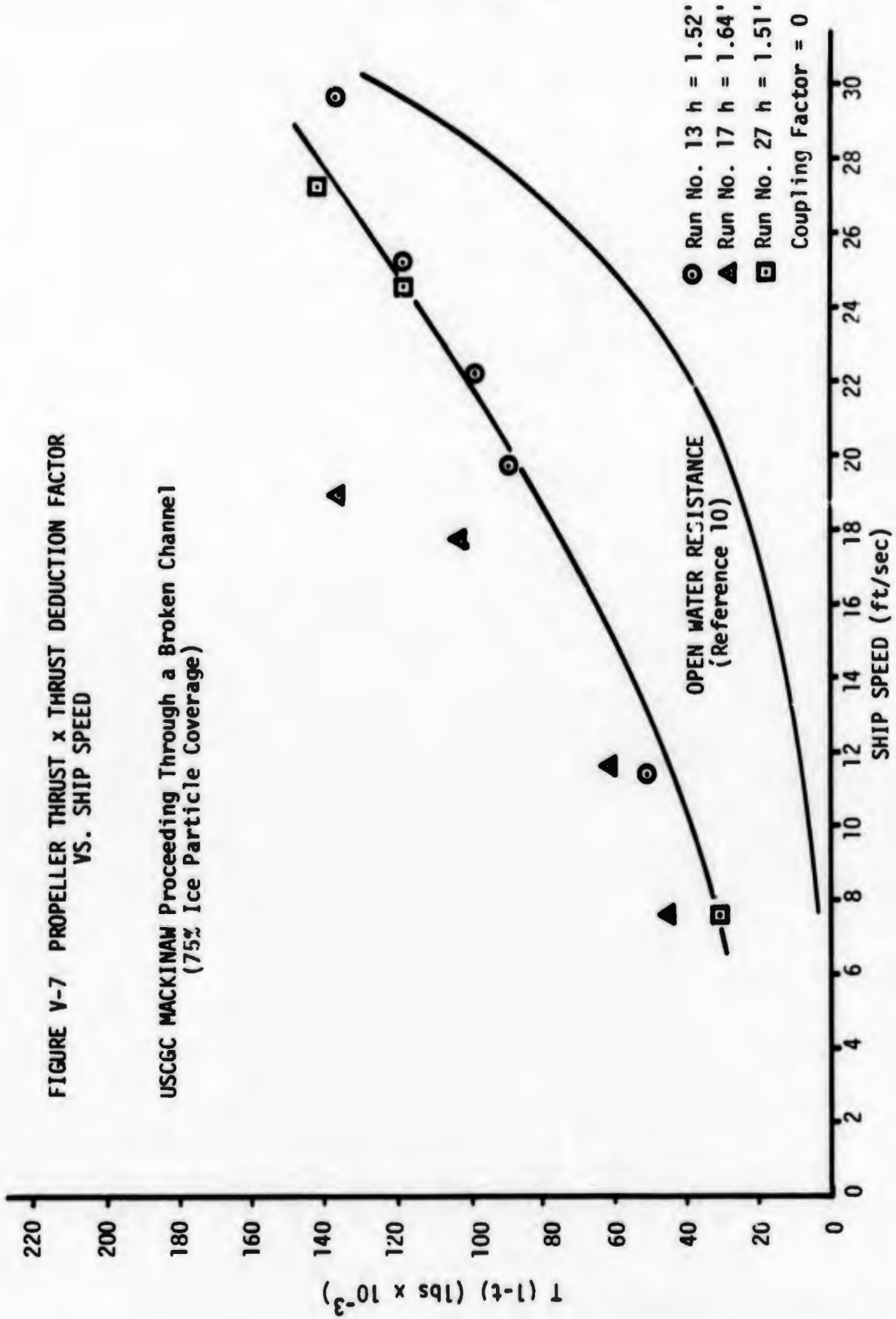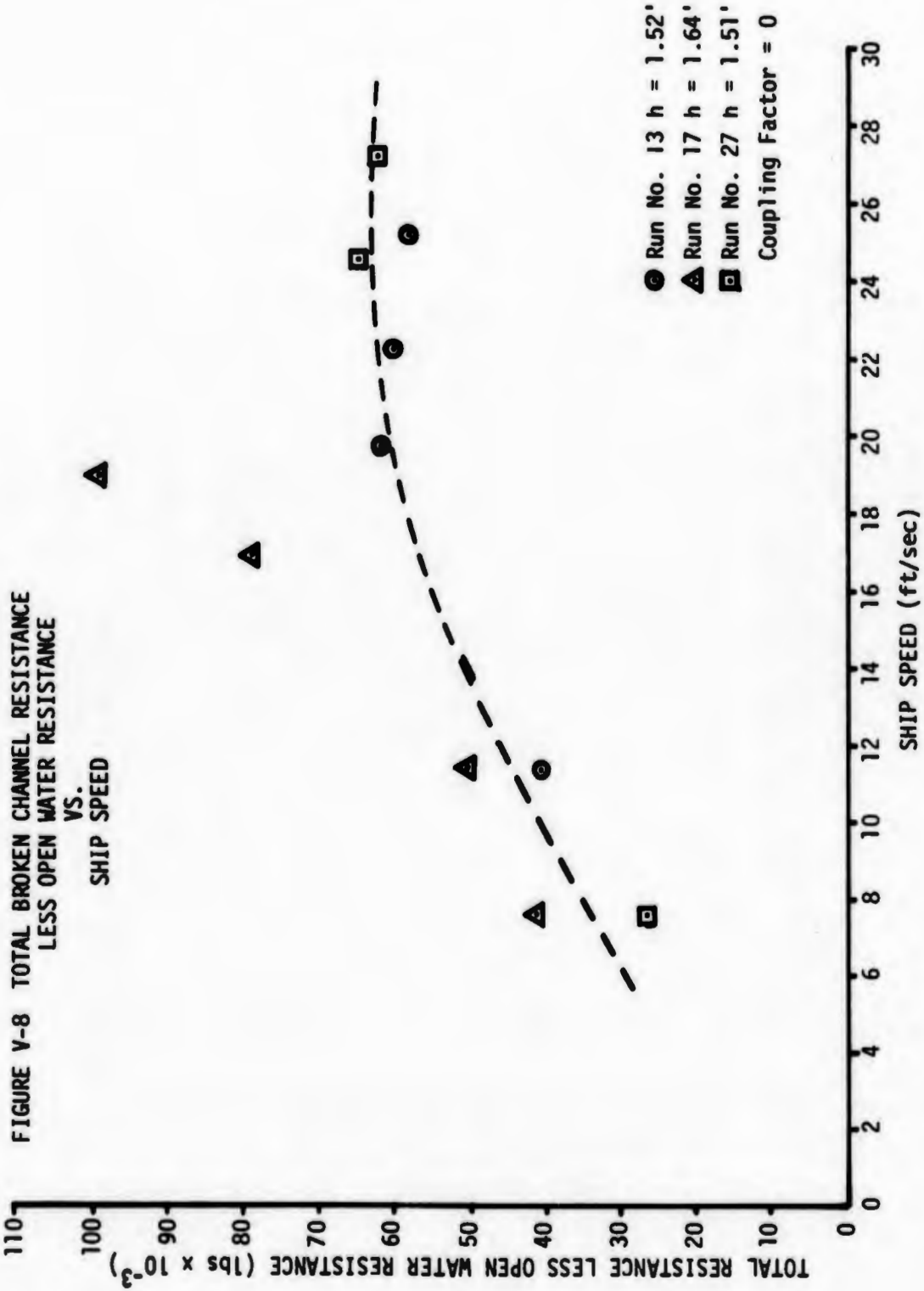
D. Ice Loads on the Hull

The computed impact force values were combined with observations of ice thickness, ship speed, and flexural strength of ice. The results are listed in Table V-9. The raw data were plotted as shown in Figure V-9. Regions of constant ice thickness were selected and the impact load plotted versus ship speed. These plots suggested that the load was a function of the product of ice thickness and ship speed. This is shown in Figure V-10. This obvious product relationship suggested that products of the dimensionless groups $(v_{ir}/\sqrt{gh})$ and $(\sigma_f/\rho_w gh)$ would reduce the data. A graphical analysis of the dimensionless data revealed that the dimensionless impact force $(F_{ice}/\rho_w gh^3)$ was highly correlated with the product of reduced Froude number and dimensionless strength. The dimensionless results of the ice impact load experiments are shown in Figure V-11.

The scatter in the data is considerable. However, considering that the impact load is dependent upon several variables which could not be measured, such as the angle of the cusp with which the hull makes contact and the elastic modulus, one would expect significant variation. Recent analysis reveals that the technique used to estimate impact load from the strain data would lead to scatter in the data and can be improved significantly for future analysis.

A best fit line to the data indicates that the dimensionless impact load may be expressed as follows:

$$\frac{F_{ice}}{\rho_w gh^3} = 50 \left[\frac{v_{ir}}{\sqrt{gh}} \cdot \frac{\sigma_f}{\rho_w gh} \right]^{1.2} \qquad [V-10]$$

Since v_{1r} in equation V-10 contains a direction cosine which may be calculated for any hull, this equation should be applicable for any hull shape. However, additional experiments similar to the one discussed here must be undertaken with different hull shapes before we will have confidence that shape is accounted for adequately by reducing ship velocity to the component normal to the hull surface.

TABLE V-9 (Cont.)

RESULTS OF ICE IMPACT EXPERIMENTS

Data Point No.	Ice Thickness (h) ft.	Velocity (v) ft/sec	Flexural Strength (σ_f) lb/in²	Impact Load (F_{ice}) lbs.	Dimen'less Impact Load $F_{ice}/\rho_w gh^3$	$\frac{\sigma_f}{\rho_w gh} \cdot \frac{v_{ir}}{\sqrt{gh}}$
19-1	0.32	12.28	137	6,200	3032.19	952.15
20-1	0.34	8.50	137	3,000	1223.20	600.61
25-1	1.71	6.28	128	12,800	41.02	36.61
26-3	1.46	5.16	128	10,600	54.58	38.29
28-2	0.86	10.77	126	31,200	786.09	173.87
29-1	0.90	17.14	126	13,400	294.57	259.26
29-2	0.82	19.96	126	9,400	273.21	347.50
30-1	0.84	22.11	126	13,000	351.49	370.96
30-2	0.82	23.12	126	11,000	319.71	401.75
30-3	0.87	23.79	126	25,000	608.41	378.54
31-5	0.94	18.61	126	20,400	393.60	263.71
32-3	0.88	22.65	107	8,800	206.94	300.30
33-1	0.87	9.42	56	13,600	330.97	66.12
34-1	0.87	4.42	56	7,600	184.95	31.05
35-7	0.87	15.93	56	10,200	248.23	112.80

TABLE V-9

RESULTS OF ICE IMPACT EXPERIMENTS

Data Point No.	Ice thickness (h) ft.	Velocity (v) ft/sec	Flexural Strength (σ_f) lb/in²	Impact Load (F_{ice}) lbs.	Dimen'less Impact Load $F_{ice}/\rho_w gh$	$\frac{\sigma_f}{\rho_w gh} \cdot \frac{v_{ir}}{gh}$
2-2	1.81	11.97	74	16,600	44.86	35.68
3-4	1.56	15.73	88	22,200	93.71	72.27
3-3	1.89	15.45	187	22,200	52.69	109.44
4-5	1.71	9.55	187	26,000	83.33	75.41
5-2	0.35	17.53	98	3,800	1420.34	847.81
5-3	1.65	13.70	98	27,800	99.18	62.08
5-4	1.77	3.53	98	12,000	34.67	12.87
5-5	1.60	8.38	98	18,800	73.55	39.22
5-6	1.66	12.03	98	20,000	70.06	56.53
6-4	1.22	13.53	139	18,000	158.85	142.66
6-6	1.28	17.71	139	15,600	119.20	173.87
6-2	1.24	18.45	139	19,800	166.42	190.18
7-1	1.18	1.57	137	7,000	68.27	15.90
7-1a	1.77	4.89	137	4,200	12.13	28.84
9-1	0.39	8.09	154	4,200	1134.60	524.28
18-1	0.32	5.89	137	3,992	1952.34	456.21
18-3	0.30	10.71	137	3,400	2018.04	914.85
18-4	0.34	12.13	137	4,000	1530.94	863.57

FIGURE V-9 SHIP SPEED
VS.
ICE THICKNESS

Subscript numbers indicate
impact load (lbs. x 10^{-3})
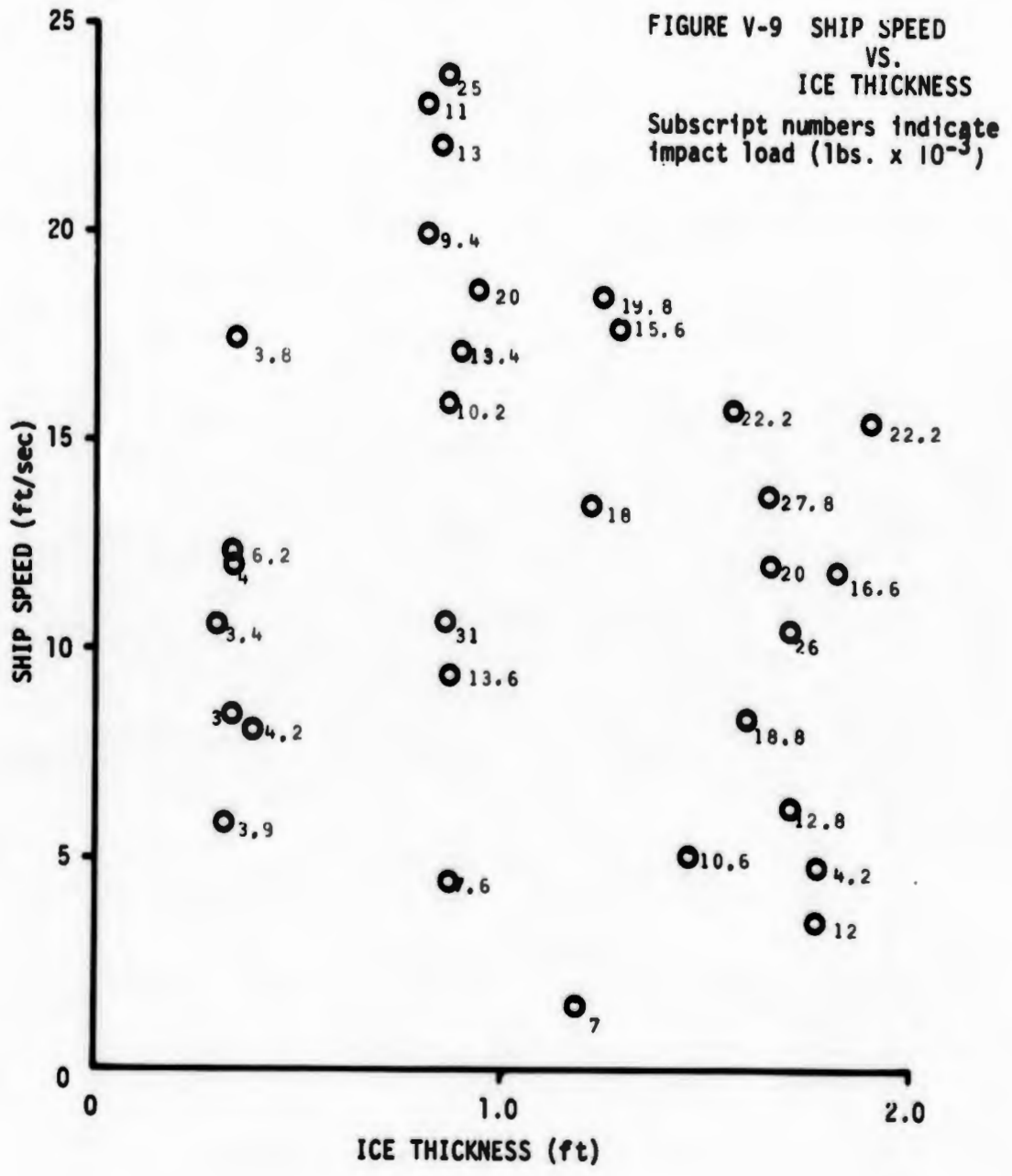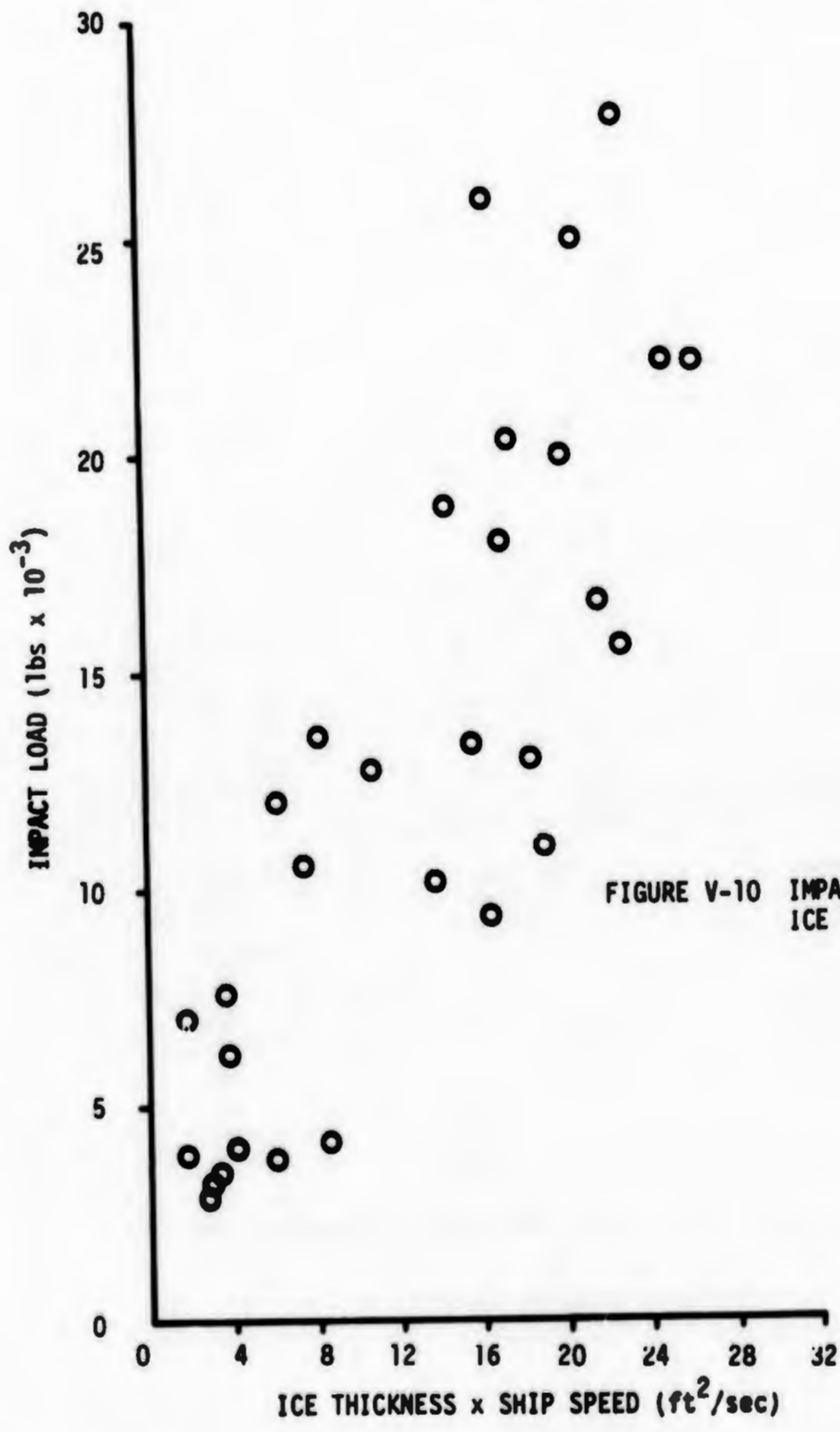
FIGURE V-10   IMPACT LOAD VS.
ICE THICKNESS x SHIP SPEED

FIGURE V-11   DIMENSIONLESS IMPACT LOAD
VS.
PRODUCT OF REDUCED FROUDE NUMBER
AND DIMENSIONLESS STRENGTH
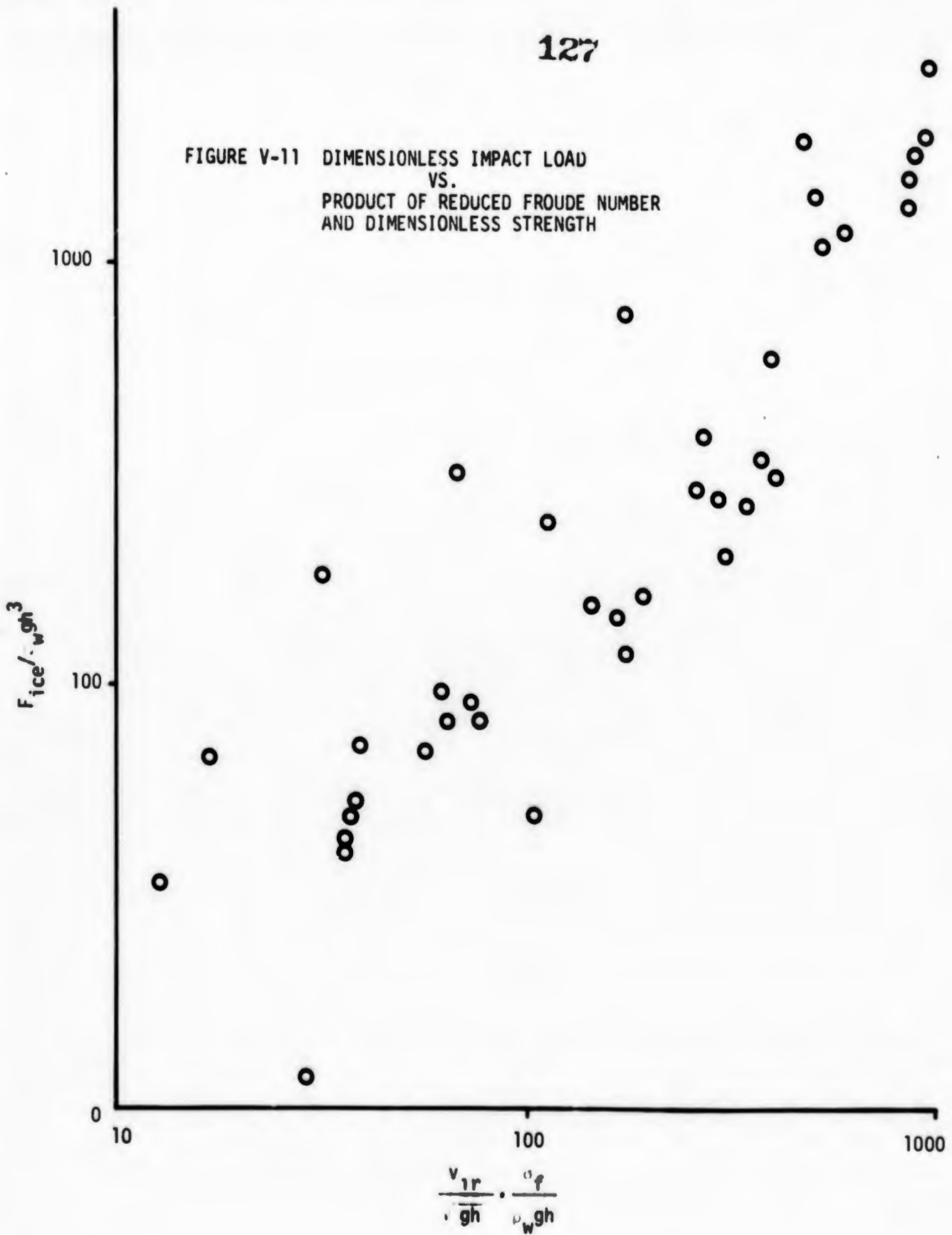
REFERENCES

1. Baier, L.A., Spooner, C.W., and McClure, A.C., Tests January 1948 on USCGC MACKINAW.

2. Comstock, John P., _Principles of Naval Architecture_, Society of Naval Architects and Marine Engineers 1967.

3. Gold, L.W., Use of Ice Covers for Transportation, 23rd Canadian Geotechnical Conference, Banff Alberta 1971.

4. Kashteljan, V.I., Poznjak, I.I., Ryvlin, A. Ja., Ice Resistance to Motion of a Ship, Sudostroenie Leningrad 1968.

5. Kline, S.J. and McClintoch F., "Describing Uncertainties in Single Sample Experiments", _Mechanical Engineering_, January 1953.

6. Lewis, J.W. and Edwards, R.Y. Jr., "Methods for Predicting Ice-breaking and Ice Resistance Characteristics of Icebreakers", Paper No. 5 SNAME Annual Meeting, November 1970.

7. Lewis, J.W. and Edwards, R.Y. Jrs., "Predicting Icebreaking Capabilities of Icebreakers", USCGC Headquarters, May 1969.

8. Schack, H. Jr., _Theories of Engineering Experimentation_, McGraw Hill Book Company, Inc. 1961.

9. Snedecor, George W. and Cochran, William G., _Statistical Methods_, Iowa State University Press

10. David W. Taylor Model Basin Tests of Model 3771, Test No. 2, February 23, 1943.

11. Popov, Faddeef, Kheisin, and Yakovlev, "The Strength of Ships Navigating in Ice" Sudostroenie, Leningrad, 1968

APPENDIX A

HULL STRAIN GAGE CALIBRATION

I. PURPOSE

During each experimental run performed in this study, strain data were recorded from an array of twelve strain gages on hull stiffeners between the Second Deck and the Platform Deck, as described in Section III of the body of the report. In order to relate the recorded strains to applied icebreaking loads, a calibration of the instrumented panel was performed by applying known loads and measuring the response of the strain gage array.

II. METHOD

The MACKINAW was moored at her pilings at Cheboygan, but moved so that a floating raft of four 12" x 12" timbers forty feet long could be positioned between the forward set of pilings and the instrumented hull panel. This raft had been constructed at the Soo and brought to Cheboygan aboard the MACKINAW. Figure A-1 illustrates the general arrangement of the raft and the ship.

The hull was loaded with a 20-ton capacity hydraulic jack set into an angle-iron frame on the raft. The frame had several different places into which the end of the jack could be set to vary the vertical location of load application. Also, the frame could be moved along the raft to vary the horizontal location. The working end of the jack was fitted with two steel pads to provide three possible variations in loaded are: 6, 36, and 144 square inches. The 36-in^2 pad was used for most of the tests.

Each calibration test run was performed by establishing a position for the jack, taking a set of zero and calibration readings on the gages, and then applying loads to the hull. At each arbitrary load level, the electrical output of each strain gage was read as a DC signal shift on an oscilloscope, and was also recorded on magnetic tape. Twelve test runs were made. A sample of the raw data is shown in Table A-1.

-A1-

III. DATA REDUCTION

The IBM subroutine REGRE was used to perform a regression analysis on the raw millivolt data from each gage for each load location, thus providing the best straight-line relationship between load and millivolts, and also defining the zero intercept. Since some of the strain gage channels were not absolutely zeroed before each test run, the zero intercept thus determined was then subtracted from the data, and the regression performed again including the calibration factors for converting millivolts to strain on each gage. A subsequent calibration of the hydraulic jack enabled a correction of the data to reflect the actual loads as a function of the pressure meter reading. Figure A-2 is a typical plot of the regression analysis for Case 7 for the 12 gages, and Figure A-3 is the computer output showing the regression coefficient (microstrain per ton) for Case 7, Gage No. 6. The final result of the calibration is shown in Table A-2 in terms of the sensitivity of each gage to each load position. Table A-3 summarizes the location of each strain gage, and Table A-4 shows the location of each load with reference to the boundaries of the panel, as illustrated in Figure A-4. These location data were measured from known boundaries such as the decks and the weld seam. Total girth distance from Second Deck to Platform Deck was scaled from Drawings CR121-1101-1 (Outside Plating, Stem to FR 69), and CR121-11030-3 (Transvers Framing Frames 22 to 34).

IV. DATA ANALYSIS

In order to gain perspective on the pattern of strain distribution, the data were plotted in various ways as functions of the panel geometry and load locations. A typical overall plot is shown in Figure A-5 for Case 2. Examining this and similar plots from the other cases, it was hypothesized that the distribution of strain along a vertical stiffener is essentially linear, but that the distribution horizontally is an exponential decay. This hypothesis is illustrated in Figure A-6, which is from the same data as Figure A-5 with the addition of the extrapolated sensitivity under the load, and the proposed distribution lines.

-A2-

The spatial distribution of strain shown in Figure A-6 agrees with what one might expect from a qualitative assessment of the stress distribution in the structure. Consider the case of the concentrated load on one of the frames. This load will be reacted by shear in the web which, in turn, feeds differential end-loads into the flanges of the frame. The reaction to these differential end-loads constitutes the bending resistance of the frame, and for a concentrated load the bending moment is linear. Thus, the distribution of end load (and strain) in the flange of the loaded frame should vary linearly with distance along the frame. The transfer of force from the loaded frame to adjacent frames must take place by shearing of the hull plating, and the theory of load transformation in stiffened skin construction* predicts a distribution of load with distance to adjacent frames which may be approximated by a cubic or exponential function. Thus, the horizontal strain distribution would be predicted to be of the type shown by Figure A-6.

The horizontal distribution was examined in more detail for the cases where the load was applied most nearly in the horizontal plane of a set of gages. Figure A-7 is a composite of the results of Cases 2, 4, and 11 for the middle row of gages, and shows that the distribution appears to have a discontinuity, but that the two parts appear exponential. Plotting them on semilog paper (Figure A-8) enables the derivation of a simple equation (as shown) for each part. The fact that the points from Cases 2, 4, and 11 fall generally on the same line indicates also that gages on any one frame in the matrix respond very much the same as gages on any other frame, and, thus, that data from one frame may be examined in detail and the results generalized. This conclusion is reinforced by study of the other cases.

The linearity in the vertical plane was investigated by looking at several cases where the load was applied at different vertical locations along the same frame. Figure A-9 shows the sensitivities of the gages extrapolated to the known location of the applied load.

---

*Stresses in Aircraft and Shell Structures, Paul Kuhn, McGraw-Hill, New York 1956, Chapter 4.

Figure A-9 indicates a number of useful things about the response of the hull along a vertical frame to applied external loads. First, the rate of change of strain versus distance from the load is quite uniform. For example, the slope of the lines for Cases 8 and 9 are almost identical, even though the load for Case 8 was applied considerably above that of Case 9. Only Gages 2 and 6 had measured responses to Cases 8 and 9 because the load was applied above Gage 2.

The second (and most useful) characteristics shown by Figure A-9 is the general uniformity of the extrapolated strain sensitivity under the load. For the 36-square-inch load areas, the values range generally between about 11 and 16 microstrain per ton, with an indication of a decrease toward the top end of the panel. Another observation is that the sensitivity is a function of load area, as might be expected; however, this observation is based on only one situation where three different areas were tried at the same location.

Finally, the lines joining the data points and the extrapolated sensitivity at the load locations have a quite symmetrical appearance, especially for Cases 2, 10, 11, and 12. (Note that Case 2 applies to Gages 3, 7, and 11.)

Taking another, and very comprehensive, approach to the distribution of strain data, the location data were transformed into absolute distances from the loads to the gages and the data plotted, as shown in Figure A-10. Here the effects of horizontal and vertical distribution are intermixed. Evidently, the exponential decay characteristic in the horizontal plane is much more pronounced than the linear vertical characteristic, resulting in a generally exponential form, but with considerable scatter.

Adjusting Hydraulic Jack Against the Hull
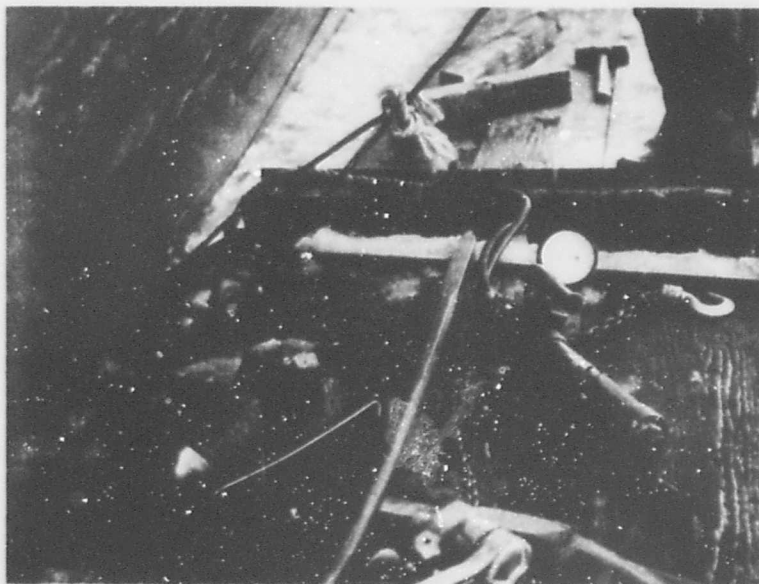
General View of Hull and Calibration Equipment

Figure A-1

Hull Strain Gage Calibration Set-up

TABLE A-1

Raw Calibration Data, Case 4

Date: 18 February 1971

Load Location: 5" forward of Frame 31
89" below weld seam

Oscilloscope Reading, Millivolts
Strain Gage

Load from Pressure Meter, Tons	1	2	3	4	5	6	7	8	9	10	11	12
0	0	0	0	0	0	0	0	0	0	0	0	0
5	20	210	130	5	25	420	150	10	20	120	80	40
6	20	240	150	5	20	480	180	20	40	170	90	40
3	20	140	100	20	30	260	110	20	30	90	50	30
2	20	85	60	15	20	120	60	20	20	40	40	30
5	30	230	150	20	30	400	170	20	40	120	90	40
4	30	190	130	15	30	320	135	20	30	110	70	40
6	30	280	190	15	40	460	210	25	40	175	100	40
3	20	140	95	15	25	240	110	20	30	80	60	30
4	20	180	130	20	30	290	140	20	35	95	75	35
5	30	250	200	20	25	380	210	25	35	120	90	40
Cal Signal	110	110	105	105	105	130	110	110	105	105	100	100
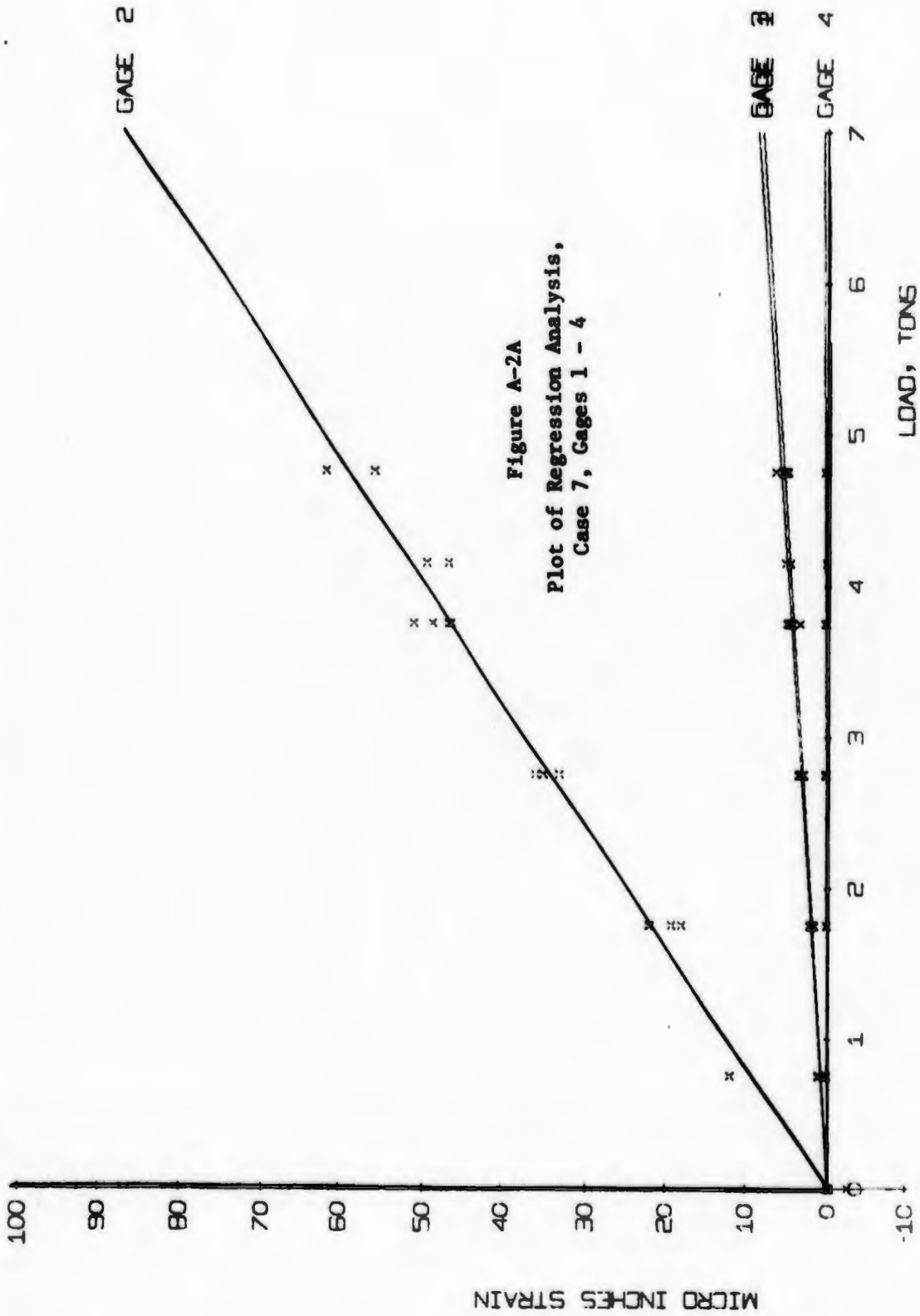
Figure A-2A

Plot of Regression Analysis,
Case 7, Gages 1 - 4

Figure A-2B

Plot of Regression Analysis,
Case 7, Gages 5 - 8

GAGE 6

GAGE 7
GAGE 5

GAGE 8

MICRO INCHES STRAIN

LOAD, TONS
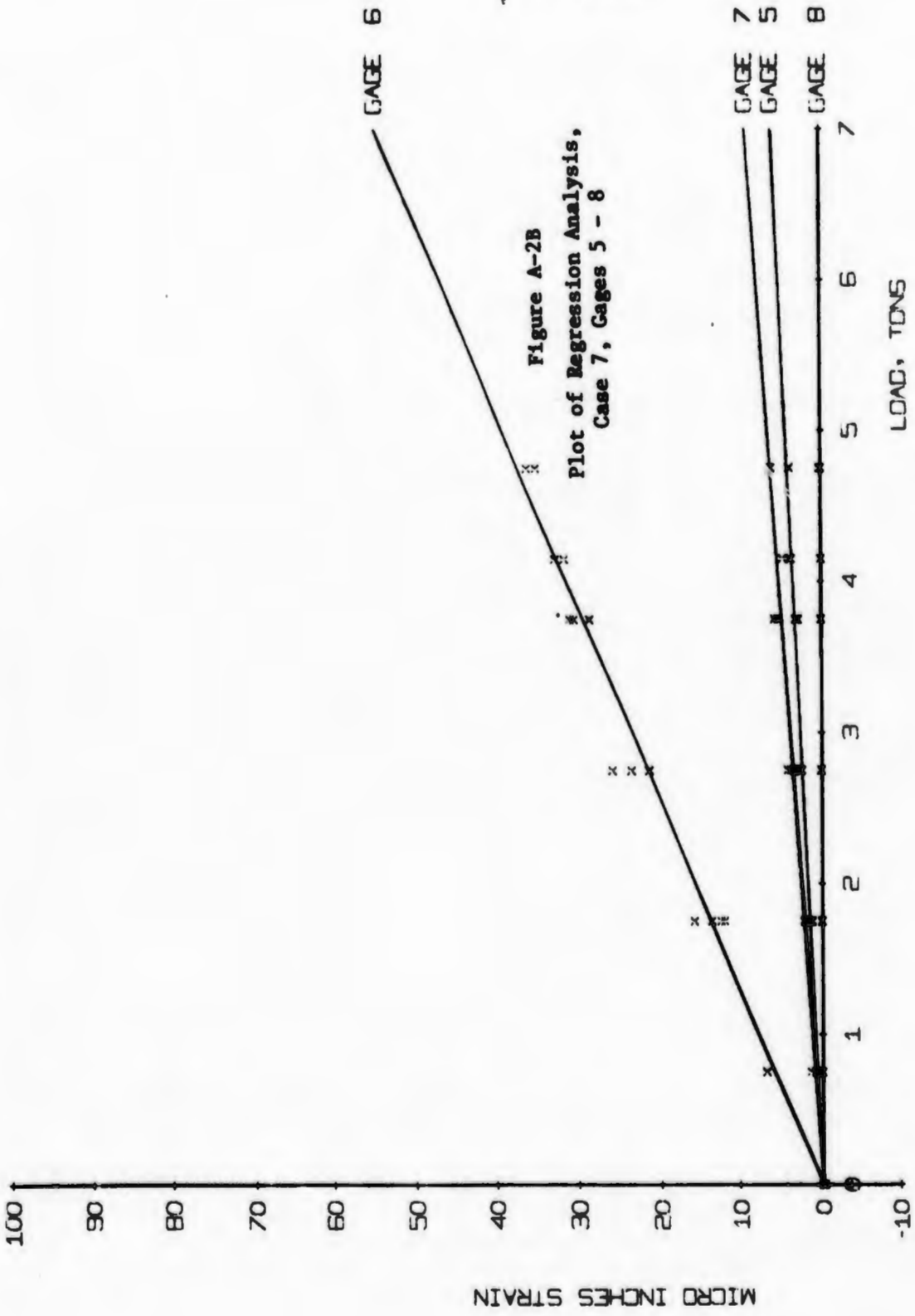
MACKINAW CALIBRATION   CASE 7

Figure A-2C
Plot of Regression Analysis,
Case 7, Gages 9 – 12
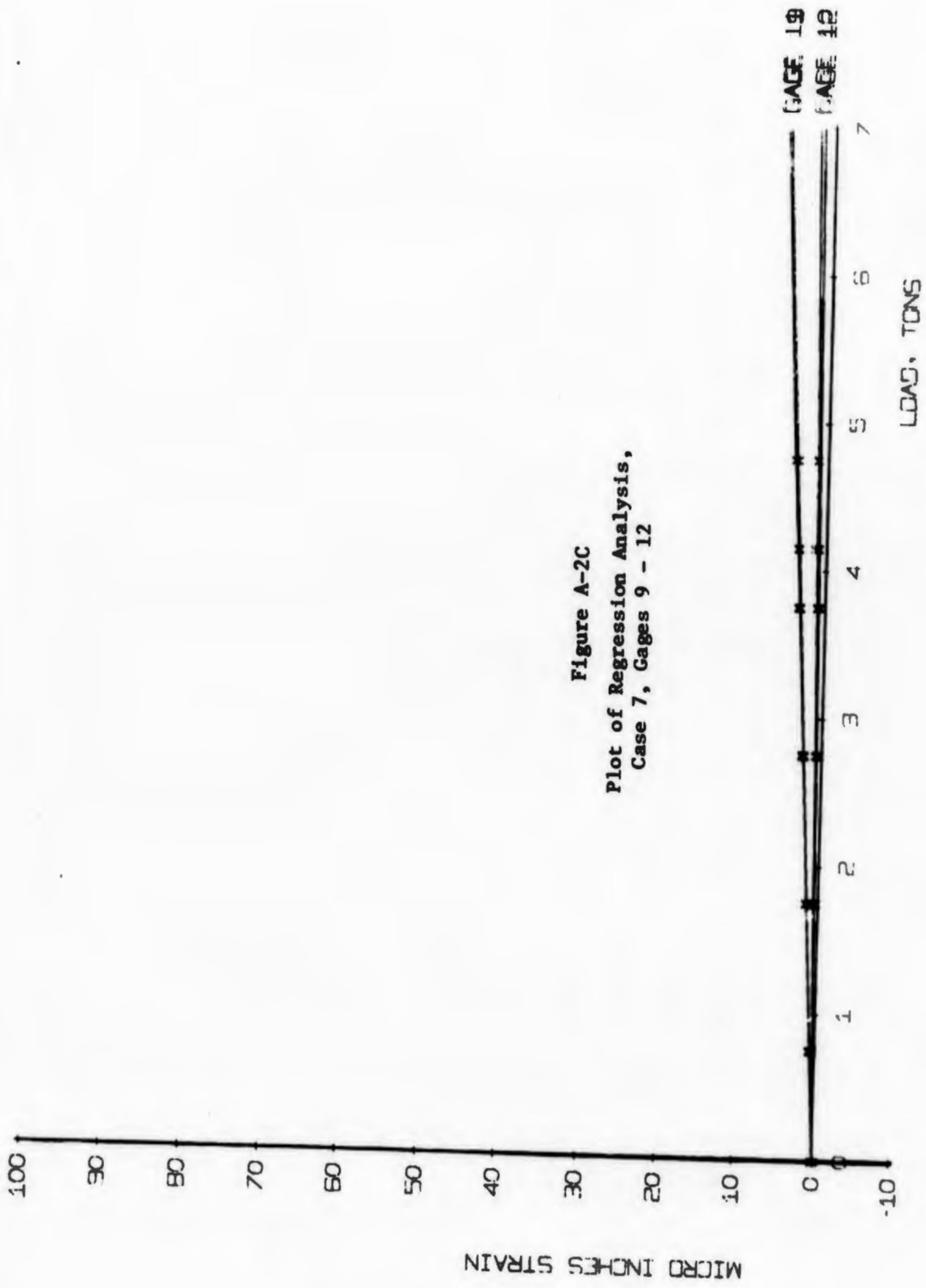
MACKINAW CALIBRATION   CASE 7

MACKINAW CALIBRATION CASE 7
ANALYSIS OF CALIBRATED STRAIN DATA -- MICRO STRAIN

VARIABLE NO.	MEAN	STANDARD DEVIATION	CORRELATION X VS Y	REGRESSION COEFFICIENT	STD. ERROR OF REG. COEF.	COMPUTED T VALUE
1	2.75263	1.40400	0.98727	7.80415	0.30491	25.59415

GAGE NO.

6	21.69191	11.09836

INTERCEPT   -0.00003

MULTIPLE CORRELATION   0.98727

STD. ERROR OF OF ESTIMATE   1.91621

ANALYSIS OF VARIANCE FOR THE REGRESSION

SOURCE OF VARIATION	DEGREES OF FREEDOM	SUM OF SQUARES	MEAN SQUARES	F VALUE
ATTRIBUTABLE TO REGRESSION	1	2161.04492	2161.04492	655.06042
DEVIATION FROM REGRESSION	17	3.29900		
TOTAL	18	2217.12793		

TABLE OF RESIDUALS

OBSERVATION	LOAD	Y VALUE	Y ESTIMATE	RESIDUAL
1	3.7	30.7543	29.2655	1.4987
2	3.7	28.5043	29.2655	-0.7612
3	3.7	28.5043	29.2655	-0.7612
4	3.7	30.3043	29.2655	1.0387
5	4.7	34.8043	37.0596	-2.2653
6	4.7	35.9293	37.0596	-1.1403
7	7.7	25.8043	21.4613	4.3429
8	2.7	23.5543	21.4613	2.0929
9	1.7	11.8543	13.6572	-1.8029
10	1.7	15.6793	13.6572	2.0220
11	0.7	6.6793	5.8530	0.8262
12	0.7	5.6793	5.8530	0.8262
13	2.7	21.3043	21.4613	-0.1570

Figure A - 3

Regression Analysis Computer Output,
Case 7, Gage 6

TABLE A-II

RESULTS OF REGRESSION ANALYSIS OF CALIBRATION DATA

Sensitivity, Microstrain per Ton

Strain Gage

Case	1	2	3	4	5	6	7	8	9	10	11	12
1	0.05	0.03	-0.02	2.66	0.15	0	0	2.76	0.12	0.19	0.18	1.63
2	0.02	0.88	6.45	0.84	0.17	0.78	13.43	0.77	0.29	0.57	2.30	0.76
3	0.12	0.83	9.46	0.97	0.13	0.81	9.94	0.97	0.26	0.74	1.27	0.87
4	0.43	4.85	3.35	0.12	0.51	7.41	3.64	0.27	0.67	3.12	1.85	0.71
5	0.28	5.20	3.51	0.05	0.25	5.71	3.37	0.08	0.40	1.65	1.40	0.23
6	0.18	5.59	3.68	0.02	0.15	3.27	2.82	0.08	0.33	0.38	0.66	0.29
7	1.14	12.37	1.22	0.07	0.84	7.80	1.28	0.01	0.82	0.28	0.85	0.20
8	1.18	7.95	0.98	-0.01	1.13	2.36	1.10	0	0.79	--	0.55	0.08
9	1.23	9.63	0.79	-0.37	1.15	4.06	0.83	-0.06	0.89	-0.81	0.75	0.14
10	1.40	6.81	1.43	0.06	1.08	8.00	1.51	0.26	1.26	3.21	1.06	0.56
11	0.70	7.30	0.66	-0.07	0.49	10.85	0.77	0.17	0.50	0.98	0.46	0.24
12	2.19	11.01	1.62	0	1.60	16.54	1.65	0.05	1.21	3.02	1.18	0.567

TABLE A-III

STRAIN GAGE LOCATIONS
(See Figure A-4)

Strain Gage	Vertical Girth Distance from 2nd Deck		Horizontal Location, Frame No.
	Absolute, in.	Normalized (to 114")	
1	64	0.562	28
2	61	0.535	30
3	62	0.543	32
4	62	0.543	34
5	82	0.720	28
6	78 1/2	0.689	30
7	80	0.702	32
8	80	0.702	34
9	99 1/4	0.870	28
10	96 1/2	0.846	30
11	98	0.860	32
12	98	0.860	34

TABLE A-IV

CALIBRATION LOAD LOCATIONS
(See Figure A-4)

Case	Load Area in.2	Vertical Girth Distance from 2nd Deck		Horizontal Location, Frame No.
		Absolute, in.	Normalized (to 114")	
1	36	72 1/2	0.636	35
2	36	74 3/4	0.656	32
3	6	67 1/2	0.592	32
4	36	77	0.675	5" Fwd of 31
5	36	70 1/2	0.618	5" Fwd of 31
6	36	51 1/2	0.451	5" Fwd of 31
7	36	66	0.575	30
8	36	48	0.421	30
9	36	57	0.500	30
10	144	75	0.658	30
11	36	75	0.658	30
12	6	75	0.658	30
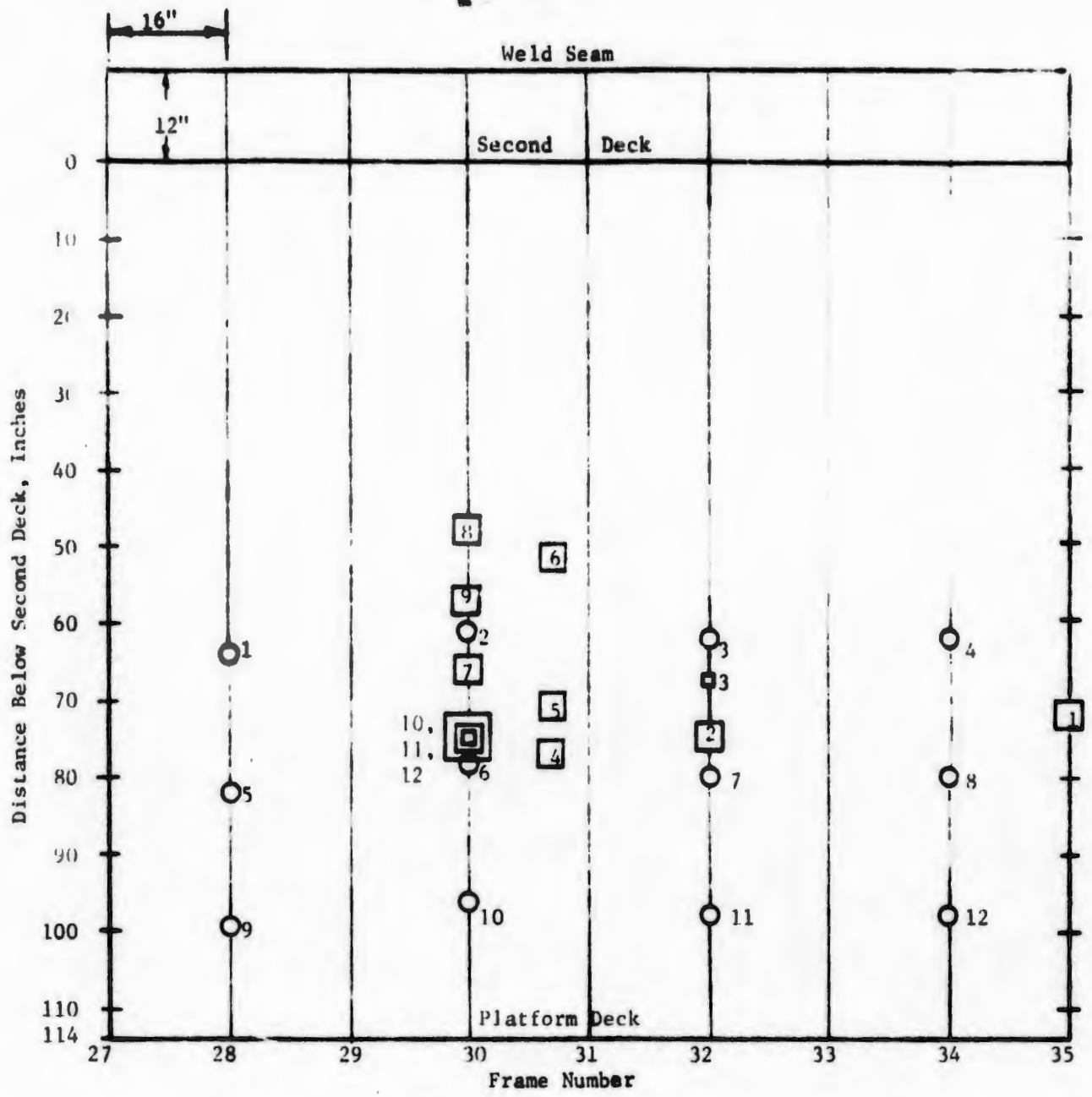
Figure A-4

Strain Gage and Load Locations
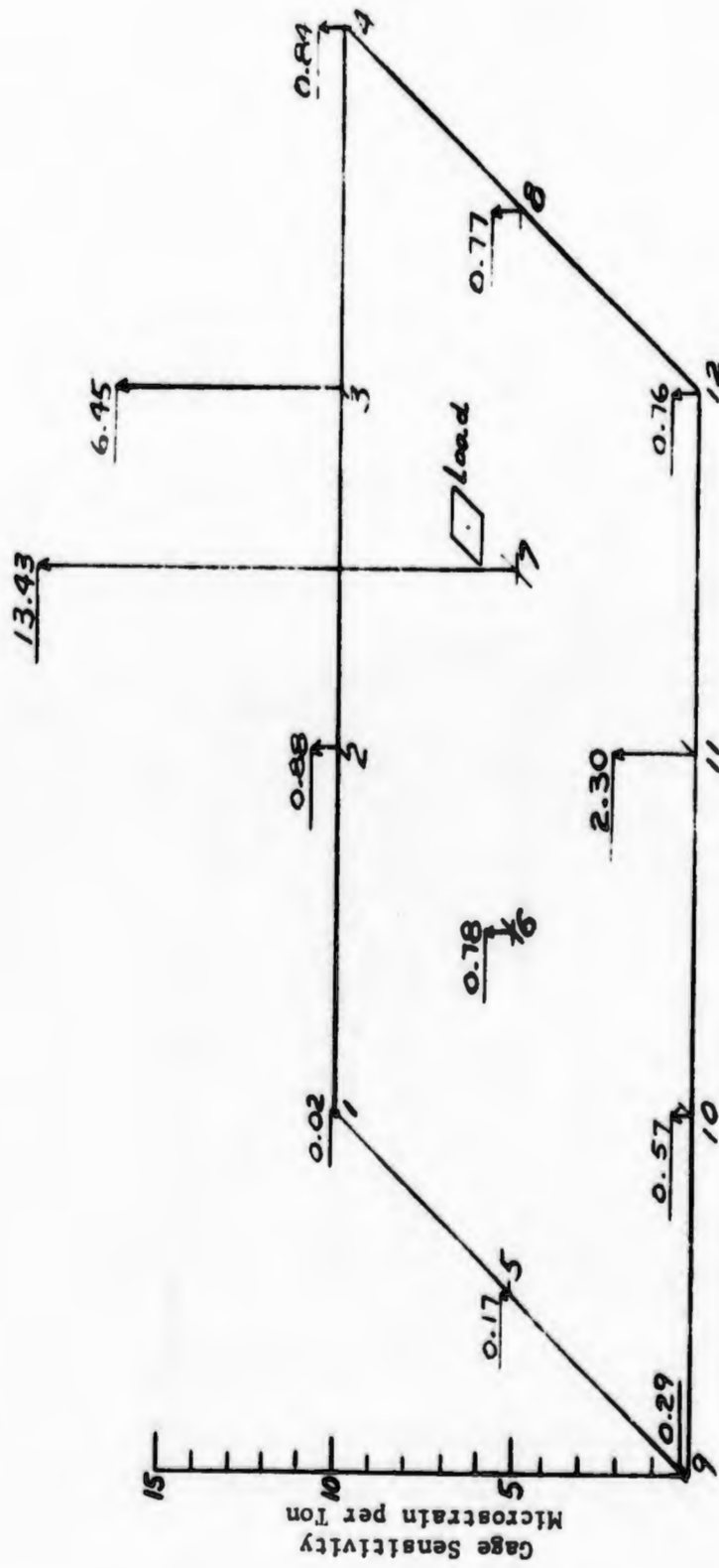
Figure A-5

Gage Sensitivities (microstrain/ton) to Applied Load, Case 2
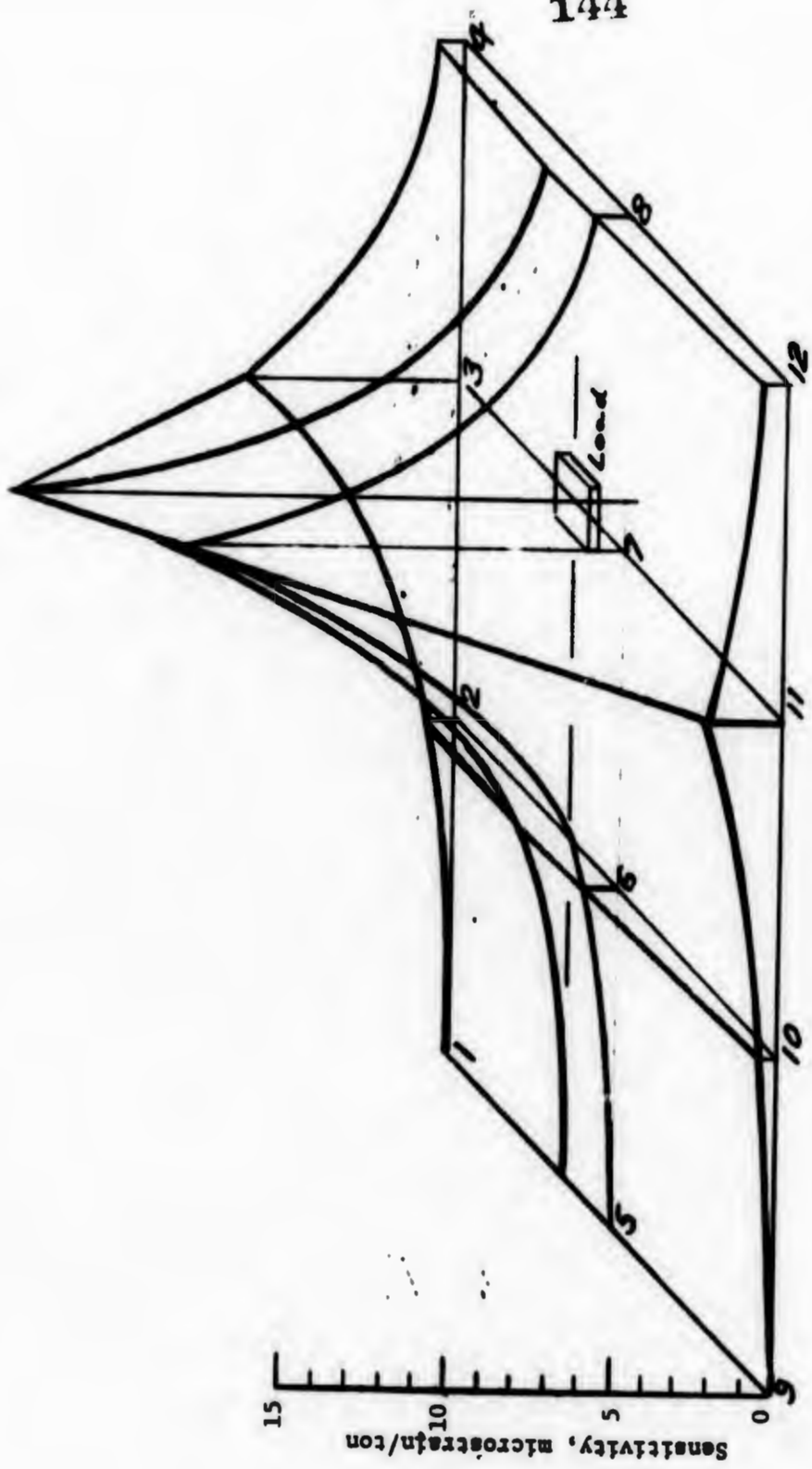
Figure A-6

Linear/Exponential Hypothesis of
Strain Distribution, Case 2
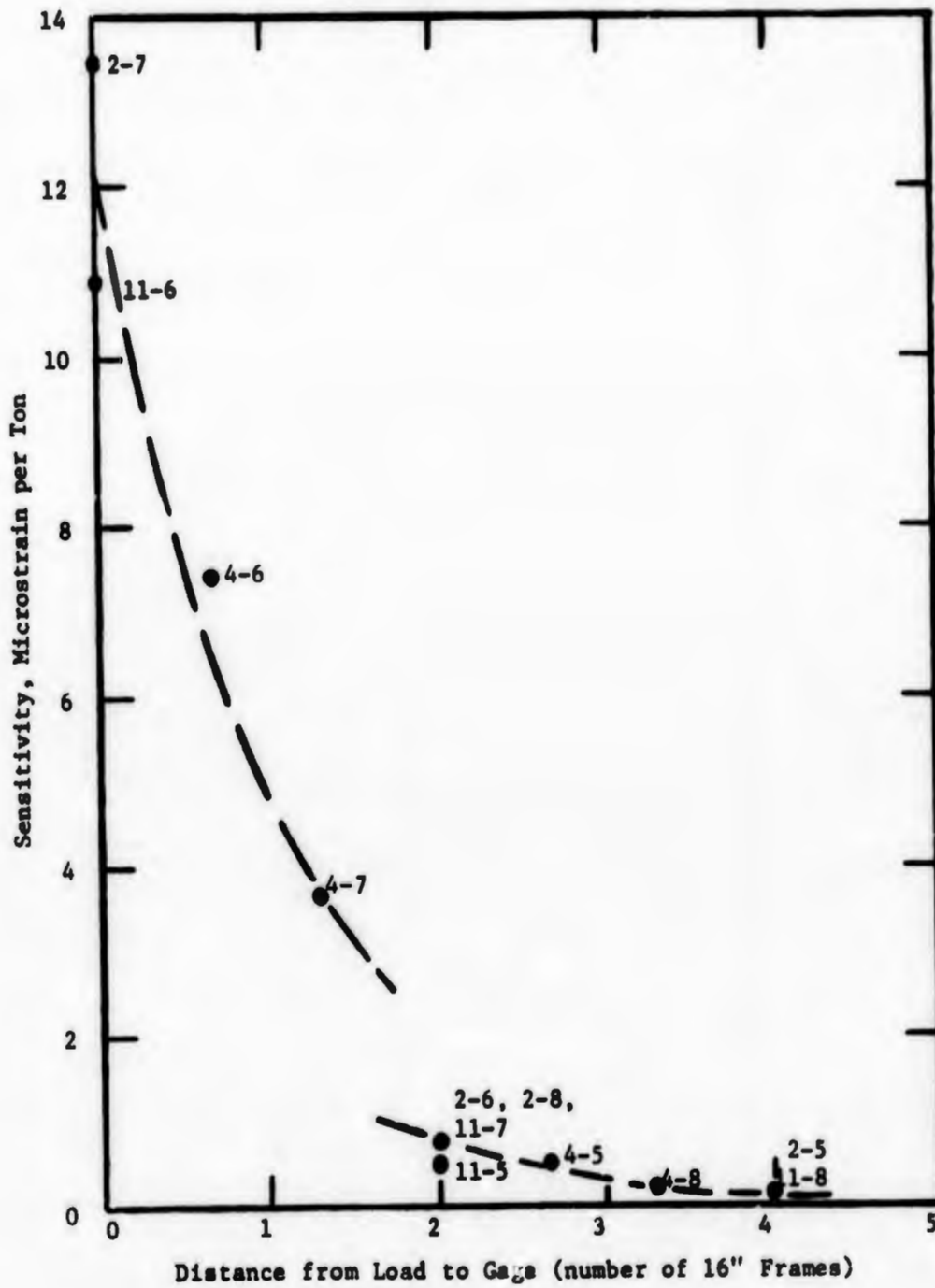
Figure A-7
Gage Sensitivity vs. Horizontal Distance, Cases 2, 4, and 11
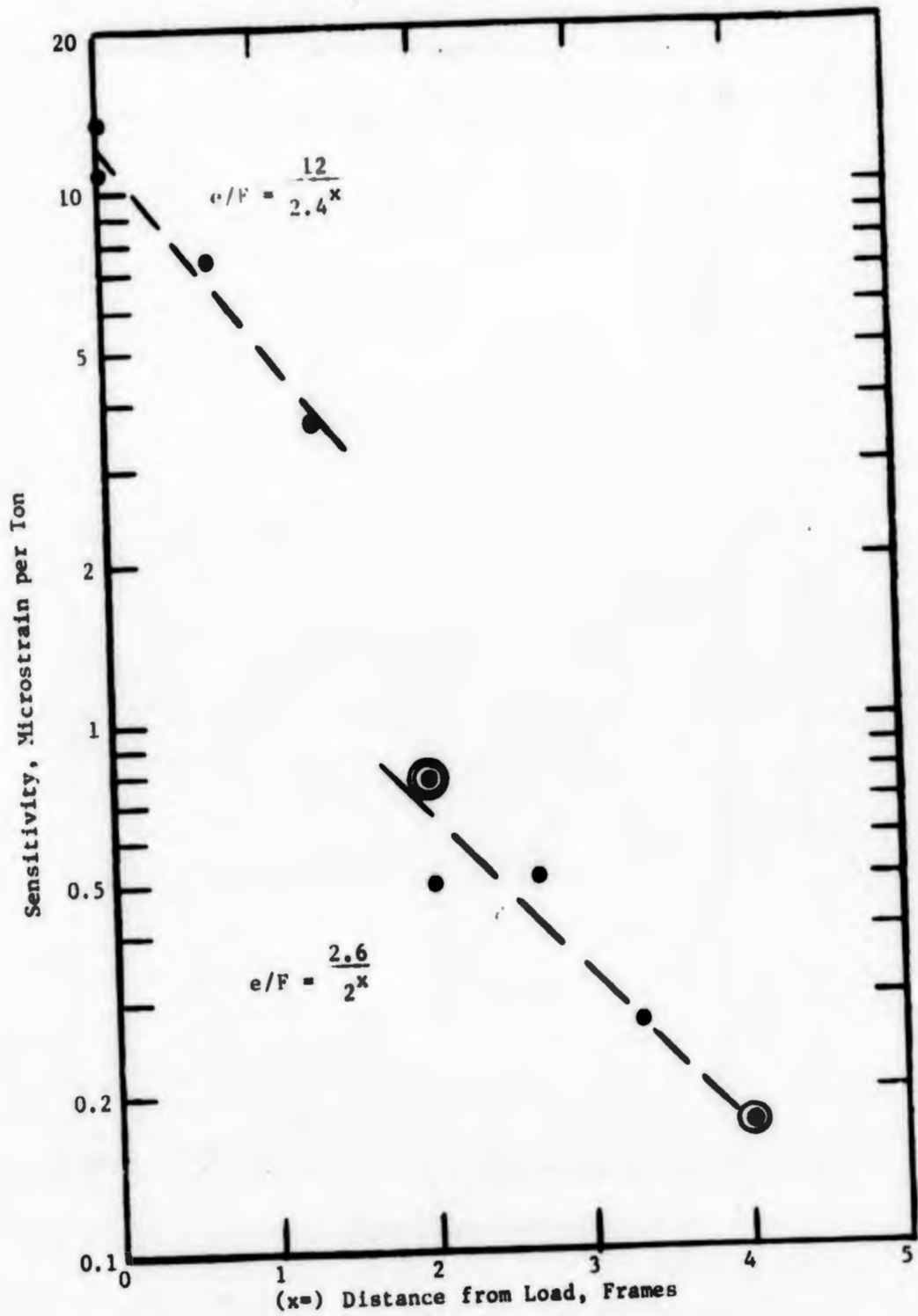
Figure A-8

Gage Sensitivity vs. Horizontal Distance, Cases 2, 4, and 11
(Semilog Plot)
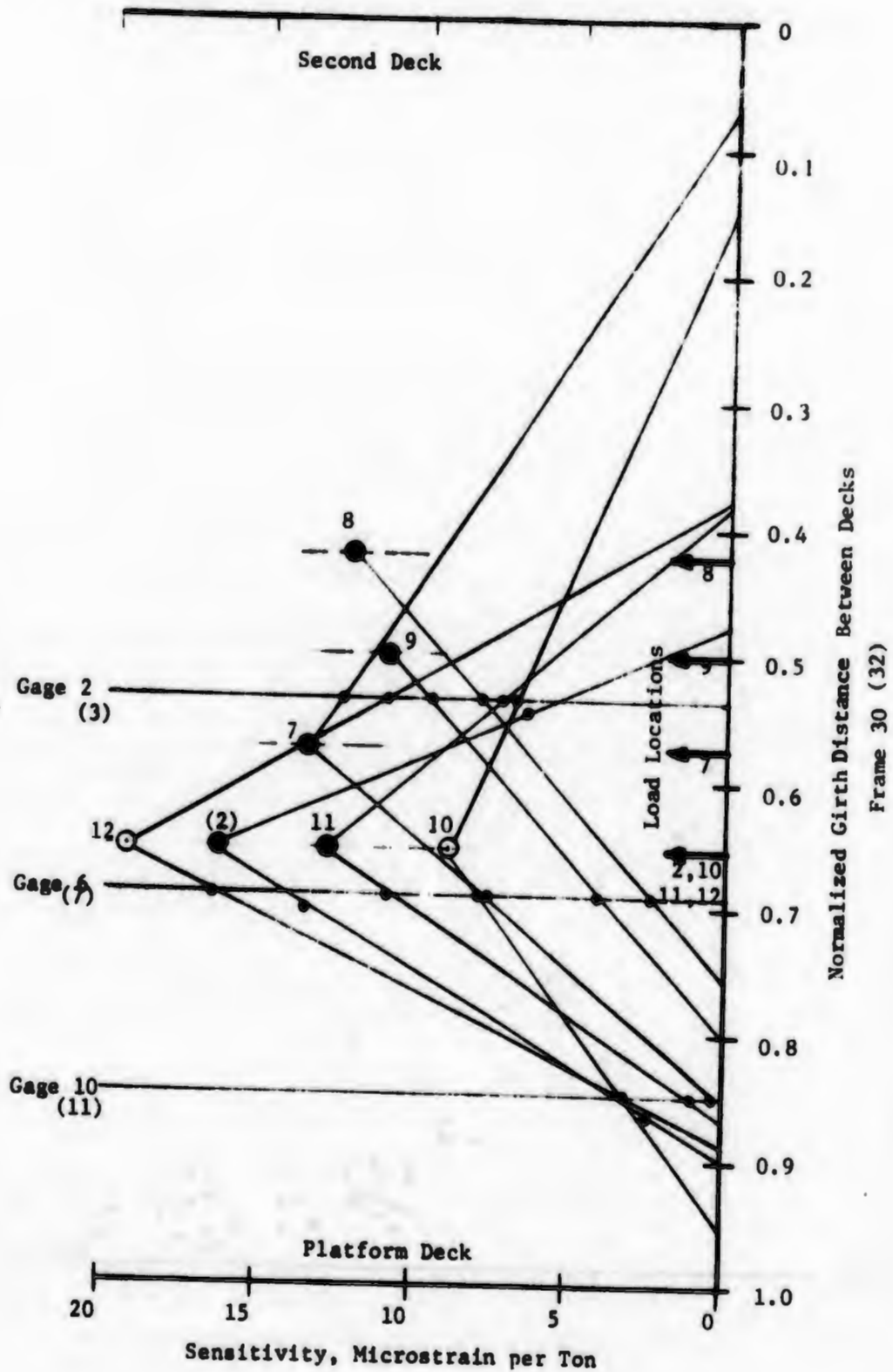
Figure A-9
Vertical Distribution of Strain Sensitivity
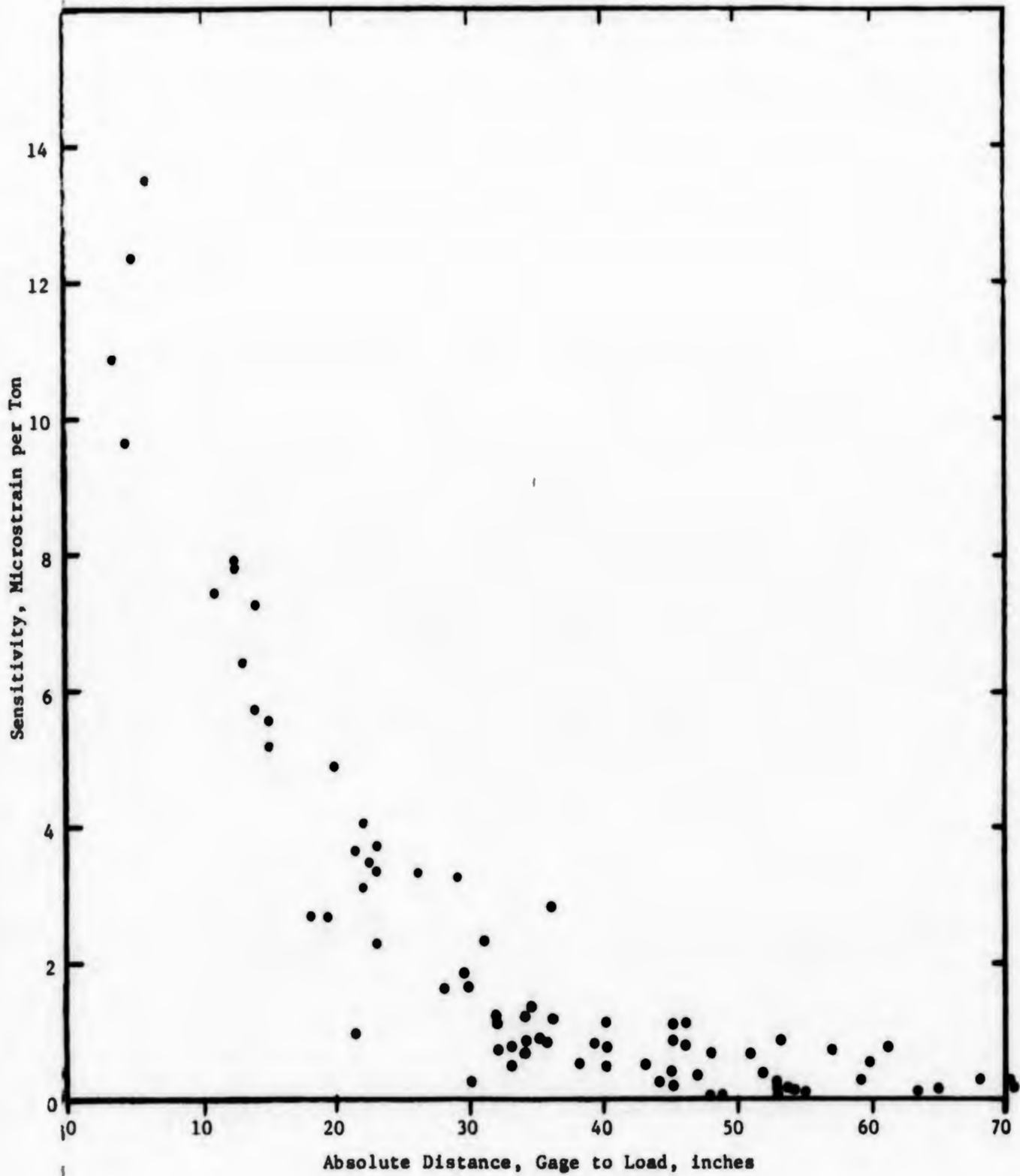
Figure A-10

Strain Sensitivity vs. Absolute Distance

APPENDIX B
EQUIPMENT SPECIFICATIONS

A. Strain Gages

    1. All gages except starboard stern shaft torque:

       Type: Kulite WUGP-1000-500 weldable semiconductor

       Resistance: 1000 ohms

       Gage Factor: +155

    2. Starboard stern shaft torque:

       Type: BLH FABD-25-35S6

       Resistance: 350 ohms

       Gage Factor: 2.0

B. Telemetry

    1. Bow shaft: NSRDC Type 499

    2. Port stern shaft: NSRDC Type 557

    3. Starboard stern shaft: Aerotherm Model 155

C. Tape Recorders

    1. Strain data: Teledyne Geotech Model 19429

          Channels: 14   Bandwidth: 0-50 Hz

          Speed: 0.3 ips

    2. Propulsion data: Ampex Model FR1300

          Channels: 14   Bandwidth: 0-625 Hz

          Speed: 1-7/8 ips

D. Oscillograph

   CEC Type 5-134

   Channels: 16   Galvanometers: 7-300 Series

The MACKINAW test program included the determination of forces on the hull due to ice loading by appropriately locating strain gauges on the hull. Initial discussion indicated a need to know the answers to a number of questions before arriving on the ship. Some of these questions were: (1) where should strain gauges be placed, both horizontally and vertically? (2) what magnitude of strain could be expected so that appropriate strain gauges could be obtained? (3) could knowledge of the distribution of measured strains be used to determine the force and area of the load causing those strains?

Three approximate methods were tried and compared with full scale tests of the USCGC WESTWIND (NSRDC Report 2134), but very little faith could be placed in the diversity of answers, most likely due to the poor modeling of a load on a stiffened plate.

To provide the required information with some degree of reliability and detail, use was made of the NASTRAN computer program. NASTRAN is a large, sophisticated computer program using a finite element method to analyze three dimensional complex structures. Due to its sophistication, it is complex and difficult to use. Details on the program and how to use it may be found in the following references:

> The Nastran User's Manual, NASA SP-222
>
> The Nastran Programmers Manual, NASA SP-223
>
> Nastran Demonstration Problem Manual, NASA SP-224
>
> The Nastran Theoretical Manual, NASA SP-221

Our initial model of the MACKINAW for use with the NASTRAN program considered a shell panel extending from Bulkhead 21 to Bulkhead 39 and from the First Platform to the Second Deck. This had been chosen as the region most likely to receive the major ice impacts. The hull had only slight curvature in this region and for the purposes of the model was assumed flat. This panel contained 20 stiffeners, all identical, heavy cant frames. The actual frames had a variation in their upper and lower ends due to the rapid change in width of the hull. However, a typical frame was assumed (Figure C-1) for all stiffeners in the model.

The shell plating was divided into a grid of 8" by 9" sections to provide coordinate information and structural characteristics. As can be seen in Figure C-2, the majority of these shell plate elements were quadrilateral. The numbers shown on the elements are the identification of both the element and the grid point at the lower left corner of the element.

The stiffeners were represented by bar elements between grid points. This type of element has no physical substance but represents the stiffener by its characteristic properties. Bar elements were numbered by adding 600 to the number of the lower grid point. Figure C-3 shows the properties of the stiffeners.

Edge fixity of the model was chosen to represent the best guess as to actual conditions. For this model the upper and lower edges were fixed and the forward and after edges (at bulkheads) assumed pinned. All grid points were constrained in rotation in the plane of the panel.

Since the elements formed a regular grid work, it was possible to prepare a short Fortran program to punch the majority of the data cards. The few additional cards were prepared by hand and combined with the computer punched deck.

This initial model was tested with three loads, applied separately in different locations. Each load consisted of a uniform pressure applied to 20 quadrilateral shell plate elements. A pressure of 637 psi represented the expected load from one meter thick ice and a ship speed of six knots. Loads A and C were located between frames 30 and 32, Load B between frames 23 and 25. Vertically, Loads A and B were located between the third and eighth grid lines above the platform deck, Load C between the fifth and tenth.

Results of exercising the model with these loads showed that the effects of the load were barely noticeable two frame spaces away from the edge of the load (Figure C-4). It was, therefore, desirable to reduce the extent of the model to reduce computing time. The reduced model extends from frame 26 to frame 34 using that portion of the initial model. This reduction of the model was offset, however, by adding to the model below the first platform to better model this lower region. This new model is shown in Figure C-5.

It was also felt desirable to represent the frame in more detail. This was done by duplicating the exact construction using plate elements as shown in Figure C-6. The extreme complexity of this model made it impractical in terms of computer time to do every frame in this manner. Therefore, only the center frame was done and the remaining frames left as before.

C-3

All load situations could be modeled by placing the load relative to this center frame with a load approaching no closer than two frame spaces to the edge of the model.

Fixity of the upper and lower ends of the frames proved to be one of the most difficult and arbitrary decisions. Inspection of the structure lead to a best guess that the upper end is pinned and rotates about grid point 1064 and that the lower end is fixed all along the lower edge of the frame.

This model was tested with Loads A and C above, then with other loads at various locations to represent possible actual ice loadings, and finally with loads approximating the ship calibration.

Figure C-7 shows micro-strain per ton of applied load for an eight ton load applied at grid point 286. This closely approximates location twelve on the actual ship calibration. Data points from the actual calibration show good correlation with the results of the NASTRAN model.

2ND DECK

FLANGE

WEB

SHELL PLATE

1ST PLTF.
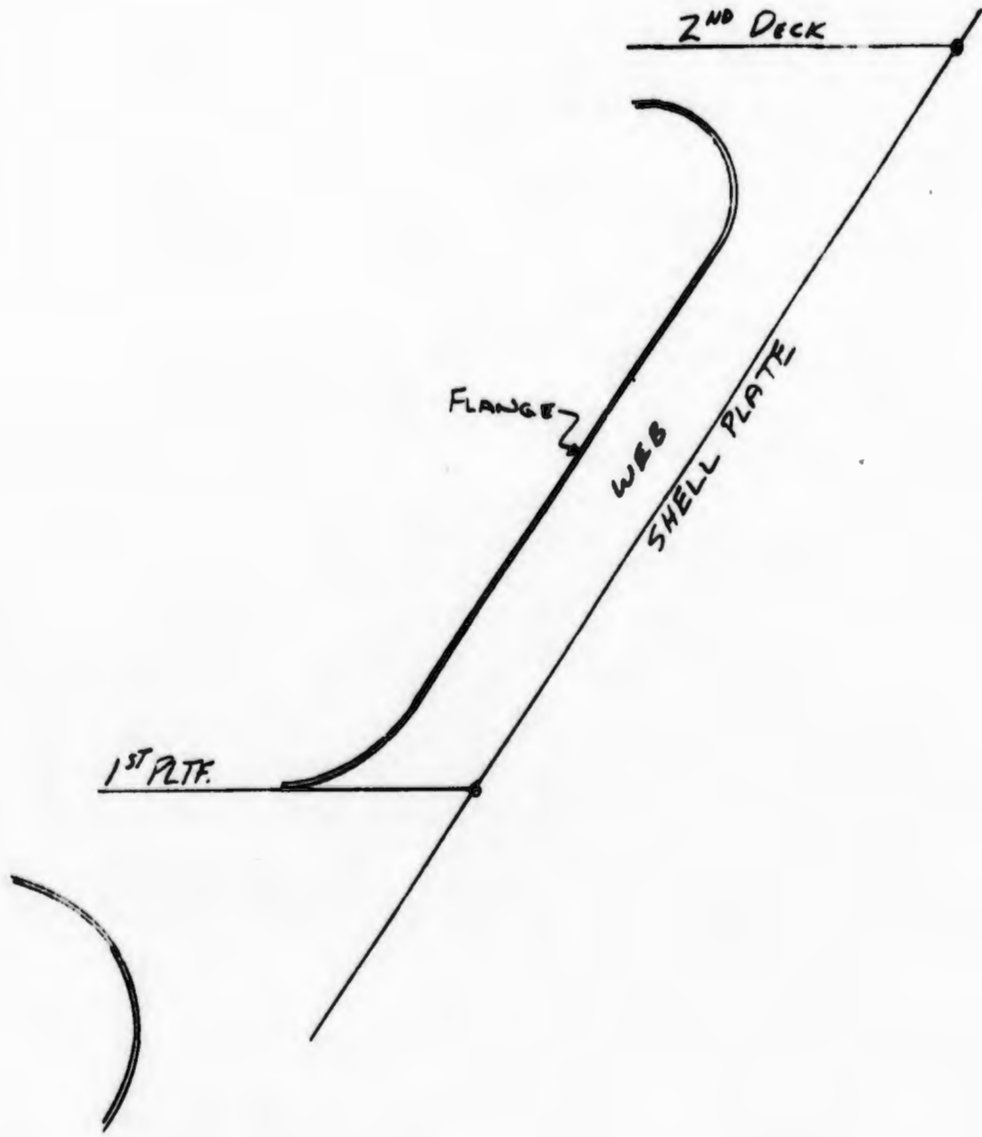
FIGURE C-1

TYPICAL FRAME CONFIGURATION
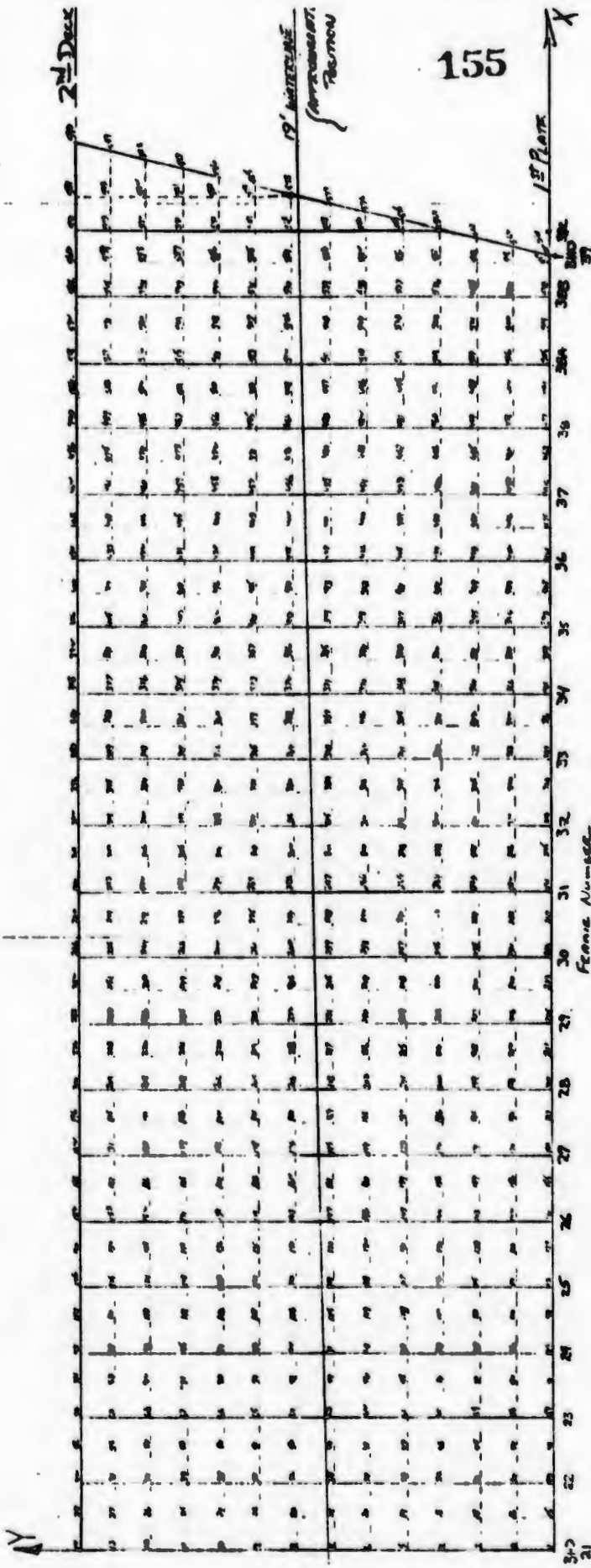
FIGURE C-2
INITIAL NASTRAN MODEL
SHELL PANEL

155

**Characteristics of stiffener only
without shell plate:**

Area: 6.75 in^2

Moment of Inertia

I_1 = 4.03 in^4

I_2 =113.5 in^4

Torsional Constant

J = 0.6845

Area Factors for Shear

K_1 = 0.445

K_2 = 0.555
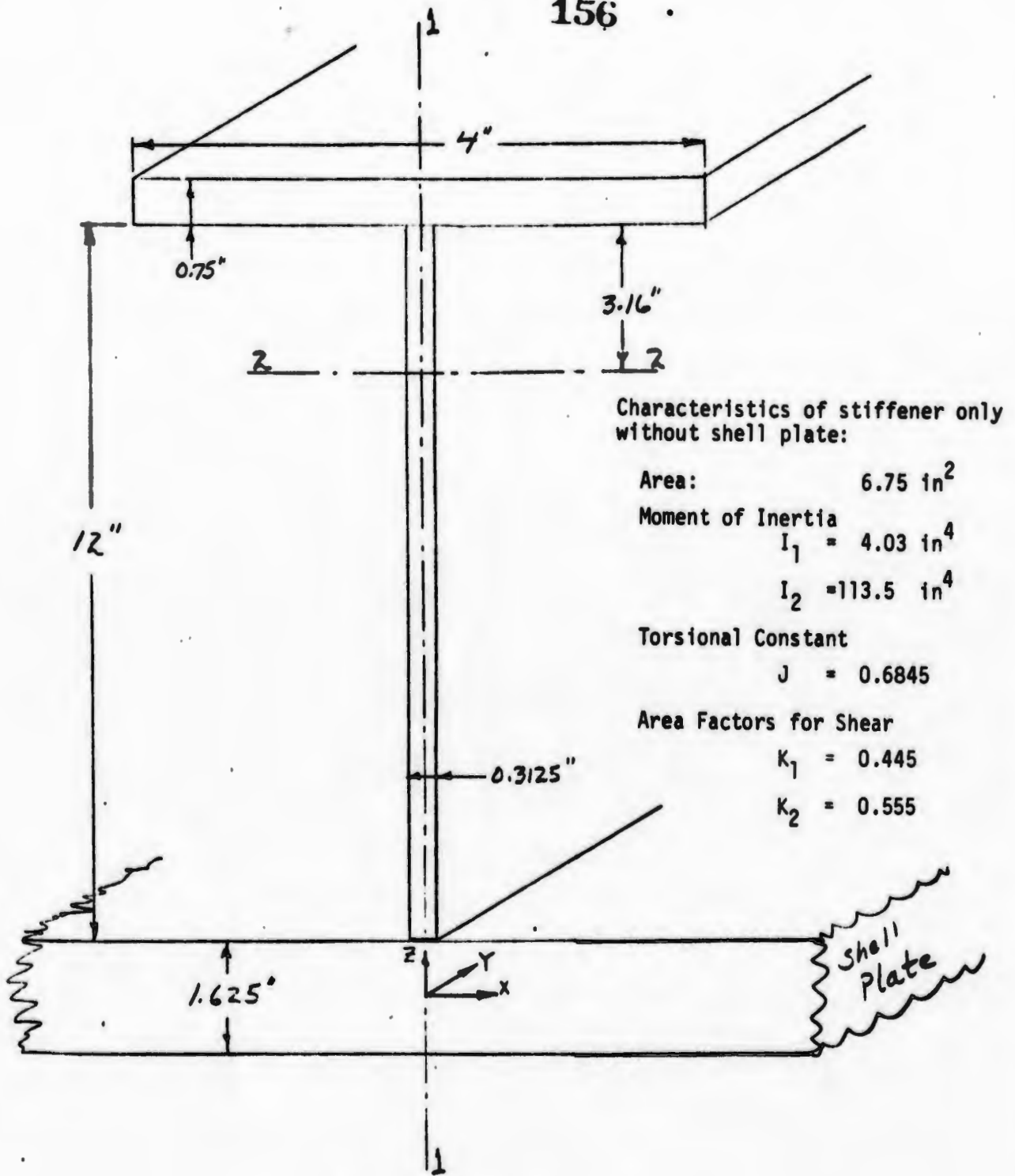
FIGURE C-3
STRUCTURAL DETAILS

Not drawn to scale
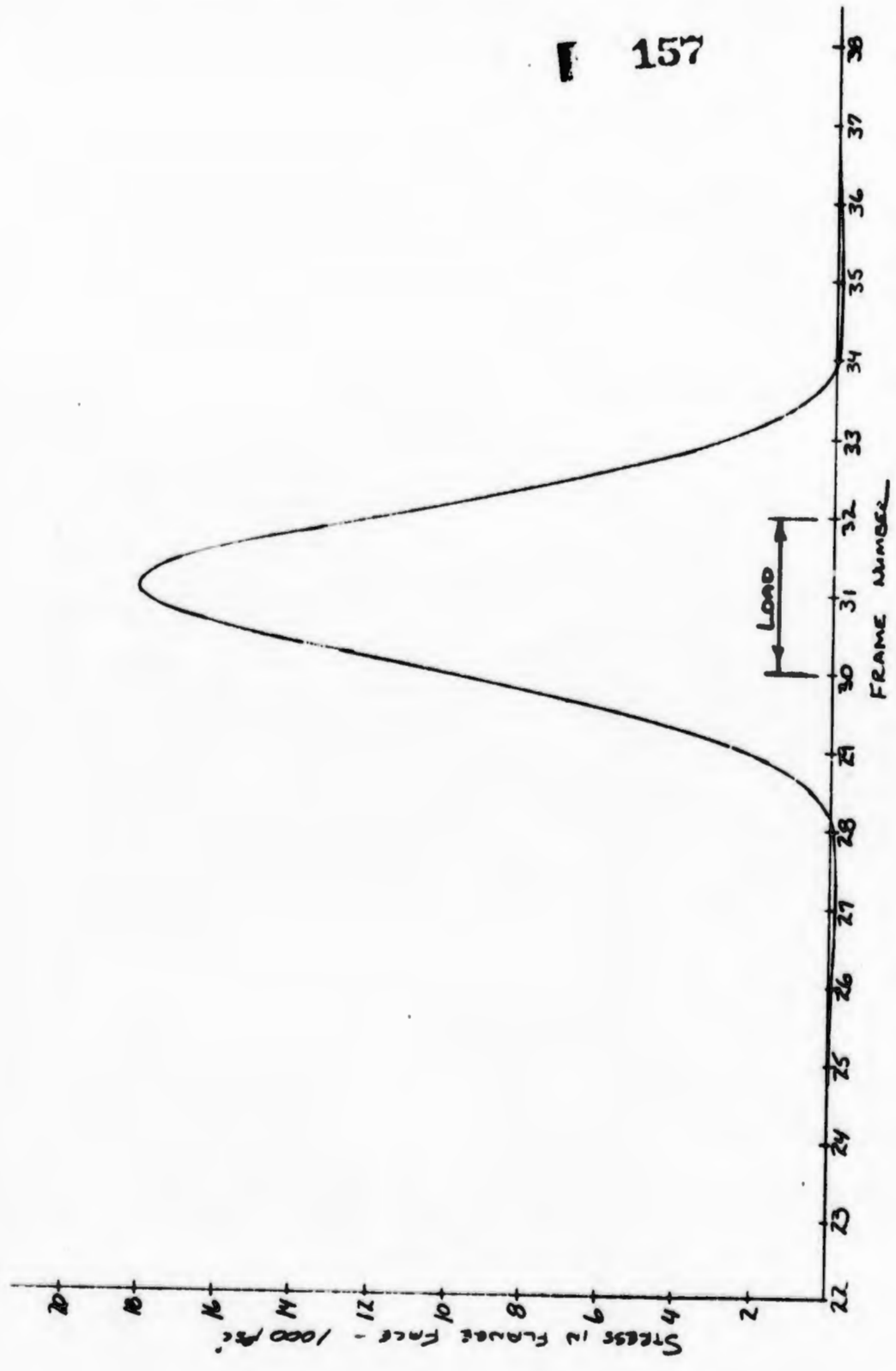
Figure C-4

Typical Nastran Results
Initial Model
Stress Along Grid Line 6

X →

2ND DECK

FRAME

1ST PLATFORM

FIGURE C-5
FINAL NASTRAN
SHELL PANEL MODEL
SCALE: $\frac{1}{2}"=1'-0"$

GRID

Y ↑

FIGURE C-6
DETAILED MODEL OF FRAME

NOTE: NUMBERS ARE GRID POINTS AND
PLATE ELEMENTS. IN SOME CASES
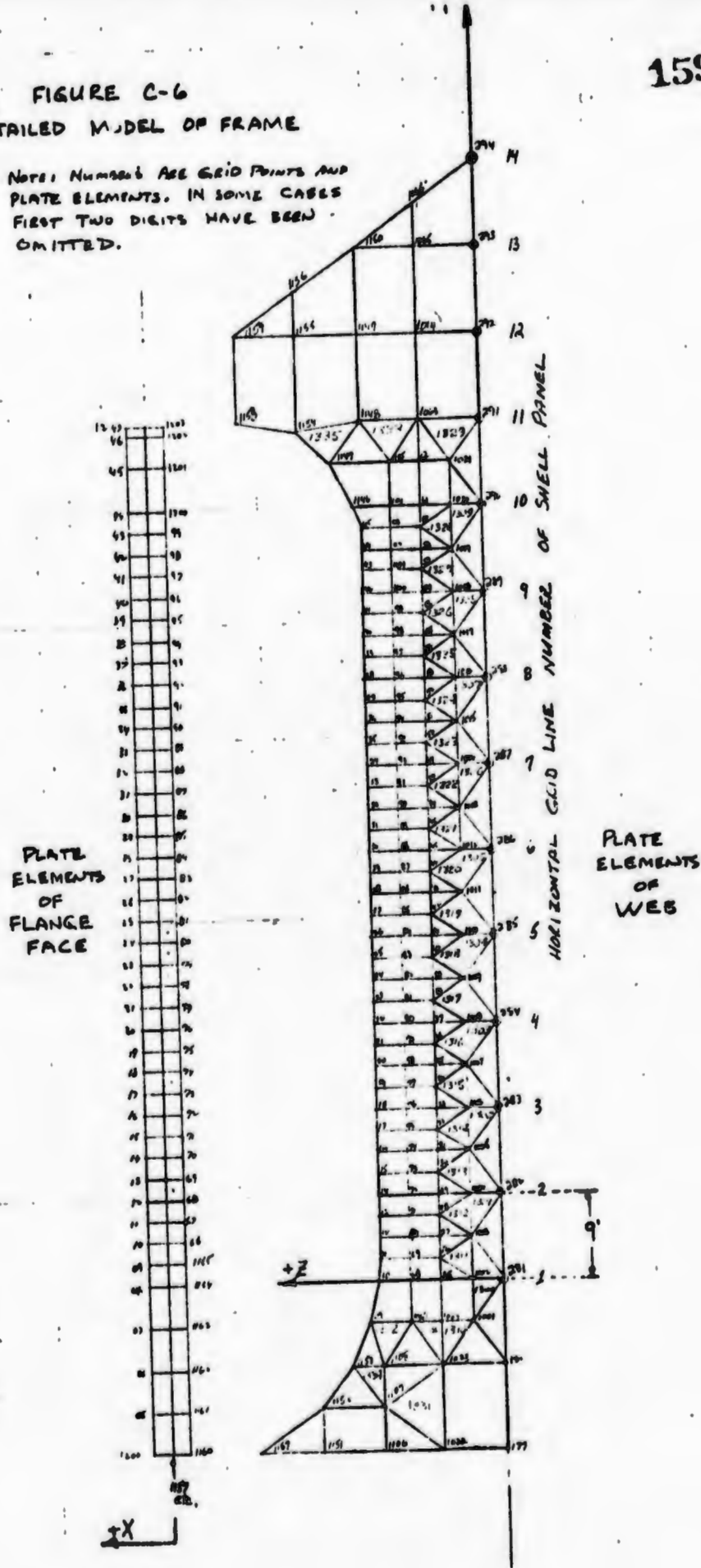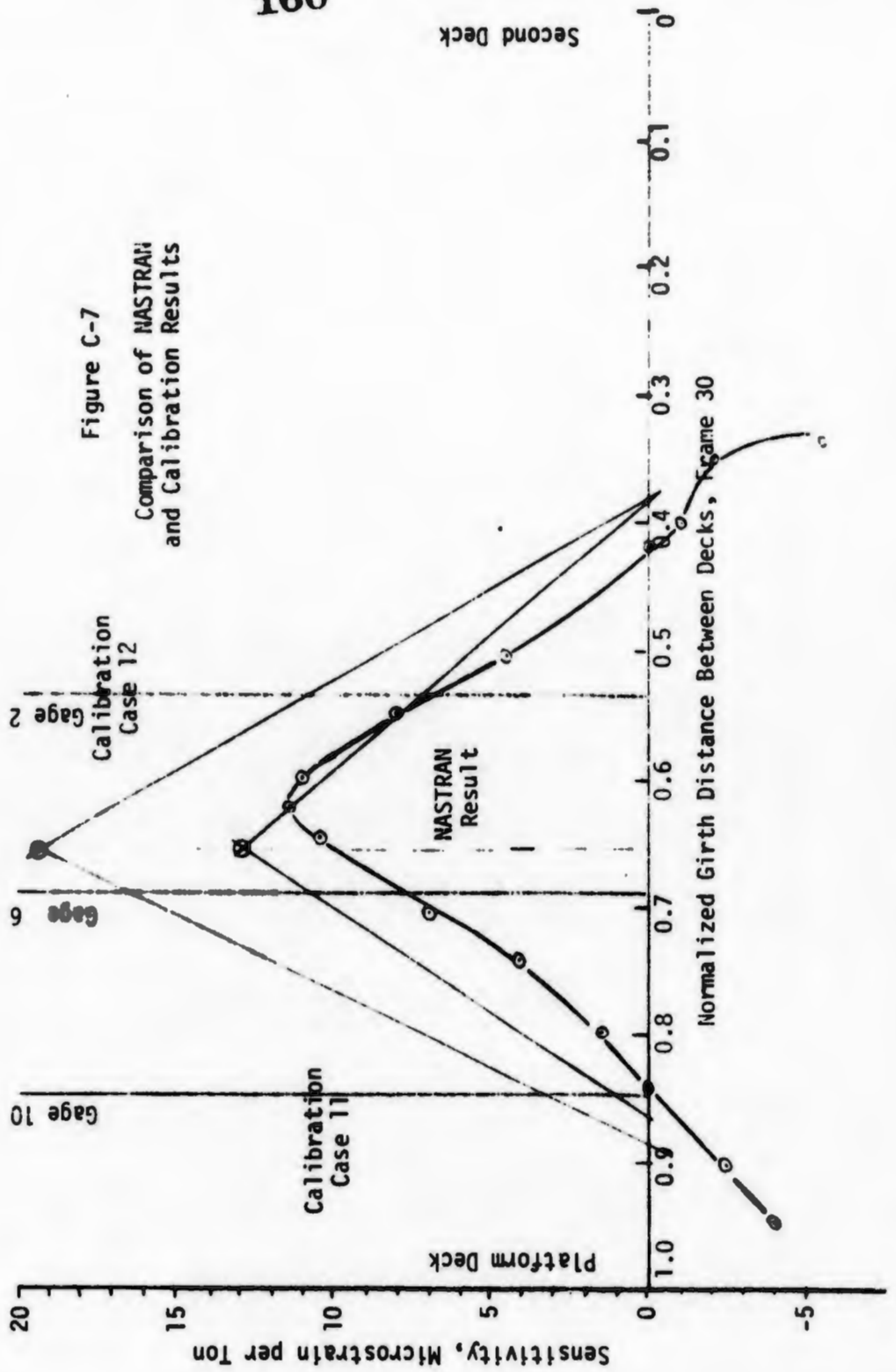FIRST TWO DIGITS HAVE BEEN
OMITTED.

PLATE
ELEMENTS
OF
FLANGE
FACE

PLATE
ELEMENTS
OF
WEB

HORIZONTAL GRID LINE NUMBER OF SHELL PANEL

159

Figure C-7

Comparison of NASTRAN and Calibration Results

APPENDIX D

COMPUTER OUTPUT

(Bound Separately)

I. INTRODUCTION

The objectives of the full-scale experiment with the MACKINAW are to determine:

1. The functions relating forward motion resistance of and powering requirements for the ship and certain ship and ice parameters;

2. The function relating force on a selected panel in the forward portion of the ship to certain ship and ice parameters.

This part of the Pre-Experimental Analysis deals only with the first objective. That objective will be met when a sufficient quantity of data with known accuracy has been collected and an empirical solution based on this data has been derived. The adequate determination of the resistance function dictated the methods used in the control of the experiment. The determination of the hull-ice force function was made with data acquired in the course of the continuous ice resistance experiment. Examination of the variables in the hypothesized hull force relationship indicates that the criteria used for control of the ice resistance experiment are reasonably compatible with those which would be used to control the hull force experiment, had it been the primary experiment of the trials.

The aim of the Pre-Experimental Analysis is to determine:

1. What variables should be measured and how accurately;

2. The minimum number of test variables required to characterize the phenomena under investigation;

3. The accuracy at the final empirical solution; and

4. A test sequence and experimental plan that will insure that sufficient data over the range of each variable of interest is collected.

II. TEST VARIABLES

The variables or parameters believed to be pertinent to this experiment are listed in Table E-1. For the purposes of this experiment it is instructive to classify these variables into three categories: 1) controllable variables; 2) dependent variables; and 3) uncontrollable variables.

The controllable variables consist of total horsepower being delivered to the propellers

$$\Sigma HP = \sum_{j=1}^{3} HP_j , \qquad\qquad [E-1]$$

and the ratio of power delivered to the forward propeller and total power delivered to all the propellers,

$$\overline{CF} = HP_1/\Sigma HP , \qquad\qquad [E-2]$$

where HP_1 is the horsepower delivered to the forward propeller. $\overline{CF}$ will hereafter be referred to as the "coupling factor". It is important to understand that these two variables are the only variables which can be effectively controlled during the experiment. The problem is to select values for these variables in such a way that the resulting values of

the dependent variables will provide the data needed to adequately characterize the ship's resistance function in ice. The exact manner in which values for these variables should be selected is discussed in Part V.

The dependent variables are T_j, Q_j, N_j, E_{B_j}, I_{a_j}, and v. By measuring these variables it will be possible to accurately determine values for the variables which will be used later as the independent variables; i.e., resistance to forward motion and total shaft horsepower requirements.

The uncontrollable variables are listed in Table E-2 and further classified into three categories according to the manner in which they will be used, i.e, independent, correction, and extraneous. The independent classification is used for those variables in which theory is available to suggest a manner in which they influence resistance and powering. Correction classification is used for variables which will be used to correct other variables to a common value using proven theories. The extraneous classification is given to variables believed to influence the resistance and powering but adequate theory does not exist to explain why.

III. REDUCTION OF VARIABLES

The objective of this experiment was stated earlier to be the determination of the functional relationship between forward motion resistance of and the hull structural forces acting on the MACKINAW and certain ship and ice parameters. This may be written in mathematical

functional notation as

$$R_{ice} = f_1 \left[h, v, \sigma_f, B, \rho_1, \rho_w', \mu_{1w}, g, \frac{HP_1}{\Sigma HP} \right] *$$ [E-3]

$$F_{ice} = f_2 \left[h, v, \sigma_f, \rho_w, g, E \right]$$ [E-4]

The objective of the experiment is thus to determine experimentally the functions f_1 and f_2.

Application of the techniques of "dimensional analysis" results in the following dimensionless equivalents of equations [E-3] and [E-4]

$$\frac{R_{ice}}{\rho_w \, g \, h^3} = f_3 \left[\left(\frac{v}{g^{1/2} \, h^{1/2}} \right) \cdot \left(\frac{\sigma}{\rho_w g \, h} \right) \cdot \left(\frac{B}{h} \right) \cdot \left(\frac{\rho_1}{\rho_w} \right) \cdot \left(\frac{\mu_{1w}}{\rho_w \, g^{1/2} \, h^{1/2}} \right) \cdot \overline{CF} \right]$$ [E-5]

$$\frac{F_{ice}}{\sigma_f \, h^2} = f_4 \left[\frac{v}{\sqrt{g \, \ell_c}} \right]^{**}$$ [E-6]

Because of the reduced number of variables, it is obviously easier to determine the functions f_3 and f_4 experimentally than it is to determine the functions f_1 and f_2.

Prior knowledge, experience, and theory suggest that the dimensionless groups contained in equation [E-5] can be combined into new dimensionless groups and thereby effect a further reduction in variables

---

*Extraneous variables have been neglected.
**The final impact load results were based on an improved relationship.

E-4

TABLE E-1

VARIABLES INVOLVED IN CHARACTERIZING
ICEBREAKING BY SHIPS

SHIP:

shaft thrust, T_j
   (j=1-bow, 2-aft port, 3-aft starboard)
ship speed, v
shaft power, HP_j
shaft torque, Q_j
shaft speed, N_j
length, L
beam, B
draft forward, H_f
draft aft, H_a
bus voltage, E_{b_j}

armature current, I_{a_j}

ENVIRONMENT:

ice thickness, h
ice flexural strength, σ_f
water density, ρ_w
ice density, ρ_i
water-ice mixture viscosity, μ_{iw}
ice-metal dry friction, f_{im}
relative wind speed, w
relative wind direction, ψ
water temperature, θ_w
air temperature, θ_a
atmospheric pressure, P_a
snow cover, $\overline{SC}$
ice elastic modulus, E
ice crushing strength, σ_c
ice surface temperature, θ_i
gravity acceleration, g
ice conditions (loose, neutral, tight)

SUBCLASSIFICATION OF THE UNCONTROLLABLE VARIABLES

INDEPENDENT:

> Ice thickness
>
> Ice elastic modulus
>
> Ice flexural strength
>
> Ice crushing strength
>
> Water temperature
>   (infer water density)
>
> Ice density
>
> Water-ice mixture viscosity
>
> Drafts
>   (infer beam and length)

CORRECTION:

> Relative wind speed
>   (correct resistance)
>
> Relative wind direction
>   (correct resistance)

EXTRANEOUS:

> Ice-metal dry friction
>
> Air temperature
>
> Atmospheric pressure
>
> Snow cover
>
> Ice surface temperature
>
> Ice conditions

by forming products of the terms as follows:

$$\mathcal{L} = \frac{\left(\dfrac{R_{ice}}{\rho_w\, g\, h^3}\right)}{\left(1 - \left(\dfrac{\rho_1}{\rho_w}\right)\right)\left(\dfrac{B}{h}\right)} = \frac{R_{ice}}{\rho_w\left(1 - \dfrac{\rho_1}{\rho_w}\right) g\, B\, h^2} \qquad \text{[E-7]*}$$

$$V = \frac{\left(\dfrac{v}{g^{1/2}\, h^{1/2}}\right)\left(\dfrac{\mu_{iw}}{\rho_w\, g^{1/2}\, h^{3/2}}\right)}{\left(\dfrac{B}{h}\right)} = \frac{\mu_{iw}\; v}{\rho_w\, g\, B\, h} \qquad \text{[E-8]}$$

These new variables will be referred to as the dimensionless loading coefficient and dimensionless velocity coefficient. Thus, equation [E-5] may be rewritten as

$$\mathcal{L} = f_5\,[V,\, \overline{CF}] \qquad \text{[E-9]}$$

The experimental determination of the functions f_5 and f_4 is the essence of this experiment and the remaining parts of this analysis are directed toward this objective.

IV. <u>MEASUREMENT ERROR ANALYSIS</u>

The objective of this phase of the analysis is to determine: 1) the magnitude of the expected error in $\mathcal{L}$, V, and $\overline{CF}$ resulting from individual variable measurement errors and, 2) the variation of this error

---

*Because the degree of uncertainty associated with determining R_{ice} is so high (see Section VI), total shaft thrust, ΣT, will be used in place of R_{ice}.

along the surface defined by equation [E-9]. The latter type of
information will be used to determine the data point frequency along
the surface.

A. <u>Error Analysis of the Variable, $\mathcal{L}$.</u>

The variable L is defined by equation [E-7]. Evaluation of this
variable involves measurement of six variables, each of which are sub-
ject to measurement error.

The precision index (8) for $\mathcal{L}$ is

$$\left(\frac{w_{\mathcal{L}}}{\mathcal{L}}\right)^2 = \left(\frac{w_{\Sigma T}}{\Sigma T}\right)^2 + \left(\frac{w_{\rho w}}{\rho_w}\right)^2 + \left(\frac{w_{\rho i}}{\rho_i}\right)^2 + \left(\frac{w_B}{B}\right)^2 + 4\left(\frac{w_h}{h}\right) \qquad [E-10]$$

where "w" is a deviation limit such that $\pm w$ encloses approximately 95 per-
cent of all readings. The precision index for $\mathcal{L}$ is written so that the
percentage error in $L(w_{\mathcal{L}}/\mathcal{L})$ is given in terms of percentage errors in
measurement of the other variables. Each of these measurement errors will
now be determined.

1. <u>Percentage error in total shaft thrust</u>

Total shaft thrust is given by

$$\Sigma T = T_1 + T_2 + T_3 \qquad [E-11]$$

The precision index, in absolute values, for ΣT is

$$w_{\Sigma T} = \left[w_{T_1}^2 + w_{T_2}^2 + w_{T_3}^2\right]^{1/2} \qquad [E-12]$$

E-6

It can be shown that the precision index, in percent values, for ΣT is equal to the percent error of any one shaft thrust measurement provided the percent error of each shaft thrust measuring system is the same; i.e.,

$$\frac{w_{\Sigma T}}{\Sigma T} = \frac{w_{T_1}}{T_1} = \frac{w_{T_2}}{T_2} = \frac{w_{T_3}}{T_3} \qquad [E-13]$$

Therefore, determination of the percentage error in ΣT is simply a matter of determining the percentage error of one thrust measuring system.

A shaft thrust measuring system can be written in equation form as

$$T = \text{const} \times K_2 \, V_{in} \, K_1 \, \varepsilon \qquad [E-14]$$

where

T = deflection of galvanometer

K_2 = gain of the telemetry system

V_{in} = strain gauge power supply voltage

K_1 = strain gauge calibration factor

ε = shaft strain

The magnicude of the deflection of the galvanometer is physically measured from an oscillograph record and is hence subject to reader error. However, this error is small when compared with the uncertainty error associated with the measuring equipment and will not be considered here.

The precision index for equation [E-14] is

$$\left(\frac{w_T}{T}\right)^2 = \left(\frac{w_{K_2}}{K_2}\right)^2 + \left(\frac{w_{V_{in}}}{V_{in}}\right)^2 + \left(\frac{w_{K_1}}{K_1}\right)^2 \qquad [E-15]$$

E-7

The percentage measurement errors in the telemetry system, strain gauge power supply and strain gauge calibration factor are all approximately one percent. Therefore, the percent error in the shaft thrust measuring system is 1.732 percent. Hence,

$$\frac{w_{\Sigma T}}{\Sigma T} = 1.732 \%$$

2. <u>Percentage error in mass density of water and ice</u>. These errors have each been assumed to be approximately equal to one percent.

3. <u>Percentage error in beam</u>. The beam of the ship is primarily influenced by changes in draft and to a lesser extent, list. The following equation will be used to obtain the beam of the ship.

$$B = 0.375 \, (H_F + H_A) + 55.8 \qquad\qquad [\text{E-16}]$$

The precision index for beam is

$$w_B = 0.375 \left[w_{H_F}{}^2 + w_{H_A}{}^2 \right]^{1/2} \qquad\qquad [\text{E-17}]$$

The draft can be measured to within approximately 0.25 feet. Therefore, following the suggestion of Kline and McClintoch (5)

$$w_{H_F} = w_{H_A} = 0.25/2 = 0.125 \text{ ft} \qquad\qquad [\text{E-18}]$$

Substituting this result into equation [E-17] gives

$$w_B = .0661 \text{ ft}$$

The percentage error is thus approximately

$$\frac{w_B}{B} = \frac{.0661}{80} \times 100 = 0.826 \text{ \%} *$$

4. <u>Percentage error in ice thickness</u>. The ice thickness which
will be used to calculate the value of L will actually be the mean value
of a number of measurements made along the track of the icebreaker; i.e.,

$$h_m = \frac{1}{n} (h_1 + h_2 + \ldots + h_n) \tag{E-19}$$

where

     n = number of ice thickness measurements

     h_i = individual ice thickness (i = 1,2,...,n)

The precision index for h is

$$w_{h_m} = \frac{1}{n} \left[w_{h_1}^2 + w_{h_2}^2 + \ldots + w_{h_n}^2 \right]^{1/2} \tag{E-20}$$

Assuming that $w_{h_1} = w_{h_2} = w_{h_3}$ etc., the equation [E-20] reduces to

$$w_{h_m} = \frac{1}{n^{1/2}} w_h \tag{E-21}$$

which shows that the error in h_m is directly proportional to the measure-
ment error for each individual ice thickness measurement and inversely
proportional to the square root of the number of ice thickness measure-
ments made. If we assume an average of around nine ice thickness measure-
ments per data point then equation [E-21] becomes

$$w_{h_m} = 0.333 \, w_h \tag{E-22}$$

---

*The percent error will vary somewhat with beam

The measurement error, w_h, is related to how accurately the ice thickness can be measured using a ruler. The minimum measurement is taken to be 1/4 inch; therefore,

$$w_h = \frac{1/4''}{2} = 1/8 \text{ in} = 0.0104 \text{ ft}$$

The percentage error in the measurement as a function of ice thickness is given in Table E-3.

This completes the analysis of the individual measurement errors associated with equation [E-12] and the measurement errors for L can now be determined. Representative values for the percent error in L as a function of ice thickness are given in Table E-4. It can be concluded that the measurement error for L is approximately 2.5 percent and fairly constant.

B. Error Analysis of the Variable, V

The variable, V, is defined by equation [E-8]. The precision index for this variable is

$$\left(\frac{w_V}{V}\right)^2 = \left(\frac{w_{\mu_{iw}}}{\mu_{iw}}\right)^2 + \left(\frac{w_V}{V}\right)^2 + \left(\frac{w_{\rho_w}}{\rho_w}\right)^2 + \left(\frac{w_B}{B}\right)^2 + \left(\frac{w_h}{h}\right)^2 \qquad \text{[E-23]}$$

Three of these percentage measurement errors have already been determined leaving the percentage measurement errors in viscosity of the slush-ice mixtures and velocity to be determined.

1. Percentage error in viscosity of slush-ice mixtures. This error is assumed to be equal to one percent.

E-10

2. <u>Percentage error in velocity</u>. Velocity measurements will be determined by measuring the time, Δt, required to traverse a certain distance, Δd. The precision index for v would then be

$$\left(\frac{w_v}{v}\right)^2 = \left(\frac{w_{\Delta d}}{\Delta d}\right)^2 + \left(\frac{w_{\Delta t}}{\Delta t}\right)^2 \qquad \text{[E-24]}$$

Assume initially that Δd = 100 feet. Such a distance can be measured accurately to within approximately 3 inches. Therefore,

$$w_{\Delta d} = 0.25/2 = 0.125$$

or

$$\frac{w_{\Delta d}}{\Delta d} = 0.00125 \text{ or } 0.13\% \qquad \text{[E-25]}$$

The time required to traverse 100 feet will be measured by two observers with stop watches.* The accuracy of such measurements would be such that $w_{\Delta t} \approx 0.5$ secs. Since the time required to traverse 100 feet is directly proportional to the ship's speed, the percentage error in measurement of Δt will vary with v as shown in Table E-5.

Table E-5 points out an area where serious measurement error could occur. When the results from this table are combined (using equation [E-24]) with the measurement error associated with distance, it is obvious that the measurement error in velocity is dependent solely on the measurement of the time interval and that the error increases with increasing velocity.

Velocity measurement error can be reduced by: 1) increasing the distance interval used to time the ship's passage as the velocity increases

---

*An electronic counter triggered by manual switches was actually used, but the error should be about the same.

175

and, 2) averaging a number of velocity readings over the same interval that ice thickness measurements are averaged. If the distance interval at speeds equal to 15 fps and above is increased to 200 feet and an average of 9 velocity measurements are made, then the percentage measurement errors of velocity shown in Table E-6 result.

The percentage error in the variable, V, can now be determined as

$$\frac{w_V}{V} = 2.682 + \frac{w_v}{v} + \frac{w_h}{h} \qquad [E-26]$$

which for a velocity of 25 fps in 0.5 feet of ice gives a percentage error equal to 2.74 percent and for a velocity of 5 fps in 2.0 feet of ice gives a percentage error equal to 1.84 percent. It can be concluded that the percentage error in V will vary approximately between these limits and that the error is greatest when the ship is operating at high speeds in thin ice.

C. Error Analysis of the Variable, $\overline{CF}$

The equation which will be used to calculate $\overline{CF}$ is

$$\overline{CF} = \frac{HP_1}{\Sigma HP} = \frac{Q_1 N_1}{Q_1 N_1 + Q_2 N_2 + Q_3 N_3} \qquad [E-27]$$

The precision index for $\overline{CF}$ (assuming N is measured without error and equal torques, Q_a, on the after propellers) can be shown to equal

$$\left(\frac{w_{\overline{CF}}}{\overline{CF}}\right) = (1 - \overline{CF})\left[\left(\frac{w_{Q_1}}{Q_1}\right)^2 + \frac{1}{2}\left(\frac{w_{Q_a}}{Q_a}\right)^2\right]^{1/2} \qquad [E-28]$$

E-12

TABLE E-3

VARIATION OF PERCENTAGE ERROR IN MEASUREMENT OF ICE THICKNESS WITH ICE THICKNESS

Ice Thickness (feet)	Percentage Error In Measurement
0.5	0.69
1.0	0.35
1.5	0.23
2.0	0.17
2.5	0.14
3.0	0.12

TABLE E-4

VARIATION OF PERCENTAGE ERROR IN THE MEASUREMENT OF L WITH ICE THICKNESS

Ice Thickness (feet)	Percentage Error In Measurement
0.5	2.69
1.0	2.49
1.5	2.42
2.0	2.41
2.5	2.40
3.0	2.40

TABLE E-5

VARIATION OF PERCENTAGE MEASUREMENT ERROR IN Δt WITH VELOCITY

v(ft/sec)	Δt	$\frac{W_{\Delta t}}{\Delta}$ x 100
5	20	2.5%
10	10	5.0
15	6.66	7.5
20	5	10.0
25	4	12.5

TABLE E-6

VARIATION OF PERCENTAGE MEASUREMENT ERROR IN MEAN VELOCITY WITH ADJUSTMENTS MADE TO TO THE DISTANCE INTERVAL

velocity (fps)	$\left(\frac{W_{V_m}}{V_m}\right)$ x 100
5	0.83%
10	1.67
15	1.25
20	1.67
25	2.08

Assuming the percent error in the measurement of torque is equal to that determined for thrust then

$$\frac{^w\overline{CF}}{\overline{CF}} = 2.1 \ (1-\overline{CF}) \qquad\qquad \text{[E-29]}$$

From this equation it can be concluded that the percentage error in the measurement of $\overline{CF}$ is approximately 2.1 percent for zero coupling and varies linearly down to 0 percent for a coupling of one.

V. TEST SEQUENCE AND EXPERIMENTAL PLAN

The problems addressed in this section are: 1) the determination of the manner in which the actual controllable variables, ΣHP and $\overline{CF}$, should be varied in order to provide consistent accuracy all along the empirically determined surfaces defined by,

$$\mathcal{L} = f_s \ [V, \ \overline{CF}] \qquad\qquad \begin{array}{c}\text{[E-9]}\\ \text{repeated}\end{array}$$

where
$$0 \leq V \leq V_{max}$$
$$0 \leq \overline{CF} \leq 1.0$$

and 2) the determination of how many data points are required to provide a meaningful empirical solution.

In making these determinations, some physical restrictions must be taken into account. First, the speed that an icebreaker can achieve in an ice field varies directly with shaft horsepower and inversely with ice thickness. This means that data points for high values of V (essentially v/h) must be collected early in the season when the ice is thin

and the speed capabilities are high. Another, somewhat more subtle restriction exists. Once the ship's propulsion machinery is setup to provide power to the forward propeller, the total shaft horsepower varies with coupling factor. The variation is shown in Figure E-1. Only a coupling factor of 0.333 provides full shaft horsepower and a coupling factor above 0.5 severely limits the shaft horsepower that can be developed..* Consequently, values of L at high values of $\overline{CF}$ and V can only be obtained early in the season when the ice is thin.

The form of the function given by equation [E-9] and the distribution of the measurement error over the surface will determine the proportion of data points to be gathered in various regions of the surface. Past experience indicates that for a constant value of $\overline{CF}$ that the functional relationship between L and V has the form

$$L = C_0 + C_1 V + C_2 V^2 \qquad [E-30]$$

It is usually suggested that data points be spaced in such a manner that equal "arc lengths" result. This concept is sketched in Figure E-2. Obviously, experimental values of the independent variable, V, must be spaced more closely together at higher values of V than at lower values in order to obtain equal arc length distribution.

The form of the functional relationship between L and $\overline{CF}$ for constant value of V is not presently known but it is hypothesized that L

* The reason for this restriction is involved with the definition of $\overline{CF}$ and the limitation on the number of diesel-generators aboard the ship.
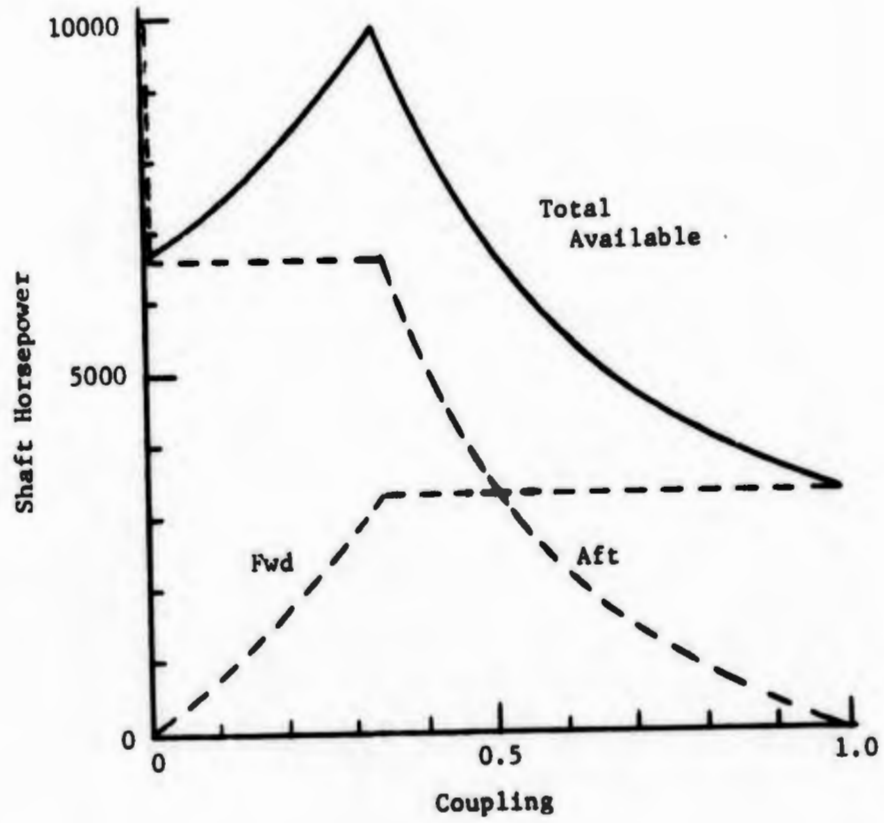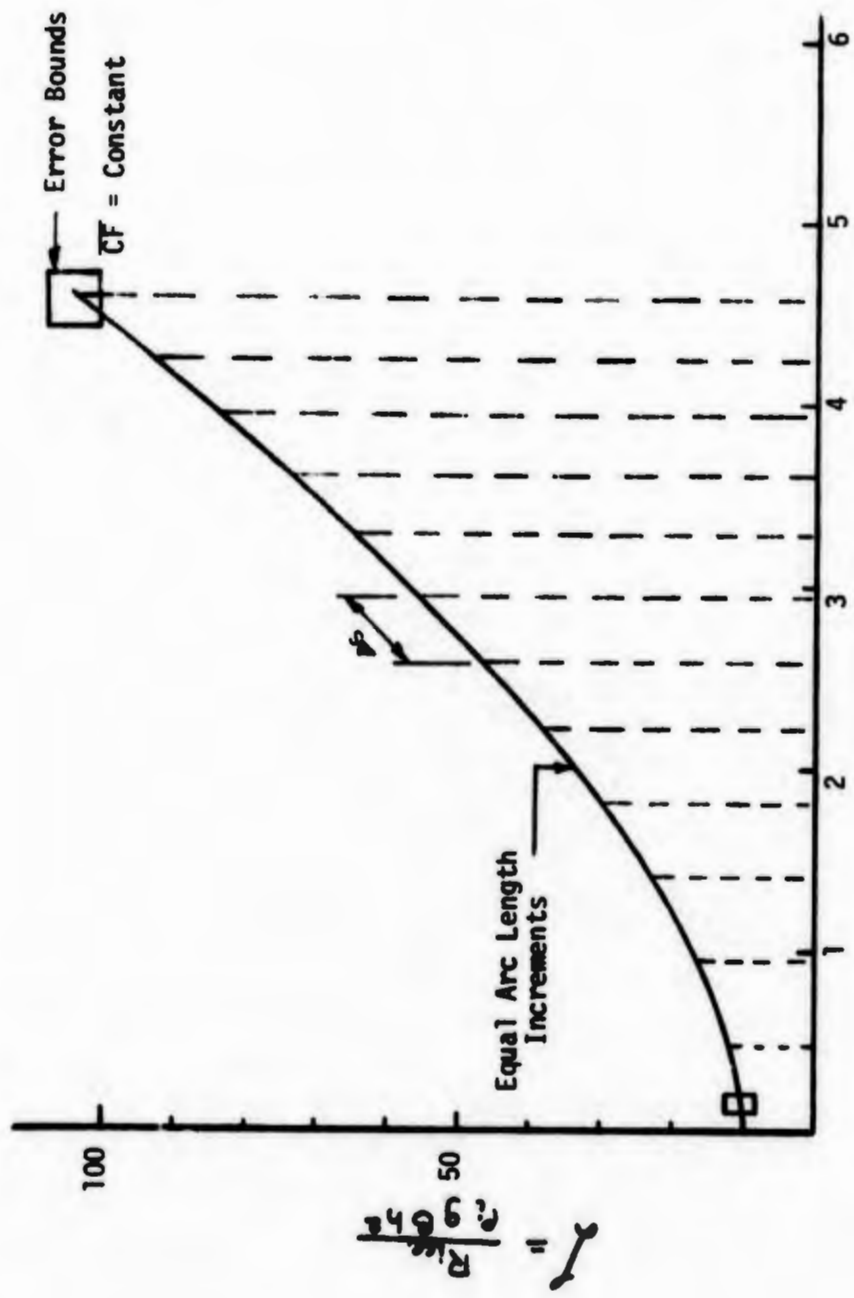
Figure E-1

Total Available Shaft Horsepower
as a Function of Coupling

Figure E-2

Dimensionless Load vs. Dimensionless Velocity
(Hypothetical Plot)

will be a mild linear function of $\overline{CF}$. In that case, equal arc length will be obtained by gathering data points at equally spaced value of $\overline{CF}$.

The next factor to consider is the distribution of measurement error. The previous section indicated that measurement error for:

1. $\mathcal{L}$ varied slightly with ice thickness tending to be greatest in thin ice,

2. V varied with v and h being greatest at high values of v and low values of h,

3. $\overline{CF}$ varied with $\overline{CF}$ in such a way that it was maximum when $\overline{CF}$ was equal to zero and minimum when $\overline{CF}$ was equal to one.

These bounds of probable error are shown by small boxes (cubes) in Figure E-2. The bounds in Figure E-2 result from the previous observations that the highest values of V will result when v is large and h is small; i.e., the exact conditions which provide maximum error in V. The relative "volumes" of the percentage error cubes distributed along the surface is a good indication of the relative number of data points to be gathered in the various regions of the surface. The relative volumes can be obtained using the percentage error equations for $\mathcal{L}$, V and $\overline{CF}$ developed in Section IV. However, before this is done, it is important to make an estimate of expected values of $\mathcal{L}$ for various values of V and $\overline{CF}$ and also to estimate the maximum V obtainable with various values of $\overline{CF}$.

To make such estimates, Figure E-3 was prepared which shows: 1) estimated thrust available for icebreaking as a function of speed and shaft horsepower extracted from reference (10); and 2) estimated ice resis-

tance as a function of speed and ice thickness based upon the dimension-less equations in reference (6). The ice resistance shown in this Figure is for a coupling factor equal to zero. For coupling factors greater than zero, the zero velocity ice resistance is estimated to be reduced linearly with increasing coupling until at a coupling factor equal to one, the resistance is equal to 80 percent of the zero coupling factor value. Assuming the minimum ice thicknesses in which tests can be conducted is six inches, then the maximum values of v_K/h (V = const x v_K/h) as a function of $\overline{CF}$ are as shown in Table E-7.

Table E-8 shows the relative distribution of data points to give approximately consistent accuracy throughout the surface defined by

$$L = f_s [V, \overline{CF}] \qquad\qquad [E-31]$$

and bounded by

$$0 \leq V \leq V_{max}$$
$$0 \leq \overline{CF} \leq 1.0$$

This distribution of data points was obtained by taking into account all the aforementioned factors on measurement error, form of the function f_s and capabilities of the icebreaker. Not shown in this table are the maximum and minimum values of v_K/h which could be obtained by conducting maximum power tests for each coupling factor and releasing tests whenever possible.

The determination of the manner in which the shipboard controllable variables, ΣHP, HP_1, HP_2 and HP_3 should be varied to obtain the
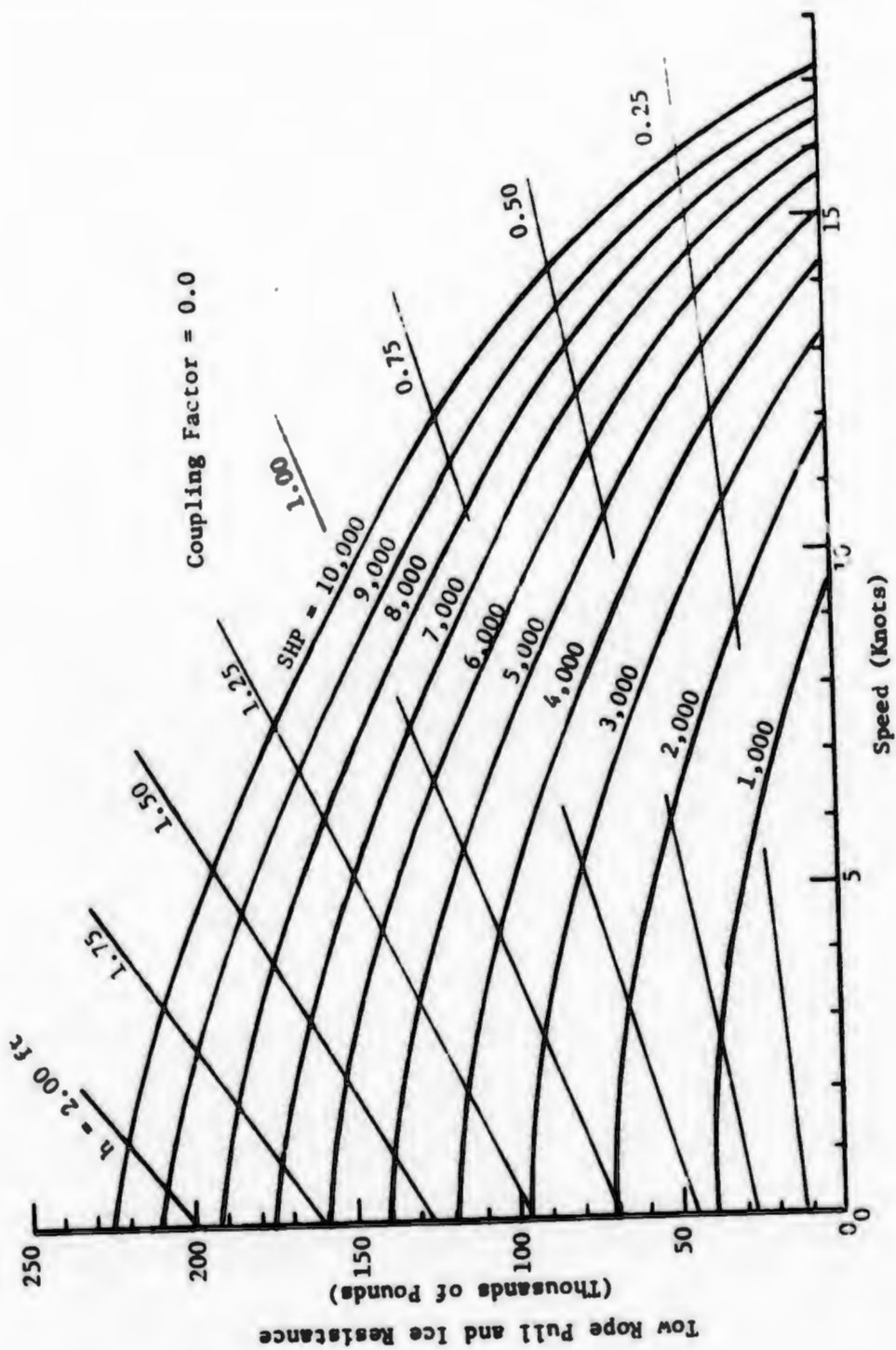
Figure E-3

USCGC MACKINAW Tow Rope Pull

TABLE E-7

MAXIMUM ATTAINABLE VALUES OF $\frac{v_k}{h}$
AS A FUNCTION OF CF

CF	MAX SHP	v_k at h = 0.5	v_k/h
0.0*	10,000	14.32	28.64
0.0**	6,800	12.25	24.50
0.25	8,800	13.70	27.40
0.333	10,000	14.40	28.80
0.50	6,700	12.40	24.80
0.75	4,700	10.40	20.80
1.00	3,300	8.90	17.80

*All diesel generator sets connected to the stern motors

**Two of six diesel generator sets connected to the bow motor

TABLE E-8

TEST SAMPLING PLAN

v_K/h \ CF	0.00	0.25	0.33	0.50	0.75	1.00
25	4*	4	4	3	--	--
20	4	4	4	3	2	--
15	3	3	3	3	2	2
10	2	2	2	2	1	1
5	2	2	2	2	1	1

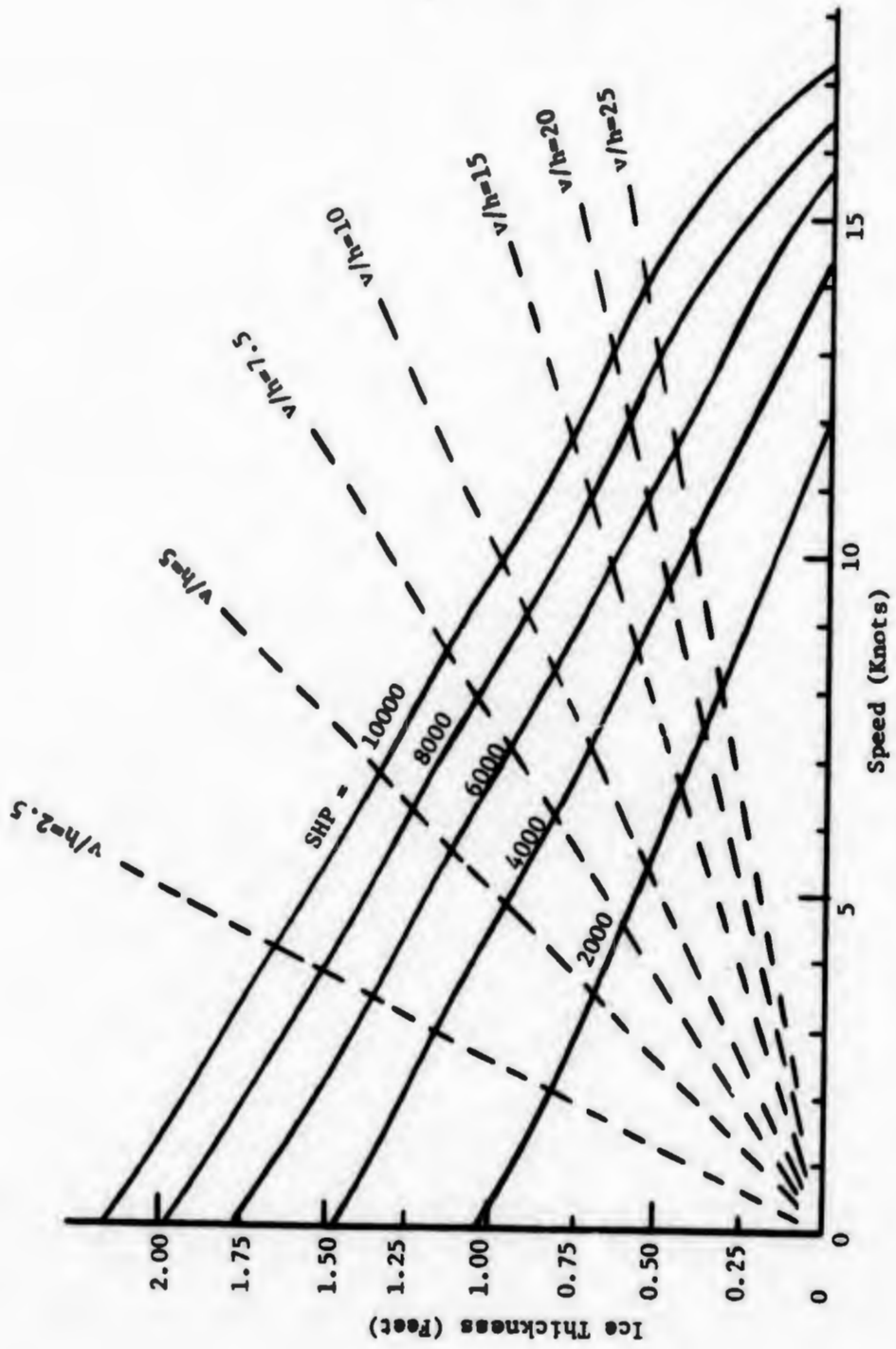*Numbers indicate relative density of sampling desired.

Figure E-4

Speed vs. Ice Thickness and Horsepower

values of $\overline{CF}$ and v_K/h given in Table E-8 must now be investigated. The first step is to cross plot Figure E-3 in such a manner that ice thickness and speed is plotted against one another with power remaining as the parameter. Lines of constant v_K/h are then superimposed on this plot (lines of constant v_K/h are straight lines in the v_K/h plane). The resulting plot is shown in Figure E-4. It is in turn cross plotted to provide Figure E-5 and E-6. These figures can be used to determine the total shaft horsepower required to obtain a desired v_K/h in a given ice thickness.

The distribution of the total horsepower (obtained from Figures E-5 and E-6) among the three shafts to achieve the desired $\overline{CF}$ is obtained from Figure E-7. The diesel speed required to generate these power levels is obtained from Figure E-8. Some caution must be taken when using Figure E-8. Should the machinery hook-up be such that only two diesel-generator sets are available for delivering power to each propeller, then Figure E-8 may not apply to the two after propellers because of the overload features on each diesel engine governor. In such cases, it will be better to set the required power on the forward propeller using diesel engine speed (the forward propeller will not be affected as above provided two diesel-generator sets are available) and set required power on the after propellers using the product of bus voltage and armature current.

Whenever possible, randomization of tests should be made in order to reduce or eliminate the influence of variations in the extraneous
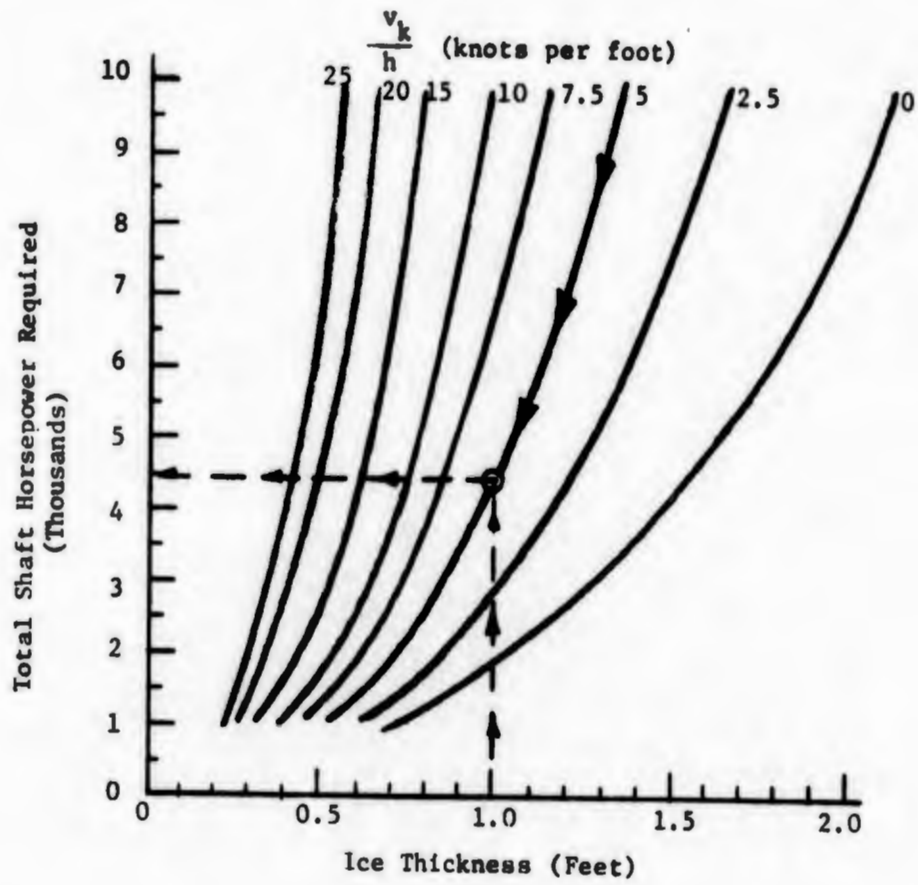
E-17

Figure E-5

Total Shaft Horsepower Required to Achieve
a Desired (v_k/h) in a Given Ice Thickness
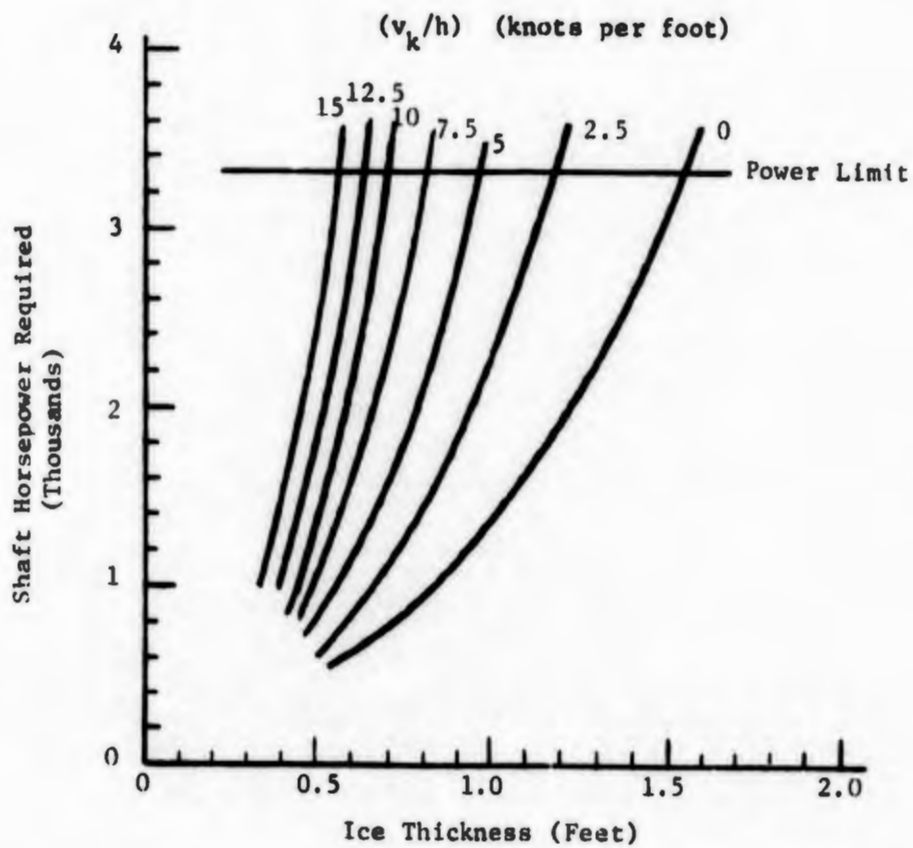(for Couplings of 0, 0.25, 0.33, 0.5 and 0.75)

Figure E-6

Shaft Horsepower Required to Achieve
a Desired (v_k/h) in a Given Ice Thickness
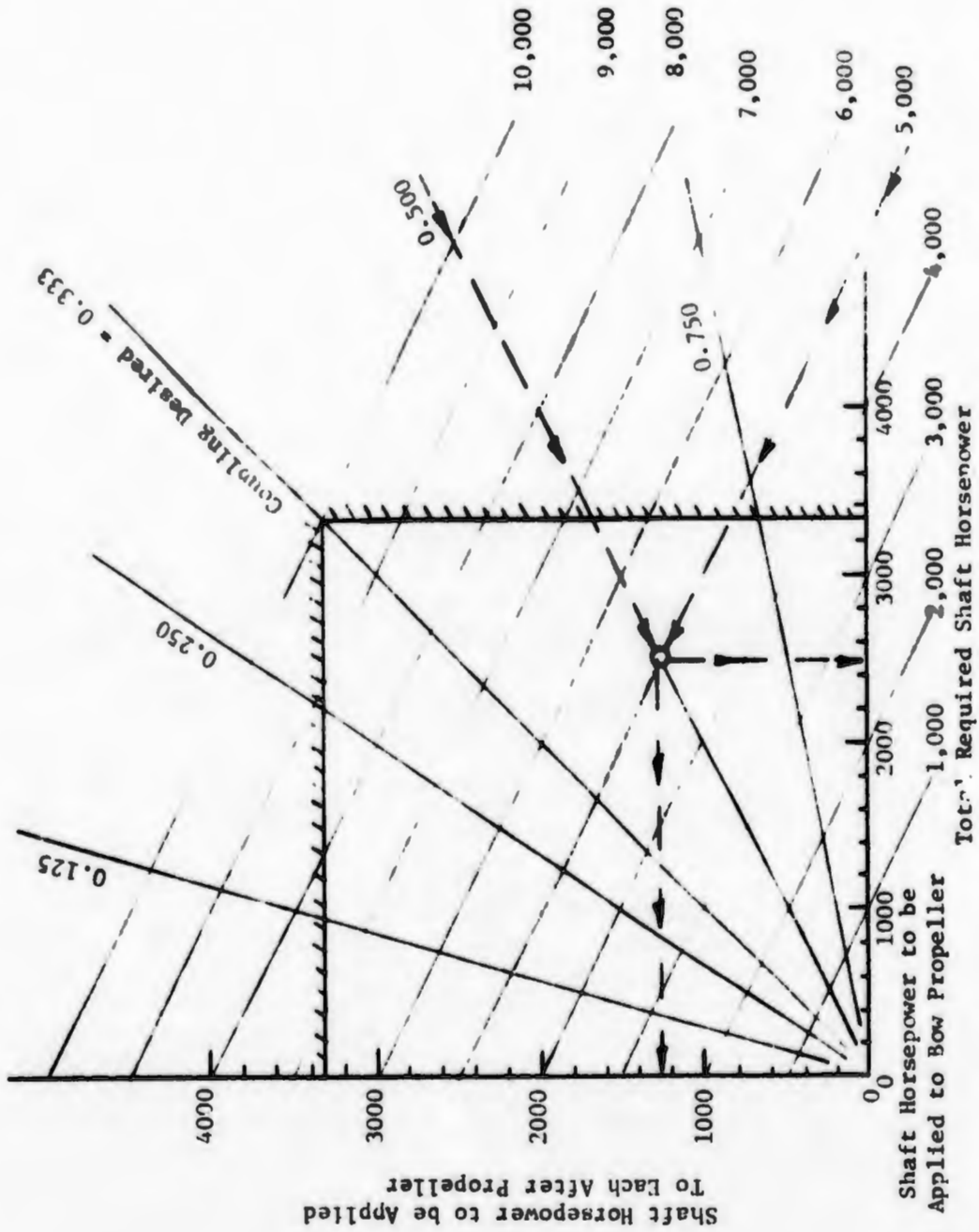(for Coupling of 1.0)

Figure F-7

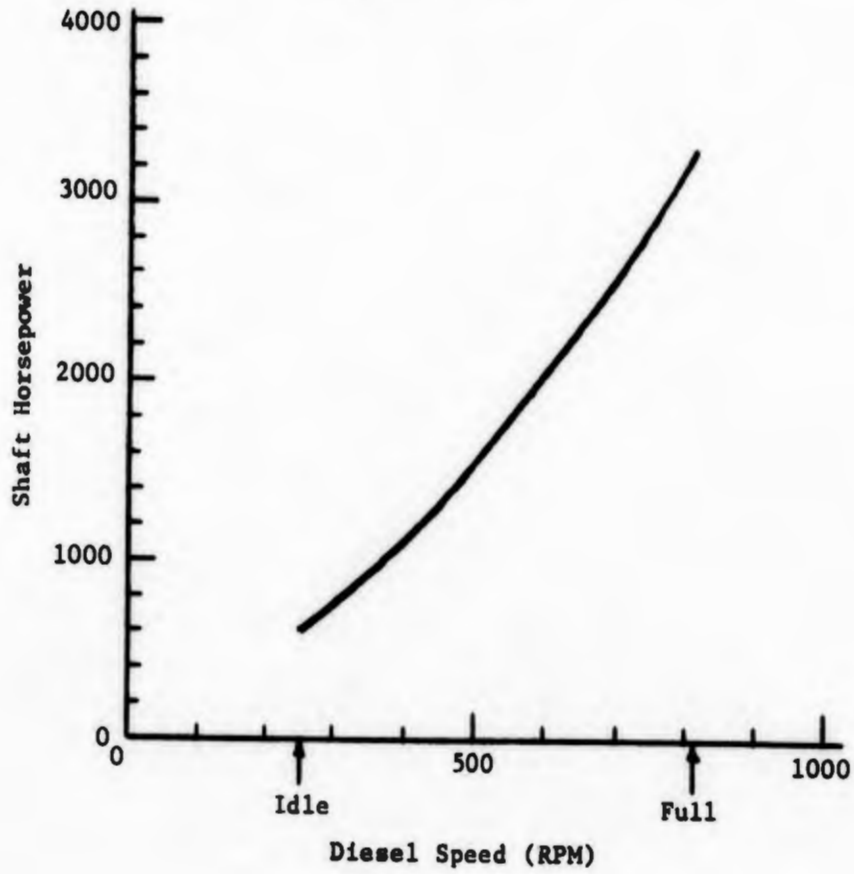Coupling Factor vs. Shaft Horsepower Distribution

Figure E-8

Output Shaft Horsepower as a Function
of Diesel Speed for Two-Engine Operations

shaft horsepower and these errors will cause

errors in determining pure ice resistance.

1. <u>Smoothing error</u>. The graph shown in Figure E-3 was developed
by fairing data available from Figures E-9 and E-10. It can be observed
that actual tow rope pull test data points were gathered only in the region
between 7 to 10,000 horsepower and 0 to 12 knots. The zero tow rope pull
intercept points were obtained from the EHP tests. It is estimated that
in the region where test data points exist that the smoothing error
would not exceed 2 or 3 percent. The further away from this area the
greater one would expect the smoothing error to be. Approximate percen-
tage smoothing errors are shown by areas in Figure E-11.

2. <u>Propagation error</u>. The propagation error will also vary with
the value of shaft horsepower and velocity. To investigate this error
consider the graphical function of Figure E-4 in equation form as

$$R_{ice} = f(SHP, v) \qquad\qquad [E-32]$$

where R_{ice} is pure ice resistance (tow rope pull in Figure E-4), SHP
is the shaft horsepower, v is the ship's speed and f is the nonlinear
function given graphically in Figure E-4. The precision index for this
equation is

$$w_{R_{ice}}^2 = \left(\frac{\partial f}{\partial SHP}\right)^2 w_{SHP}^2 + \left(\frac{\partial f}{\partial v}\right)^2 w_v^2 \qquad\qquad [E-33]$$

where the partial derivatives are to be evaluated graphically at the point
of interest. Using equation [E-33] and the data developed in the text for
errors associated with measuring SHP and v, one can readily determine the

E-19

percentage propagation errors for R_{ice}. Representative values are given in Table E-9. It may be concluded that as velocity increases and horsepower decreases, the propagation error associated with determining R_{ice} increases.

A standard method for combining smoothing and propagation errors does not exist. One method would be to combine the errors using a square law relationship. For example,

$$(\text{total error in } R_{ice})^2 = (\text{smoothing error})^2 + (\text{propagation error})^2$$

Using this method gives total errors in predicting R_{ice} ranging from about 2 percent at low velocities to around 9 percent at high velocities.

The consequences of this error can only be appreciated by studying its effect on the variable L. Using the above results in place of $w_{\Sigma T}/\Sigma T$ in equation [E-10] gives a percentage error ranging from those shown in Table E-4 up to around 9.5 percent. This is significantly larger than the error shown in Table E-4. Additionally the error in L would now be extremely speed dependent meaning that for high values of the variable V there will now exist large errors in L as well as V. The up-shot of all this would be that many more data points would have to be gathered at the high speed-low ice thickness condition in order to guarantee uniform accuracy over the entire range of the empirical solution.

SHAFT HORSEPOWER & TOWROPE PULL
FOR
U.S.C.G. ICE BREAKER
ESTIMATED FROM SELF PROPELLED TESTS WITH MODEL 3771
STERN PROPS. DRIVING, ZERO THRUST ON BOW PROP.
STERN PROPS. NO. 2412-13, BOW PROP. NO. 2414   DISPL. 5138 TONS

e = TOWING EFFICIENCY = $\frac{101.33 \, PV}{33000 \, SHP}$

P = TOWROPE PULL IN POUNDS IN S.W.
V = SHIP SPEED IN KNOTS.
A = PROPELLER DISC. AREA IN SQ. FT.
ρ = 1.99 = WATER DENSITY

SPOT	SPEED
○	0 KTS.
●	3 KTS.
⊖	6 KTS.
●	9 KTS.
⊖	12 KTS.

TEST NO. 2 a

DAVID W. TAYLOR MODEL BASIN   24 FEB. 1943

E. 21

Estimated from Self-Propelled Tests with
Model No. 3771 Using Propellers 2412-13-14
Test No. 3 David Taylor Model Basin
20 February 1943
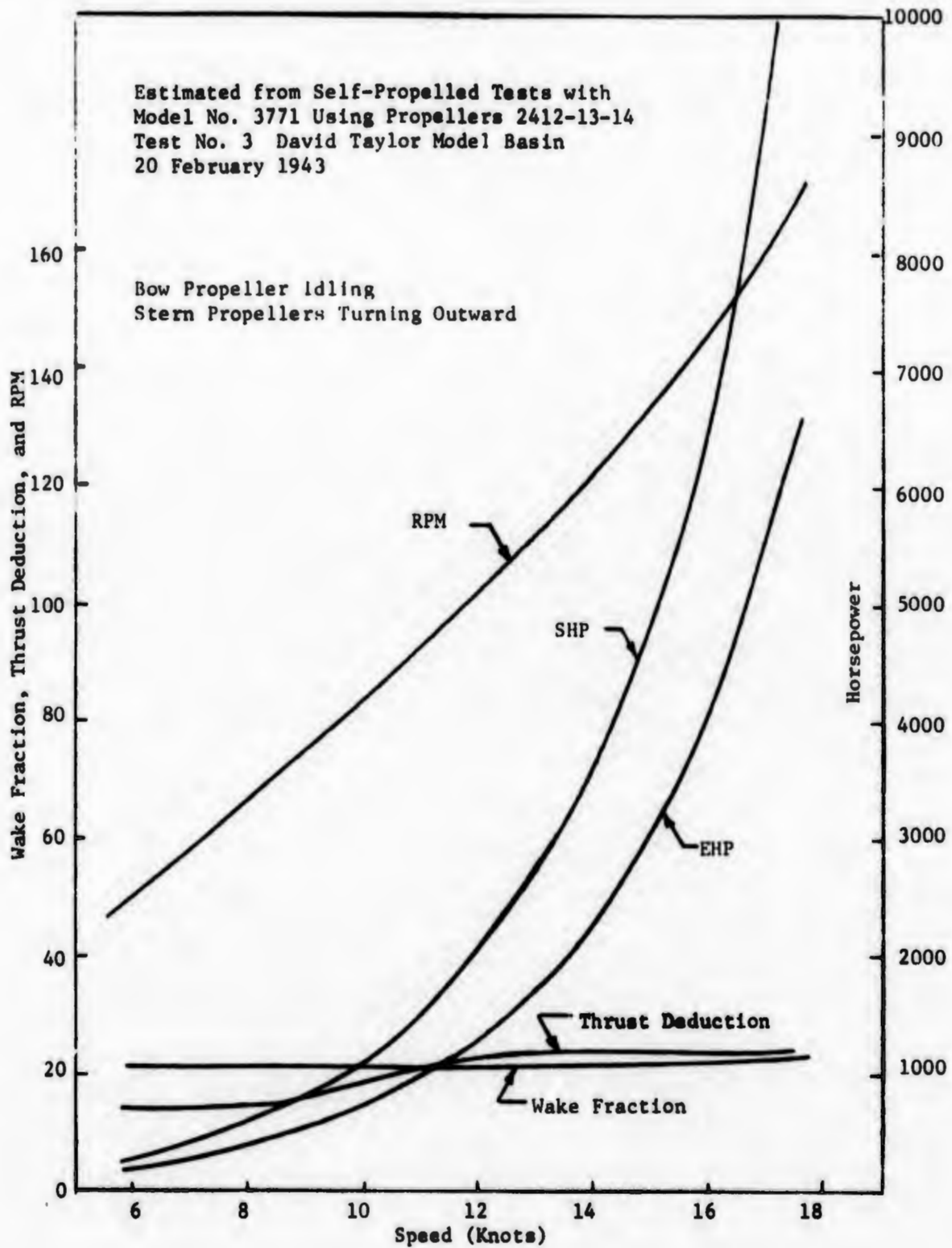
Bow Propeller Idling
Stern Propellers Turning Outward

Figure E-10

Shaft Horsepower & RPM Curves
for Coast Guard Icebreaker

E-2-2
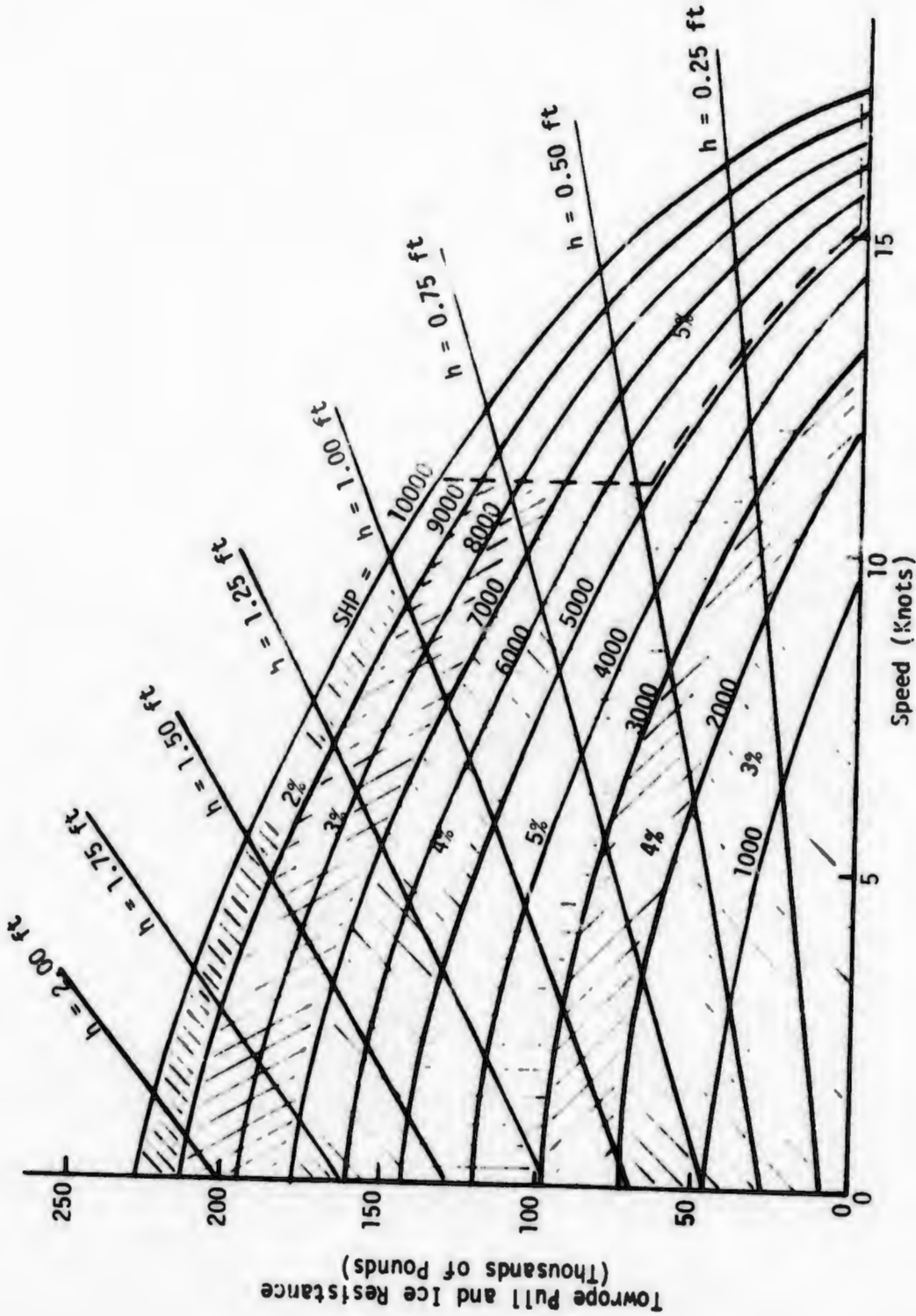
FIGURE E-11

USCGC MACKINAW Towrope Pull Data
(Error Bounds Indicated)

Speed (Knots)

Towrope Pull and Ice Resistance
(Thousands of Pounds)

E-23

TABLE E-9

REPRESENTATIVE PERCENTAGE ERRORS IN DETERMINING R_{ice} AS A RESULT OF ERROR PROPAGATION

v(fps)	SHP	R_{ice} (tans)	$\dfrac{W_{R_{ice}}}{R_{ice}} \times 100$
25	10000	84	7.4%
5	10000	211	1.1
10	5000	112	3.6